On Switched Control Systems and Model Predictive Control under Uncertainty: Theory and Applications

by

Xinxin Shang
B.Sc., Harbin Institute of Technology, 2016
M.Sc., Harbin Institute of Technology, 2018

A Dissertation Submitted in Partial Fulfillment of the Requirements for the Degree of

DOCTOR OF PHILOSOPHY

in the Department of Mechanical Engineering

We acknowledge and respect the Lək̓ʷəŋən (Songhees and Xʷsepsəm/Esquimalt) Peoples on whose territory the university stands, and the Lək̓ʷəŋən and W̱SÁNEĆ Peoples whose historical relationships with the land continue to this day.

On Switched Control Systems and Model Predictive Control under Uncertainty: Theory and Applications

by

Xinxin Shang
B.Sc., Harbin Institute of Technology, 2016
M.Sc., Harbin Institute of Technology, 2018

Supervisory Committee

Dr. Yang Shi, Supervisor
(Department of Mechanical Engineering)

Dr. Daniela Constantinescu, Departmental Member
(Department of Mechanical Engineering)

Dr. Xiaodai Dong, Outside Member
(Department of Electrical and Computer Engineering)

ABSTRACT

Hybrid systems are a widely applied class of dynamic systems, leveraging both continuous and discrete variables to characterize practical physical processes, including discrete variables like switches and logic, as well as continuous variables like position and velocity. As a powerful tool to model a variety of control systems, it has been widely applied in control system design and utilized in a large number of practical applications, such as aerospace, industrial electronics, and biomedical engineering. Since the seminal work published in Automatica in 1999 by Prof. Bemporad (Professor of Control Systems, IMT School for Advanced Studies Lucca, Italy), more and more control scientists and engineers have been increasingly devoted to studying the fundamental theories and applications of hybrid systems. Along with this historical research road, this dissertation focuses on:

- Theories: Stability and stabilization (Chapter 3), robustness (Chapter 4), data-driven model predictive control (MPC) (Chapter 5)
- Applications: Path planning and obstacle avoidance (Chapter 6), mobile communication networks, and hydrogen refueling station optimization (Chapter 7)

In the following, a brief introduction will be given.

In Chapter 1, a brief introduction to a class of hybrid systems is provided, including their stability and stabilization methods, as well as a typical case, i.e., switched systems. Moreover, a comprehensive review of MPC variants designed for handling uncertain hybrid systems is also presented.

In Chapter 2, preliminary concepts and notations are introduced, providing the foundational understanding required for the subsequent chapters.

In Chapter 3, an asynchronous stabilization of discrete-time switched linear systems under dwell-time constraints is presented. This research investigates the stability and control of systems that switch between different modes in an asynchronous manner, and a novel convex stability criterion is developed, facilitating efficient control design.

Following that, in Chapter 4, from a more practical perspective for stabilizing switched systems, a new control strategy is provided to minimize the error between nominal and disturbed states by employing ellipsoidal techniques and demonstrates how system stability can be maintained despite disturbances.

In Chapter 5, a lightweight data-driven approach is developed to construct a novel data-driven MPC framework to control an unknown linear system. The proposed theories ensure two of the most critical properties in MPC frameworks: system stability and recursive feasibility, even under significant uncertainties.

Then, Chapter 6 is devoted to the scenario-based MPC for path planning and obstacle avoidance with chance constraints. This work provides solutions for dealing with uncertainties in real-time decision-making under safety-critical conditions.

In Chapter 7, a representative application is presented, demonstrating how the fundamental theories developed in previous chapters can address practical requirements. The application involves modeling the hydrogen refueling processes as hybrid systems and leveraging MPC to optimize energy costs while satisfying safety constraints (e.g., temperature and pressure).

Finally, the conclusion and future works of the dissertation are presented in Chapter 8.

Contents

List of Tables

List of Figures

ACKNOWLEDGEMENTS

First and foremost, I would like to express my deepest gratitude to my supervisor, Dr. Yang Shi, for his unwavering support, guidance, and inspiration throughout my doctoral journey. his profound expertise, insightful feedback, and patience have been invaluable in shaping my research and academic growth. I am particularly thankful for his encouragement during challenging moments, as well as his ability to challenge me intellectually while fostering an environment of trust and independence. The opportunities he has provided, from collaborative research projects to presenting my work, have significantly enriched my experience and broadened my horizons.

Next, I would like to thank the committee members, Dr. Daniela Conatantinescu and Dr. Xiaodai Dong, for their insightful comments. I also would like to thank the external examiner, Dr. Yajun Pan, for her constructive suggestions in improving my dissertation and kindness help for my research.

Moreover, I would like to extend my heartfelt gratitude to my lab colleagues and friends from Applied Control and Information Processing Lab (ACIPL), University of Victoria (UVic), whose support and camaraderie have made my doctoral journey both enriching and enjoyable. As a caring senior sister, Qian Zhang extended her kindness and support to me from the moment I arrived in this unfamiliar and brand-new country, helping me smoothly begin my PhD journey. As knowledgeable and generous senior brothers, Jicheng Chen and Kunwu Zhang have provided tremendous assistance throughout my PhD studies, life, and personal growth during these years. Meanwhile, I am deeply grateful to all the members of the lab, from senior alumni to junior peers, including Prof. Qi Sun, Dr. Tianyu Tan, Prof. Henglai Wei, Prof. Yuan Yang, Mrs. Chen Ma, Prof. Changxin Liu, Prof. Yaning Guo, Prof. Binyan Xu, Mr. Huaiyuan Sheng, Mr. Zhang Zhang, and Mr. Chonghan Ma, who have already graduated, as well as those still pursuing their studies, including Tianxiang Lu, Yue Song, Yufan Dai, and Rui Pan. Their support and companionship have been invaluable throughout my journey.

In addition, I would like to express my deepest gratitude to my project supervisor, Yunli Wang, for her invaluable support throughout the completion of the project. Her insightful guidance, constructive feedback, and unwavering encouragement have been instrumental in shaping both the progress of this work and the quality of my writing.

Lastly, I want to express my heartfelt gratitude to my parents, Prof. Xiang Shang and Prof. Lu Tian, my aunt, Miss Yun Tian, and my boyfriend, Songlin Zhuang,

for their unwavering love and support over the years. Their encouragement and care have been an essential part for me to complete this journey.

Xinxin Shang
Victoria, BC, Canada,
March, 2025

To my beloved family

Acronyms

MPC model predictive control

LTI linear time-invariant

PID proportional-integral-derivative

RMPC robust MPC

SMPC stochastic MPC

SCMPC scenario-based MPC

DMD dynamic mode decomposition

EDMD extended DMD

NLP nonlinear programming

SVD singular value decomposition

MINLP mixed-integer nonlinear programming

LMI linear matrix inequality

RPI robust positive invariant

AS asymptotically stable

GAS globally asymptotically stable

GES globally exponentially stable

GUES globally uniformly exponentially stable

DT dwell-time

ADT average dwell-time

PDT persistent dwell-time

PWA piecewise affine

CPS cyber physical system

FHCSCP finite horizon conditional scenario program

HRS hydrogen refueling station

FCEV fuel cell electric vehicle

DTDLF dwell-time dependent Lyapunov function

QTDLF quasi-time dependent Lyapunov function

BMI bilinear matrix inequality

UAV unmanned aerial vehicle

USV unmanned surface vehicle

Chapter 1

Introduction

This chapter provides the introductory knowledge of hybrid systems and variants of model predictive control (MPC) methodologies such as classical, robust, stochastic, data-driven, and switched MPC. Subsequently, an overview of this dissertation consisting of theories and practical applications is presented.

1.1 Hybrid systems

Hybrid systems are a class of dynamic systems characterized by the interaction between continuous and discrete dynamics. They have been widely used to model many practical systems and processes such as smart grids [1], robotic systems [2], communication networks [3], hydrogen refueling stations [4], and biomedical processes [5].

These systems integrate continuous-time control systems, such as those governed by differential equations, with discrete-event systems modeled by state machines or automata. Hybrid systems are prevalent in various applications, including automotive systems, robotics, and aerospace, where the integration of different types of dynamics is crucial for performance and reliability. Switched systems are a specific subclass of hybrid systems where the primary focus is on systems that switch between different subsystems, each with its own continuous dynamics. The switching is typically governed by predefined rules or external signals [6].

The key components of a hybrid system include the following (shown in Figure 1.1):

- **Continuous dynamics:** Represented by continuous-time control systems, such as linear systems described by $\dot{x} = Ax + Bu$, where x is the state vector,

u is the control input; A and B are system dynamic matrices.

- **Discrete dynamics:** Modeling using finite-state automata or state machines, where the system transitions between discrete states based on specific conditions or inputs.
- **Interaction mechanism:** The continuous and discrete components interact, with the continuous state influencing the discrete transitions and vice versa. For example, a car's automatic transmission system uses speed (a continuous variable) to decide the moment to shift gears (a discrete event).

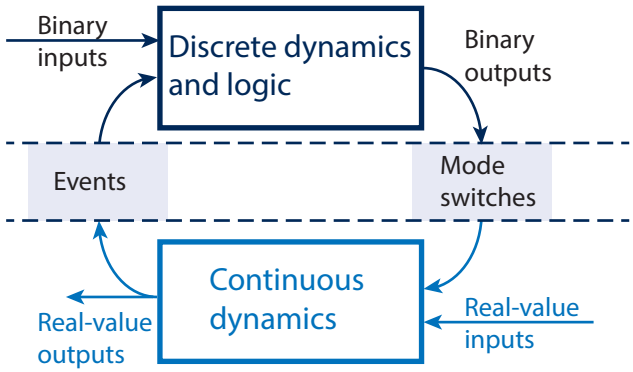

Figure 1.1: Diagram of the hybrid system including the continuous dynamics, logic-based discrete dynamics, and their interaction mechanism.

The field of hybrid systems is inherently interdisciplinary, leading to various perspectives across different research communities. For instance, computer scientists often utilize hybrid systems to describe algorithm logic, focusing on the discrete behavior of the system while assuming the continuous dynamics are relatively simple. In this context, fundamental concerns include well-posedness, simulation, and verification. Conversely, researchers in the domain of systems and control theory often treat hybrid systems as continuous systems with switching, placing more emphasis on the properties of the continuous state. For them, key issues revolve around stability analysis and control synthesis.

In this dissertation, discrete-time systems characterized by discrete switching events, commonly referred to as switched systems, are studied. A switched system can be derived from a hybrid system by ignoring the specifics of the discrete behavior and instead considering all possible switching patterns within a predefined class of behaviors. This shift in focus marks a notable departure from hybrid systems, particularly in the analysis phase. In switched control design, the details of the switching

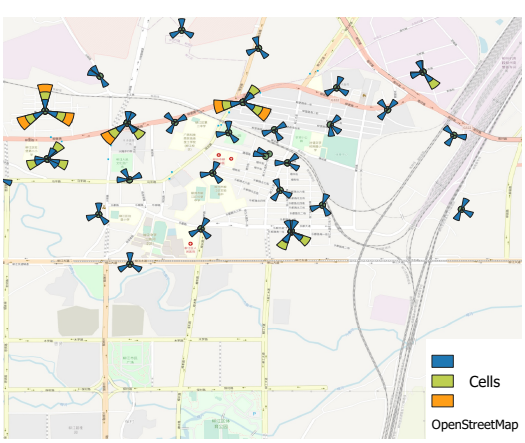

(a) Communication base station

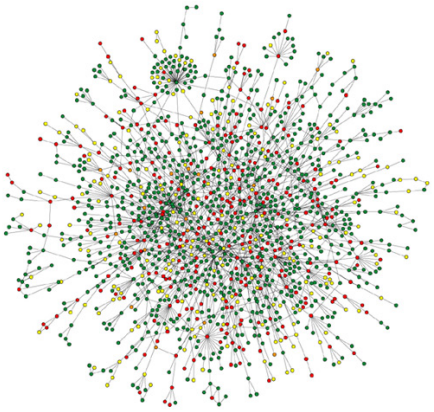

(b) Complex network

(c) Hydrogen refueling station (HRS)

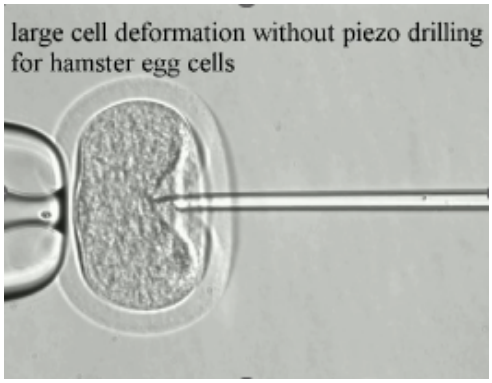

(d) Egg cell injection

Figure 1.2: Hybrid systems in our life.

mechanism become more critical, although typically only the essential characteristics of the discrete behavior are analyzed and utilized. While switched systems can originate from hybrid systems, we will focus exclusively on switched systems and generally avoid explicit references to this connection.

Hybrid systems and switching dynamics are widely present in our real life. Figure 1.2 shows many systems that contain hybrid properties. The communication base station shown in Figure 1.2a and the complex networks shown in Figure 1.2b are systems that have system structure switching. The hydrogen refueling station (HRS) in Figure 1.2c has an input switch. Another kind is like this biosystem in Figure 1.2d, the object, the egg cell, is switching at the moment when the pipette is inserted into the surface.

In the following section, a brief literature review of the stability analysis and control of switched systems is introduced.

1.1.1 Stability and stabilization

As a typical class of hybrid systems, switched systems have been well investigated from both the academic and industrial communities in the last decades. A switched system is composed of a collection of subsystems and a switching event that indicates the active subsystem mode at each time instant [6]. It has been widely applied to model many practical systems with multiple-mode characteristics, including systems with time delay [7,8], with intermittent failures [9,10], with external triggers [11,12], and with operating regions [13,14], etc. So far, the research on switched systems has attracted significant attention on different aspects, e.g., stability analysis [15,16], controller synthesis [17,18], and filter design [19,20].

The stability of switched systems focuses on how the system's overall stability is affected by switching between different subsystems. Switched systems are composed of multiple continuous-time subsystems, and stability analysis seeks to ensure that the system remains stable despite the switching process.

Controlling switched systems presents several challenges due to the complexity of modeling and analyzing systems that involve both continuous and discrete dynamics. The first one is stability analysis. Ensuring the stability of a switched system, especially under frequent switching or in the presence of uncertainties, is a complex task that requires advanced mathematical tools and methods. Another potential problem is computational complexity. An ideal control strategy for the switched system is optimal control, but it causes a demand for solving large-scale optimization problems, which can be computationally intensive.

1.1.2 Classification of switched systems

From the view of the timing and nature of the switching events, switched systems with time constraints can be categorized into different classes, including dwell-time (DT) switched systems, average dwell-time (ADT) switched systems, and persistent dwell-time (PDT) switched systems.

- **DT switched system**: This type of switched systems is classified according to the switching signal that occurs at predefined discrete time instants. The system transitions between modes only at specific, regularly spaced time intervals [15].

- **ADT switched system**: This type of switched systems is defined where the switching between modes is governed by a constraint on the average dwell time.

The average dwell time refers to the average duration for which the system remains in one mode before switching to another. This concept is used to ensure stability by limiting the frequency of switching events [21].

- **PDT switched system**: This type of switched systems is characterized by the time spent in each mode satisfying a lower bound known as the persistent dwell time. This condition ensures that the system remains in each mode for at least a minimum amount of time before switching to another mode [22].

1.1.3 Control of switched systems

The control of switched systems requires specialized strategies that can handle both continuous evolution of system states and discrete changes triggered by events or conditions. Meanwhile, considering the challenges mentioned above, several typical approaches have been developed to control the switched system.

- **Switched control:** In this approach, the system switches between different controllers or subsystems based on certain conditions, such as the states of the system or external inputs. Each controller is designed to handle specific operating conditions, and the switching logic ensures that the transition between controllers is smooth and does not cause instability.

- **Optimal control:** Optimal control strategies for switched systems involve determining the best control actions and switching sequences to optimize a given performance criterion, such as minimizing energy consumption or maximizing efficiency. This often requires solving complex optimization problems that account for both continuous dynamics and discrete events.

- **MPC:** This control framework originates from traditional optimal control methodology, with two key advantages: receding-horizon optimization and constraint satisfaction. MPC is an advanced control strategy that has the ability to use a model of the switched system to predict future behavior and optimize control actions over a finite prediction horizon. For switched systems, MPC must handle both the continuous evolution of the system and the discrete transitions, making it a powerful but computationally demanding approach.

Table 1.1: Overview of MPC approaches.

METHODS	SYSTEM FEATURES
Classical MPC	nominal systems (uncertainty-free)
RMPC	systems with additive and/or multiplicative disturbances (hard constraints)
SMPC	systems with additive and/or multiplicative disturbances (chance constraints and/or expectation of objective function)
Data-driven MPC	online/offline data collection, systems with unknown dynamics/coefficients
Switched MPC	hybrid (switched) systems with time constraints

1.2 Model predictive control (MPC) with hybrid systems

1.2.1 MPC overview

MPC for switched systems involves solving an optimization problem that accounts for both continuous and discrete dynamics. This is often referred to as mixed-integer nonlinear programming (MINLP) systems or piecewise affine (PWA) systems, where the system's behavior is piecewise linear depending on the current mode or state. In this section, a literature review of MPC is illustrated.

This section presents the fundamental concepts and applications of MPC. The following four types of MPC will be briefly introduced: Classical MPC, robust MPC (RMPC), stochastic MPC (SMPC) and data-driven MPC. A brief overview of all the features of these MPC approaches are summarized in Table 1.1, and the literature review of these approaches are discussed in the following subsection.

A basic operating procedure of MPC is introduced in [23, 24]. Figure 1.3 shows this process intuitively. The blue dashed lines are constraints of states, and the red dashed lines are constraints of inputs. The red dash-dot line represents the output setpoint of the states, which is the control target of states. The blue curve indicates the actual and predicted state trajectory, and the green poly-line indicates the actual and predicted control action. At each time instance k, the MPC is solved, and a series of system states and control inputs among the control horizon and prediction horizon is obtained to control the system states converge to the setpoint. The control horizon might be shorter than the prediction horizon of states. A mathematical equation that

describes the system model is identified:

$$x_{k+1} = f(x_k, u_k) \tag{1.1}$$

and several equations and inequalities reflecting physical constraints are considered:

$$\begin{aligned} F(x_k, u_k) &\leq 0 \\ G(x_k, u_k) &= 0 \end{aligned} \tag{1.2}$$

where $f(\cdot, \cdot)$ denotes the dynamic mapping from the state and the input at time k to state at time $k+1$, $F(\cdot, \cdot)$ and $G(\cdot, \cdot)$ represent inequality and equality constraints, respectively. At the time k, the system's future behavior (such as the state

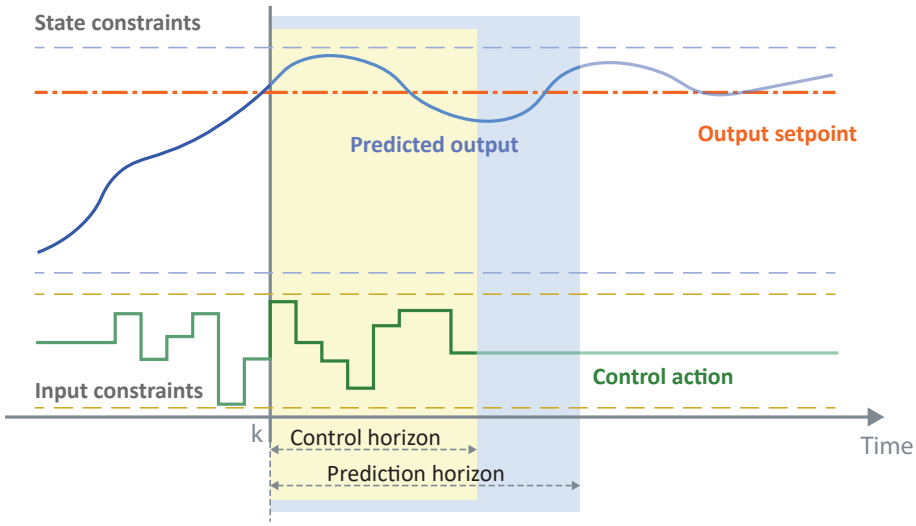

Figure 1.3: The schematic diagram of MPC.

trajectory) is computed based on the identified model in (1.1) and control inputs $\mathbf{u}_k := \{u_{0|k}, u_{1|k}, \ldots, u_{N-1|k}\}$, where the subscript "$p|k$" denotes p time instant ahead from time k. The length of this prediction, denoted by N, is called "prediction horizon" on which a cost function $J_k(x_k, \mathbf{u}_k)$ is defined that often involves both system's future states and control inputs. Here, the system's future states on the horizon can be predicted by the current system state x_k, control inputs $\mathbf{u}_k$, and the identified system model in (1.1). An optimization problem $\mathbb{P}_k$ is to be solved at time k with the cost function of $J_k(x_k, \mathbf{u}_k)$ subject to constraints in (1.2). The optimal solution

of $\mathbb{P}_k$ generates a control sequence:

$$\mathbf{u}_k^* := \{u_{0|k}^*, u_{1|k}^*, \ldots, u_{N-1|k}^*\}. \tag{1.3}$$

After applying the first element of the control sequence $\mathbf{u}_k^*$ in (1.3), i.e., $u_{0|k}^*$, the system state x_k moves one step ahead and transitions to the next state x_{k+1}.

Compared to other control frameworks, MPC has three key distinguishing features [25, 26]:

1) Direct consideration of various types of physical constraints, such as input constraints, state constraints, time constraints, etc.

2) Online prediction of system's future behavior based on the identified system model.

3) Receding-horizon optimization of a predefined cost function that involves both system's future behavior and physical constraints.

It is worthwhile to highlight the three features of MPC:

- The first feature is capable of flexibly introducing practical constraints into the MPC control framework, such as quadratic constraints for obstacle avoidance, integer variables for discrete events, etc. Particularly, if the constraints can be violated to a certain extent for better performance, the problem boils down to the so-called SMPC.

- The key point of the second feature lies in the difficulties in getting a precise mathematical description of a "system model", which motivates the study of data-driven MPC problems.

- The third feature attracts a lot of attention in developing effective and efficient numerical algorithms for online optimization.

Till now, there are a lot of available optimization toolboxes that can be integrated to MPC, such as CVX, GUROBI, IPOPT, etc. Some representative applications are listed as follows:

1) Robotics: flying robots [27], parafoil and payload systems [28], and wheeled vehicles [29].

2) Industrial electronics: pulse width modulation (PWM) inverters [30], direct power control [31], power converter [32], and power electronics [33].

3) Process control: chemical processes [34], multirate networked industrial process control [35], steam generators [36], and process economic performances [37].

4) Power plant: super-heaters [38], power management for hybrid electric vehicles (HEVs) [39], microgrids [40], and thermal energy storage systems [41].

6) Multi-agent systems: schemes for consensus [42] and transportation networks [43].

7) Cyber-physical systems: resilient control under attacks [44] and systems with multiple state delays [45].

Although many common control schemes such as proportional-integral-derivative (PID) control are popular control methodologies in practical applications, MPC shows its unparalleled advantages in handling complex control problems that often involve multi-variables, constraints, and online optimization.

1.2.2 MPC for systems with uncertainties

In the classical MPC framework, the controlled plant of a system is assumed to be well known, i.e., the system's future behavior can be precisely described by an exactly known mathematical equation in a deterministic form. However, due to practical reasons such as unavoidable modeling errors or unpredicted external disturbances, control systems always involve uncertain model structures or parameters. The concepts of robust control and stochastic control is therefore introduced and further integrated into classical MPC, leading to two related but distinct research topics, i.e., RMPC and SMPC. In Table 1.2, representative RMPC and SMPC schemes for handling systems with uncertainties are presented.

Two typical uncertainties generally considered in dynamic systems are additive uncertainties and unstructured uncertainties (or multiplicative uncertainties). To handle linear/nonlinear systems with additive/unstructured uncertainties, four methods are developed, which are shown in Table 1.2.

1.2.3 Robust MPC

The primary goal of robust control is to design controllers that ensure the closed-loop system remains stable and meets predefined performance criteria, even in the presence

Table 1.2: Representative RMPC and SMPC schemes for uncertain systems.

	Methods	Additive disturbances		Unstructured uncertiainties	
		Linear system	Nonlinear system	Linear system	Nonlinear system
RMPC	min-max	[46, 47]	[48, 49]	[50]	[49]
	tube-based	[51, 52]	[53]	[54, 55]	[56]
SMPC	analytical	[57–60]	[61–63]	[64, 65]	[66]
	randomized	[67–69]		[70, 71]	[72]

of uncertainties. Incorporating robust control principles into classical MPC has led to significant advancements in RMPC research. Along with the research on RMPC, min-max RMPC and tube-based RMPC have been two popular frameworks.

Min-max RMPC. Classical MPC has inherently robust stability to a certain degree (details can be found in Chapter 3 of the book [73]). However, in the presence of state and control input constraints, the robustness margin may be super small or even nonexistent. Alternatively, one of the promising solutions for obtaining the robustness guarantee is the min-max MPC method, which can simultaneously handle parametric uncertainties and external disturbances, achieving a desired control performance with a smaller region of attraction (compared to that of classical MPC).

Min-max MPC is theoretically more robust than classical MPC but is hindered by its high computational complexity, thus its use in real-world applications. However, the progress in optimization techniques and the increasing affordability of hardware with powerful computational capabilities enable min-max MPC to be a more feasible solution [74].

Tube-based RMPC. Another promising method for handling uncertain systems is tube-based RMPC. The main idea is to ensure that all possible realizations of the disturbed state trajectory lie in a pre-computed uncertainty tube under the closed-loop MPC framework. The key steps of tube-based RMPC are how to design the "center" and "diameter" of cross sections which can form the tube together, and simultaneously guarantee closed-loop system stability and the recursive feasibility of the derived RMPC algorithm. One of the representative works was reported in [51] in which the authors presented a general framework of tube-based RMPC. This framework later motivated many subsequent theoretical research works and practical applications.

The tube-based RMPC can be classified into several categories in accordance with

the type of the tube:

- **Rigid tube-based RMPC**. Rigid tube represents the tube constructed from the invariant set around the nominal trajectory, ensuring that the actual system state remains within a bounded region despite disturbances [51]. This is the most classical type of tube but is more conservative in general [53].
- **Homothetic tube-based RMPC**. Homothetic tube-based RMPC is another approach that builds on the concept of flexible tube shapes to handle system uncertainties and disturbances. Unlike the rigid tube approach, the homothetic tube allows for scaling and translation of the tube, enabling better adaptability to varying conditions, therefore achieving improved performance [54].
- **Elastic tube-based RMPC**. Elastic tube-based RMPC is a robust control approach that extends the concept of tubes around nominal trajectories by allowing the tube to be both scaled and reshaped dynamically. Compared with the homothetic tube which can only vary the size of each cross-section, the elastic tube allows the modification of the shape, which increases the flexibility of this approach [55].

1.2.4 Stochastic MPC

As introduced in Section 1.2.3, the main advantage of RMPC is the guarantee of system stability and algorithm feasibility even if the system suffers from disturbances. However, RMPC algorithms have several limitations that prevent them from being used in practical applications:

1) It is conservative in some cases where the plant to be controlled can accept violations of the constraints to some degree, in order to obtain more economic benefits or improve the overall efficiency [75].

2) The RMPC algorithms turn the statistical properties of the uncertainties into an upper bound, but actually the uncertainties may seldom reach the upper bound.

3) For some specific systems, the system properties cannot guarantee the satisfaction of the robust constraints; hence, the system must tolerate some constraint violations [76].

To overcome these limitations, researchers have presented a series of SMPC control schemes to describe, analyze, and synthesize the controlled systems in a more general way since RMPC can be seen as a special case of SMPC. The SMPC methodology formulates the uncertainties with their statistical descriptions, such as the probability distribution function or expectation, being particularly closer to the nature properties.

The so-called "hard constraints" used in RMPC are reformulated as "stochastic constraints" which will allow violations of constraints as long as the overall violations follow a predefined probability. The cost function of the optimization problem is also transformed into a corresponding modality.

SMPC has been successfully applied in some applications where a reasonable number of violations can be allowed or cannot be avoided. The representative applications include intelligent building systems, optimal operation of energy systems, intelligent vehicle path planning and control, and so on.

On the other hand, SMPC can be classified into two groups from the theoretical perspective [76], as shown in Table 1.3: Analytical method constructs a stochastic tube with the terminal set, and converts the chance constraints to deterministic inequalities by particular matrix manipulations; The scenario-based method randomly generates uncertain parameters that are subject to specific distributions, and accordingly obtains the optimal control input.

Table 1.3: Two representative SMPC control schemes.

Methodology	Expected value	Joint constraints	Independent constraints
Analytical	[64, 66]	[77–80]	[65]
Sample-based	N/A	[69, 81, 82]	N/A

The primary advantage of SMPC, compared to RMPC, lies in its stochastic constraints feature. It essentially allows the system to violate constraints as long as a predefined probability of such violations can be followed, and therefore, provides a larger solution space for potentially better performance [59]. Due to this feature, SMPC is widely used in a lot of constraints-nonsensitive applications, where the pre-set upper and lower bounds are allowed to be slightly violated. For instance, in [83], the authors employed an SMPC strategy for building climate control that also integrated predictions of weather in the next hours so as to increase energy efficiency while respecting desired occupant comfort. Simulation and experimental results demonstrate

that SMPC significantly outperforms other control methods, like rule-based control and performance bound control.

However, traditional SMPC algorithms, e.g., algorithms developed in [83], are often of high computational complexity since they involve the mathematical operation of high-dimensional system state or input probabilities. To address this issue, a variant of standard SMPC methods, termed scenario-based MPC (SCMPC), is presented. The main idea of SCMPC is to address uncertainties by considering multiple possible future scenarios, each representing a different realization of the stochastic variables. Scenarios are typically generated by sampling from the probability distributions of the uncertain parameters or disturbances.

Tube-based SMPC. The authors in [79, 84] presented a seminal framework for tube-based SMPC that can ensure system stability and feasibility by calculating a stochastic tube and further letting the terminal state of the system always be within this tube in the established optimization problem.

In [65], the authors proposed the tube-based SMPC for linear systems with both additive and multiplicative disturbances, considering probabilistic constraints. The main technique is the utilization of vertices of polytopic sets to cover all uncertainties with a prescribed probability, for the purpose of reducing the conservativeness. Although the conservativeness is lowered to some extent by such a mathematical operation, the main idea still follows robust control or RMPC where the worst case among all uncertainties is taken into account. For the further reduction of conservativeness in the field of SMPC, the authors in [57] presented a novel concept called explicit technique in 2010. This technique can turn probabilistic constraints into deterministic constraints while respecting constraints under the predefined probability. In particular, the authors ingeniously put probabilistic constraints to a finite-dimensional algebraic matrix where each element contains the preset probability and states/inputs variables. The equivalence between the probabilistic constraints and deterministic constraints is strictly demonstrated by illustrating the operation of this algebraic matrix, and the recursive feasibility of the derived algorithm and the stability of the considered system are guaranteed.

Although the explicit technique, developed in the seminal work of SMPC in [57], has addressed the probabilistic constraints problem, it still has two main limitations. On the one hand, this technique only works for state or input constraints in a simple form, such as

$$\Pr(x_k \leq h) \geq p,$$

where x_k represents system state at time k, h and $p \in [0, 1]$ are preset constants, and $\Pr(\cdot)$ is the probability function; it cannot fit a more general case like $\Pr(f(x) < h) > p$. On the other hand, the price to pay for the conversion from stochastic constraints to deterministic constraints is the high computational cost of iteratively calculating the algebraic matrix. To extend the SMPC to a more general case and further relax the computational cost, the authors in [70] developed a one-step-ahead sample-based SMPC method. The main idea of this method is to draw samples subject to preset probabilistic constraints from the current time instant k to $k+1$ (only one step), and thereafter turn this problem to RMPC formulation from $k+1$ to the terminal time instant. Actually, this is a promising solution since its first step belongs to SMPC, and the rest belongs to RMPC. The authors also claimed that this approach would decrease the conservativeness a little more than the explicit SMPC approach. This idea also inspires scenario-based SMPC, which will be reviewed in the next section.

It should be noted that since the explicit SMPC theoretical framework was established in 2010, a large number of works were reported by extending explicit SMPC to different control disciplines, such as distributed control [85–87]. For instance, in [85], the authors developed a cooperative distributed SMPC algorithm that allows the system to violate predefined constraints as long as the violations follow a preset probability.

Scenario-based SMPC. Although explicit SMPC provides a complete theoretical framework for handling probabilistic constraints with both recursive feasibility and stability guarantees, the high computational cost limits its widespread usage. An open problem arises: Can we invent a method similar to rolling dice to address the design and optimization issues of SMPC? Actually, a naive idea to handle the probabilistic constraints can be formulated as follows:

Step 1: Draw samples from possible uncertainties (subject to probabilistic constraints).

Step 2: Solve the optimization problem (note that the optimization problem does not contain any uncertainties once we consider a specific sample).

Step 3: Check the optimization result to see whether the solution is feasible.

Step 4: Decide if we use the solution in Step 3; If not, turn to Step 1 and repeat the aforementioned steps.

The authors in [88] first presented a rolling dice idea similar to the above four steps, which marks the beginning of the study of SCMPC. The authors proved that

the probability of violations of constraints will decrease while the number of samples increases, which aligns well with our basic thinking. The most important conclusion of the paper is how to determine the minimal number of samples to meet the requirement of the probability of constraints since it provides an effective approach to identifying when to stop the sampling process. However, the crucial properties of the system, like recursive feasibility and stability, are not proved. Moreover, the computational cost remains high, as the number of optimization problems corresponds to the number of samples.

To reduce the computational burden in [88], D. Bernardini and A. Bemporad came up with a clever method that contains two steps for searching for the best solution. The first step is to refine samples that have the potential to induce the best solutions [89]. The authors introduce the concept of optimization tree to screen effective samples which may need to be calculated in the optimization process where a set of linear matrix inequalities is introduced. In the second step, users need to solve optimization problems whose number is equivalent to refined possibly best samples. Although this approach efficiently avoids some unnecessary calculations in the first step, it still contains several optimization problems to be solved.

To further lower the computational cost as well as the conservativeness, S. Georg updated the algorithm in [89], and significantly reduced the number of calculations [69]. The main idea of [69] is to draw samples in the first step, where each sample corresponds to a vector of uncertain parameters, and a deterministic cost function. In the second step, all the cost functions are added together to form a new cost function, and users only need to solve the optimization problem (consisting of the new cost function and previous deterministic constraints) once to obtain a solution. The authors strictly proved that such a solution is feasible and can ensure the system stability.

Risk-sensitive MPC. The main idea of risk-sensitive MPC is to incorporate risk awareness into the control optimization process, explicitly accounting for uncertainties and potential risks in the system. A general risk-sensitive objective function often takes the form:

$$J = \mathbb{E}\left[\sum_{k=0}^{N-1} \ell\left(x_k, u_k\right)\right] + \lambda \cdot Risk\ Measure,$$

where

- $\mathbb{E}[\cdot]$ is the expectation operator,

- $\ell(x_k, u_k)$ is the stage cost (e.g., tracking error, control effort),
- λ is the risk-sensitive parameter (tuning the trade-off between performance and risk),
- *Risk Measure* quantifies the risk.

Unlike traditional MPC, which typically focuses on optimizing expected performance (e.g., minimizing average cost), risk-sensitive MPC aims to balance performance with the sensitivity to risk arising from system uncertainties, such as disturbances, noise, or model inaccuracies. Interested readers can refer to [90, 91].

1.2.5 Data-driven MPC

An accurate mathematical model is crucial for control tasks, but is often difficult to obtain, especially for high-dimensional complex processes. Therefore, it is in high demand to develop novel control approaches that can be implemented directly based on data [92]. In the last decade, data-driven MPC has been one of the promising methods for addressing this emerging challenge [93]. The main advantages of data-driven MPC include directly handling constraints, prediction-based optimization, and model-free control input generation.

Existing results on data-driven MPC can be classified into indirect and direct approaches [94]. The **direct approaches** solve the control problem directly by data, such as reinforcement learning-based MPC [95, 96]. Most direct approaches generally need abundant initial data for training or a good enough initial guess of the system dynamics at the beginning. The **indirect approaches** involve identifying the model parameters from data which is then used in a certainty-equivalent control design. Indirect approaches consider advanced system identification methods, such as deep learning and recurrent neural networks [97]. For example, the interpolated Koopman operator is a kind of indirect approach to transfer the high-dimensional nonlinear system to a low-dimensional surrogate model that is used for prediction in the MPC optimization problem [98]. In [99], a robust data-driven MPC scheme based on the Hankel matrix is proposed with guaranteed closed-loop stability and robustness, but it requires a sufficiently large input-output data set which satisfies the persistent excitation condition.

Compared with the above indirect approaches that require sufficient offline calibration data, direct approaches are very suitable for a class of practical scenarios

in which the offline identified models cannot reflect the dynamics of the *in situ* system. For instance, the connections among smart grids change rapidly to respond to the time-varying energy demand [100], and the crowd and fluids flows vary unpredictably with both time and space [101], just to mention a few. Since system dynamics is constantly evolving, these examples necessitate a precise and rapid online model adaptation to accurately capture real-time changes. Relying solely on offline-identified models, without considering real-time variations, nonlinearities, external disturbances, or parameter drift, may lead to degraded system performance and, in extreme cases, result in system instability.

1.2.6 Switched MPC

Switched MPC emerged from the need to address the challenges posed by switched systems, a class of systems characterized by the ability to transition between multiple dynamic modes. One of the earliest works related to switched MPC is the seminal paper by Bemporad and Morari, which addressed control of hybrid systems and laid the foundation for predictive control strategies tailored for switched systems [102].

One of the typical methods to handle this problem is Lyapunov-based switched MPC. This approach leverages a Lyapunov function as a stability criterion while accounting for the mode-switching behavior in predictive control. In [103], the switched MPC problem is examined within the Lyapunov-based MPC framework, assuming a known switching pattern. To ensure the recursive feasibility of the switched MPC algorithm, mode transition constraints are incorporated, and multiple Lyapunov constraints are applied to guarantee the convergence of the system states. In [104], the design of MPC for switched linear systems is formulated as a combinatorial optimization problem. To address stability issues, a regional control law leveraging a piecewise Lyapunov function is investigated.

Time constraints are crucial to switched systems since they dominate the switching frequency and period of the system dwelling at each subsystem, which decides the system stability and control performance. Thus, some research works have been devoted to developing different kinds of MPC methods for switched systems under different types of time constraints.

- For DT switched systems, the switched MPC design is implemented under DT constraints by accounting for all possible truncated switching sequences within the prediction scheme [105].

- The MPC algorithm for switched nonlinear systems under ADT switching signals demonstrates that recursive feasibility and asymptotic stability of the closed-loop system can be ensured if each subsystem has a stabilizing MPC controller and the average dwell-time condition is satisfied [106].
- PDT has been shown to offer greater generality and flexibility as a time constraint compared to dwell-time or average dwell-time. MPC methods leverage this flexibility to solve the co-optimization problem of switched systems while ensuring recursive feasibility and stability under time constraints [107].

1.3 Organization and contributions

Considering the hybrid system and the advanced controller discussed in the literature review, this study explores several key problems, including stabilization analysis, the design of an advanced MPC controller, and its applications in real-world projects. Figure 1.4 illustrates the overall organization of this dissertation, with detailed descriptions of each chapter provided in the following sections.

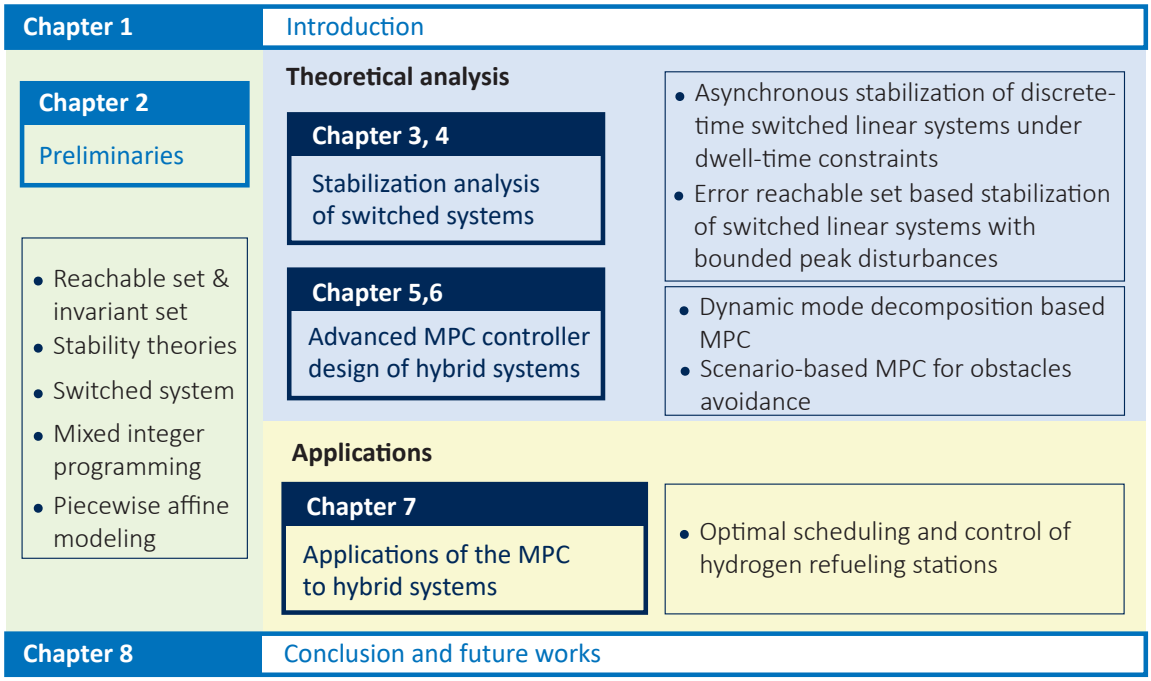

Figure 1.4: The organization of the dissertation.

- **Chapter 2** introduces the notations used in the dissertation and some preliminary results that will be used in the dissertation.

- **Chapter 3**. This chapter investigates the asynchronous stabilization problem for a class of discrete-time switched linear systems under dwell-time constraints. A novel concept called "basic pattern" is proposed to precisely characterize all the admissible sequences of switched systems under asynchronous switching. Compared to existing methods which are devoted to constructing different Lyapunov functions for achieving less conservative stability conditions, here we report a convex stability criteria of asynchronously switched linear systems based on the established basic patterns. The derived stability conditions depend on an integer parameter that can be possibly unbounded to achieve the non-conservativeness. The convex feature of the proposed stability criterion further facilitates the computation of the l_2-gain and H_∞ control problems. Simulation results verify the validity of the derived theories and demonstrate that the proposed control method outperforms several existing approaches reported in the literature.

- **Chapter 4**. This chapter studies the error reachable set based stabilization problem for a class of discrete-time switched linear systems with bounded peak disturbances under PDT constraints. A double-clock-dependent control scheme is proposed to split the disturbed switched system into a nominal system and an error system, and assign to each system a controller scheduled by a clock. A necessary and sufficient convex stability criterion is presented for the nominal system, and is further extended to the stabilization controller design with a nominal clock. In the presence of bounded peak disturbances, another stabilization controller with an error clock is developed for the error system, with the purpose of "minimizing" the reachable set of the error system by the ellipsoidal techniques. It is demonstrated that the disturbed system is also globally exponentially stable in the sense of converging to an over-approximation of the reachable set of the error system, i.e., a union of a family of bounding ellipsoids, that can also be regarded as the cross-section of a tube containing the trajectories of the disturbed system. Simulation studies are provided to verify the effectiveness of the developed results.

- **Chapter 5**. This chapter integrates the dynamic mode decomposition, a

lightweight model identification technique, into data-driven MPC, and presents the analysis of the recursive feasibility and stability. The contributions are three-fold: (1) converting the effect of additive disturbances into multiplicative uncertainties, (2) the calculation of the upper bound on dynamic mode decomposition (DMD) predictor errors, (3) the calculation of the upper bound on DMD predictor errors, and (4) the trimodal control mechanisms to guarantee the closed-loop stability and recursive feasibility.

- **Chapter 6**. This chapter investigates the problem of path planning with obstacle avoidance under stochastic constraints. The contributions are three-fold: (1) formulating the path planning problem with a preferred probability of constraint violation, enabling cost optimization under stochastic conditions, (2) proposing a novel concept of candidate paths to represent all possible combinations of linear constraints, addressing the non-convexity of obstacle constraints, (3) developing a conditional scenario algorithm to transform the non-convex optimization problem into convex sub-problems, making it compatible with the SCMPC framework. Finally, the proposed approach is validated through simulations, demonstrating its effectiveness in ensuring obstacle avoidance and recursive feasibility.

- **Chapter 7**. This chapter illustrates a case study of optimal control for hybrid systems. This case involves the so-called HRS Optimization. In this practical example, we investigate energy-saving strategies for HRS by developing a coordinated control framework to minimize energy consumption during the refueling process.

- **Chapter 8**. This chapter concludes this dissertation and presents future research directions about hybrid system control.

Chapter 2

Preliminaries

In this chapter, we will provide some notations utilized in this dissertation. We will also give some definitions of basic concepts and theories including reachable set and invariant set, stability theories, switched systems, mixed-integer nonlinear programming (MINLP), and piecewise affine (PWA) functions.

2.1 Notations

In this dissertation, $\mathbb{R}$ denotes the dimensional Euclidean space; $\mathbb{R}_+$ denotes the set of non-negative real numbers; $\mathbb{R}^n$ represents the vector space for n-tuples of real numbers; $\mathbb{R}^{n\times m}$ represents the real matrix containing n rows and m columns; $\mathbb{Z}$ denotes the set of integers; $\mathbb{Z}_+$ denotes the set of non-negative integers; $\mathbb{Z}_{\geq t} := \{k \in \mathbb{Z}_+ \mid k \geq t\}$; $\mathbb{Z}[t_1, t_2] := \{k \in \mathbb{Z}_+ | t_1 \leq k \leq t_2\}$.

For a set $\mathcal{P}$, we use $|\mathcal{P}|$ to denote the cardinality. $\mathcal{P}_i$ denotes the ith element, and $\mathcal{P}_{i,j}$ denotes the jth element of $\mathcal{P}_i$. $\bar{\sigma}(\cdot)$ denotes the largest singular values. The l_2-norm of a sequence $\omega \in l_2[0,\infty)$ is denoted by $\|\omega\|_{l_2} := (\sum_{k=0}^{\infty} \omega_k^{\mathrm{T}}\omega_k)^{1/2}$. The set of $n \times n$ symmetric positive definite matrices is denoted by $\mathbb{S}^n_{\succ 0}$.

For a list $\mathcal{A}$, we use $|\mathcal{A}|$ to denote the list length. $\mathcal{A}_i$ denotes the ith element of $\mathcal{A}$, and $\mathcal{A}_{i,j}$ denotes the jth element of list $\mathcal{A}_i, i = 0, 1, \ldots, |\mathcal{A}| - 1$, $j = 0, 1, \ldots, |\mathcal{A}_i| - 1$. A^{T} denotes the transpose of A. $\|x\|_S = d(x, S)$ denotes the distance of a point $x \in \mathbb{R}^{n_x}$ from a set $S \subset \mathbb{R}^{n_x}$ and is defined by $d(x, S) := \inf_{\hat{x}}\{d(x, \hat{x}) \mid \hat{x} \in S\}$, where $d(x, \hat{x})$ denotes the distance between x and $\hat{x}$.

The notation $\|\cdot\|_\infty$ denotes the infinity norm of vectors or matrix. Also, $\|x\|_Q^2$ denotes the shorthand of $x^\top Qx$. $\mathbf{0}$ denotes the vector whose elements are all 0.

The maximization of a vector in a linear programming problem is given as $y_l = \max_{j\in\{1,\dots,m\}} H_l^{(j)} x$. It means an element-wise optimization problem, such that for every lth element of vector y, the maximum solution can be found by the index j.

Moreover, in this dissertation, $\mathbb{E}$ denotes the expectation operator; $\mathcal{U}([\theta_1, \theta_2])$ denotes the uniform distribution on the interval $[\theta_1, \theta_2]$; $\mathcal{N}(\mu, \sigma^2)$ denotes the normal distribution with mean of μ and variance of σ^2.

2.2 Basic concepts

2.2.1 Reachable set and invariant set

Consider an autonomous system in the state-space representation

$$\dot{x}(t) = f(x(t)). \tag{2.1}$$

This system is defined in a proper open set $\mathcal{O} \subseteq \mathbb{R}^n$. Its positive invariance is defined as follows.

Definition 2.1. *(Positive invariance). ([108], Definition 4.1). The set $\mathcal{S} \subseteq \mathcal{O}$ is said to be positive invariant w.r.t. (2.1) if every solution of it with initial condition $x(0) \in \mathcal{S}$ is globally defined and satisfies $x(t) \in \mathcal{S}$ for $t > 0$.*

Definition 2.2. *(Robust positive invariant (RPI)). ([108], Definition 4.3). The set $\mathcal{S} \subseteq \mathcal{X}$ is said to be RPI if, for all $x(0) \in \mathcal{S}$, the solution $x(t) \in \mathcal{S}$ holds for all $t > 0$.*

Definition 2.3. *(Distance from a set). ([108], Definition 4.5). Given a set $\mathcal{S} \subset \mathbb{R}^n$ and a point $y \in \mathbb{R}^n$, the distance is defined as*

$$\operatorname{dist}(y, \mathcal{S}) = \inf_{w\in\mathcal{S}} \|y - w\|_*, \tag{2.2}$$

where $\|\cdot\|_*$ is any relevant norm.

Definition 2.4. *(Positive invariant set). ([108]). The closed set $\mathcal{S}$ is positive invariant, if for all t_0, the condition $x(t_0) \in \mathcal{S}$ implies $x(t) \in \mathcal{S}$ for $t \geq t_0$.*

Consider a discrete-time system

$$x_{k+1} = f(x_k). \tag{2.3}$$

A λ-contractive set is a concept used in control theory and stability analysis, particularly in MPC and invariant set theory. It describes a set of states that contract under a given system's dynamics by a factor λ in each step. The contractive set is defined on the basis of the Minkowski function. Hence, the definition of the Minkowski function (gauge function) and the contractive set $\mathcal{S}$ of a discrete-time system are given as follows.

Definition 2.5. *(Minkowski function). ([109]). A function $\Psi : \mathbb{R}^n \to \mathbb{R}$ is said to be a Minkowski function if the following conditions are satisfied*

(a) $\Psi(x+y) \leq \Psi(x) + \Psi(y)$, *for all* $x, y \in \mathbb{R}^n$,

(b) $\Psi(x) \geq 0, \Psi(x) = 0 \Leftrightarrow x = 0$, *and for* $\mu > 0$, $\Psi(\mu x) = \mu\Psi(x)$.

Definition 2.6. *(Contractive set). ([108]). The set $\mathcal{S}$ is contractive for the system*

$$x_{k+1} = f(x_k, u_k, w_k), \tag{2.4}$$

where disturbance $w \in \mathcal{W}$ and input $u \in \mathcal{U}$, if and only if there exists a control function $u(x) \in \mathcal{U}$ such that, for every $x \in \mathcal{S}$, the following condition holds

$$\Psi_{\mathcal{S}}(f(x, u, w)) \leq \lambda, \quad \text{for all } w \in \mathcal{W},$$

where $\Psi_{\mathcal{S}}(x)$ is the Minkowski function of $\mathcal{S}$, for some $0 \leq \lambda < 1$. In this case, the set $\mathcal{S}$ is said to be λ-contractive.

2.2.2 Stability theories

In this section, some basic definitions of stability theories are briefly summarized to illustrate the following chapters.

Definition 2.7. *($\mathcal{K}, \mathcal{K}_\infty, \mathcal{KL}$, and $\mathcal{PD}$ functions). ([26], Definition B.3).*

- *A function $\alpha : \mathbb{R}_+ \to \mathbb{R}_+$ belongs to class $\mathcal{K}$-function if it is continuous, $\alpha(0) = 0$, and strictly increasing;*
- *A function $\theta : \mathbb{R}_+ \to \mathbb{R}_+$ belongs to class $\mathcal{K}_\infty$-function if it is a class $\mathcal{K}$ and unbounded ($\sigma(s) \to \infty$ as $s \to \infty$);*

- *A function $\beta : \mathbb{R}_+ \times \mathbb{Z}_+ \to \mathbb{R}_+$ belongs to class $\mathcal{KL}$-function if it is continuous and if, for each $t \geq 0, \beta(\cdot, t)$ is a classs $\mathcal{K}$-function and for each $s \geq 0, \beta(s, \cdot)$ is non-increasing and satisfies $\lim_{t\to\infty} \beta(s,t) = 0$;*

- *A function $\gamma : \mathbb{R} \to \mathbb{R}_+$ belongs to a class of positive definite function if it is zero at zero ($\gamma(0) = 0$), and positive everywhere else.*

The definitions of asymptotically stable (AS), globally asymptotically stable (GAS), globally exponentially stable (GES), and globally uniformly exponentially stable (GUES) are given as follows.

Definition 2.8. *(AS). ([26], Definition B.11). Suppose that the set $\mathcal{S}$ is positive invariant and the set $\mathcal{A} \subseteq \mathcal{S}$ is closed, and positive invariant for (2.3). The set $\mathcal{A}$ is asymptotically stable in $\mathcal{S}$ for (2.3) if there exists a $\mathcal{KL}$-function $\beta(\cdot)$ such that, for each $x \in \mathcal{S}$*

$$|\phi(i;x)|_{\mathcal{A}} \leq \beta\left(|x|_{\mathcal{A}}, i\right) \quad \forall i \in \mathbb{Z}_{\geq 0}. \tag{2.5}$$

Definition 2.9. *(GAS). ([26], Definition B.8). The (closed, positive invariant) set $\mathcal{S}$ is GAS for (2.3) if it can satisfy any of the following statements.*

- *It is locally stable and globally attractive.*

- *There exists a $\mathcal{KL}$ function $\beta(\cdot)$ such that, for each $x \in \mathbb{R}^n$*

$$|\phi(i;x)|_{\mathcal{S}} \leq \beta\left(|x|_{\mathcal{S}}, i\right) \quad \forall i \in \mathbb{Z}_{\geq 0}. \tag{2.6}$$

Definition 2.10. *(GES). ([26], Definition B.9). The (closed, positive invariant) set $\mathcal{S}$ is GES for (2.3) if there exists a $c > 0$ and a $\gamma \in (0,1)$ such that $|\phi(i;x)|_{\mathcal{S}} \leq c|x|_{\mathcal{S}}\gamma^i$ for all $x \in \mathbb{R}^n, i \in \mathbb{Z}_{\geq 0}$.*

Definition 2.11. *(GUES). ([110]). The equilibrium $x = 0$ of the system (3.5) is said to be GUES, if there exist positive constants μ and c such that $\|x(k)\| < ce^{-\mu k}\|x(0)\|$ holds for all $\hat{\sigma} \in S_{\text{dwell}}[\tau, \Delta]$ (Definition 2.14), all $x(0) \in \mathbb{R}^{n_x}$, and all $k \in \mathbb{Z}_+$.*

Definition 2.12. *(Lyapunov function). ([26], Definition B.12). Suppose that X is positive invariant and the set $\mathcal{S} \subseteq X$ is closed and positive invariant for (2.3). A function $V : X \to \mathbb{R}_{\geq 0}$ is said to be a Lyapunov function in X for the system (2.3)*

and the set $\mathcal{S}$ if there exist functions $\alpha_1, \alpha_2 \in \mathcal{K}_\infty$, and continuous function $\alpha_3 \in \mathcal{PD}$ such that for any $x \in X$, the following conditions hold:

$$V(x) \geq \alpha_1 \left(|x|_{\mathcal{S}}\right), \tag{2.7a}$$

$$V(x) \leq \alpha_2 \left(|x|_{\mathcal{S}}\right), \tag{2.7b}$$

$$V(f(x)) - V(x) \leq -\alpha_3 \left(|x|_{\mathcal{S}}\right). \tag{2.7c}$$

2.2.3 Swiched systems

A switched system is composed of a finite number of dynamic subsystems and a switching rule to regulate the switching behavior among them. It can model many practical systems with hybrid characteristics, such as electrical devices/circuits, networked control systems, time-delay systems, etc. A general switched system is defined as follows.

Definition 2.13. *(Switched system). ([111]). A switched system is described by a collection of indexed differential (or difference) equations*

$$\dot{x}(t) = f_{\sigma(t)}(x(t), u(t)), x(0) = x_0,$$
$$y(t) = g_{\sigma(t)}(x(t), u(t)),$$

where the input is $u \in \mathbb{R}^m$, $x \in \mathbb{R}^n$ is the continuous state vector, and $\sigma(t) \in \{1, 2, \cdots, M\} \triangleq Q$.

As mentioned in Chapter 1, according to different types of switching mechanisms, switched systems can be classified into state-dependent switching or time-dependent switching, where the latter includes three typical sets of switching signals. These three sets are defined as follows.

Definition 2.14. *(DT). ([112]). The set $S_{\text{dwell}}[\tau]$ is a DT set of switching signals, if any consecutive discontinuities of σ are separated by no less than τ, $\tau \in \mathbb{Z}_+$. The constant τ is called the dwell time.*

Definition 2.15. *(PDT). ([113]). The set $S_{\text{p-dwell}}[\tau, T], \tau > 0, T \in [0, \infty]$ is a PDT signal set, if there is an infinite number of disjoint intervals of length no smaller than τ on which σ is constant, and consecutive intervals with this property are separated by no more than T. The constant τ is called the persistent dwell time, and T is the period of persistence.*

Definition 2.16. *(ADT). ([21]). In the context of switched systems, the ADT set* $S_{a-dwell}[\tau_D, N_0]$ *is defined as:*

$$S_{\text{a-dwell}}[\tau_D, N_0] = \left\{ \sigma(t) \mid N(t) \leq N_0 + \frac{t}{\tau_D}, \quad \forall t \geq 0 \right\},$$

where

- $S_{a-dwell}[\tau_D, N_0]$ *is the set of all admissible switching signals under the given average dwell time condition.*
- $N(t)$ *represents the total number of switches up to time* t*.*
- N_0 *is a fixed nonnegative constant, ensuring that a limited number of switches can occur even in small time intervals.*
- τ_D *is the average dwell time, ensuring that on average, each subsystem remains active for at least* τ_D *before switching.*

It is seen that PDT set is more general than DT and ADT sets because $S_{\text{dwell}}[\tau] = S_{\text{a-dwell}}[\tau, 1] = S_{\text{p-dwell}}[\tau, 0]$. For any switching signal $\sigma \in S_{\text{a-dwell}}[\tau_D, N_0]$, it holds that $\sigma \in S_{\text{p-dwell}}[\delta\tau_D, \delta\tau_D(N_0 - \delta)/(1 - \delta)]$, $\delta \in (0, 1)$.

2.2.4 Basic concepts of MPC algorithm

In Chapter 1, we present a literature review of MPC, and in the following chapters, we will apply and develop MPC schemes to handle the posted control problems with practical constraints. Here, we introduce some basic ideas of MPC algorithm.

Classical MPC. In the following, we review and introduce a classical MPC framework with quadratic cost function and linear constraints in the discrete-time domain. Consider a class of discrete-time linear time-invariant (LTI) systems in the state-space form:

$$x_{k+1} = Ax_k + Bu_k, \tag{2.8}$$

where $x_k \in \mathbb{R}^{n_x}$ and $u_k \in \mathbb{R}^{n_u}$are the system state, input, and output, respectively. The k is the discrete-time instant, taking values in the set of non-negative integers $\{0, 1, 2, \ldots\}$. The state x_k of the system is assumed to be measurable and made available to the controller at each sampling instant. The matrices A and B are the system dynamics matrices.

Suppose that the controlled system in (2.8) is subject to linear constraints. These constraints may involve both states and inputs restrictions and are commonly formulated as the following set of linear inequalities:

$$Fx_k + Gu_k \leq \mathbf{1}, \tag{2.9}$$

where $F \in \mathbb{R}^{n_C \times n_x}$, $G \in \mathbb{R}^{n_C \times n_u}$ and the inequality applies elementwise. The n_C denotes the dimensions of state and input constraints and $\mathbf{1}$ denotes the unit vector. The cost function in the quadratic form is often given as follows:

$$J(x_0, \{u_0, u_1, \dots\}) := \sum_{k=0}^{\infty} (\|x_k\|_Q^2 + \|u_k\|_R^2),$$

where the matrix Q is a symmetric positive definite matrix and the R is a symmetric positive semi-definite matrix, playing roles as weighting matrices of system states and inputs, respectively. The pair (A, B) is assumed to be stabilizable and the pair (A, Q) is observable. The reason for the requirement of stabilization is that classical MPC needs a state-feedback control gain K to stabilize the system, and the reason for the requirement of observability is that valid states must be contained in the cost function of the quadratic term $x_k^{\mathrm{T}} Q x_k$ in classical MPC. As a result, the optimal solution of the cost function is a control sequence $\{u(0), u(1), \dots\}$ of infinite length and what we need to do is to solve the following minimization problem:

$$J^*(x_k) := \min_{\{u_k, u_{k+1}, u_{k+2}, \dots\}} J(x_k, \{u_k, u_{k+1}, u_{k+2}, \dots\}). \tag{2.10}$$

The optimization problem in (2.10) is unsolvable due to the infinite dimensions of decision variables. The dual-mode MPC framework then proposed by H. Michalska and D. Q. Mayne in [114] can turn it into a finite-dimensional problem, and explicitly ensure system stability by switching to a precomputed stabilizing control law once the system reaches a terminal region. This paradigm separates the prediction horizon into two parts: $[k, k+N)$ and $[k+N, \infty)$. Then, the cost function in (2.10) can be rewritten as:

$$J(x_k, u_k) := \sum_{i=0}^{N-1} \left(\|x_{i|k}\|_Q^2 + \|u_{i|k}\|_R^2 \right) + \|x_{N|k}\|_W^2, \tag{2.11}$$

where W is the solution of the Riccati equation

$$W = A^{\mathrm{T}}WA + Q - A^{\mathrm{T}}WB(B^{\mathrm{T}}WB + R)^{-1}B^{\mathrm{T}}WA, \tag{2.12}$$

and the control input u_k is solved online.

Tube-based RMPC. Consider a class of discrete-time linear systems with additive disturbance in the form of:

$$\begin{aligned} x_{k+1} &= Ax_k + Bu_k + w_k, \\ x_k &\in \mathcal{X}, u_k \in \mathcal{U}, \end{aligned} \tag{2.13}$$

where $x_k \in \mathbb{R}^{n_x}$ and $u_k \in \mathbb{R}^{n_u}$ are system state and control input, and $w_k \in \mathcal{W} \subseteq \mathbb{R}^{n_x}$ is external disturbance [73].

Suppose that there exists a state feedback gain $K \in \mathbb{R}^{n_u \times n_x}$ such that $A_K := A + BK$ is stable. A set Z is defined as a disturbance invariant set for the closed-loop system $x_{k+1} = A_K x_k + \omega_k$. Then, it holds that:

$$A_K Z \oplus W \subseteq Z,$$

where $\oplus$ represents the Minkowski set addition. Due to the invariant property, the set Z often serves as the terminal set for the disturbed system, i.e., the optimization problem in RMPC additionally involves the following terminal constraints:

$$x_{N|k} \in Z \subseteq \mathcal{X},$$

which actually enforces that the predicted state at the last step on the prediction horizon enters the disturbance invariant set. Therefore, the state trajectory will always stay in the disturbance invariant set and no longer move outside, under the control of MPC control input supplemented by the state-feedback control law. Note that state constraint would not be violated because

$$x_{k+1} = A_K x_k + \omega_k \in A_K Z \oplus W \subseteq Z.$$

This tube plays the key role in guaranteeing the recursive feasibility and further the system stability (since $x_{N|k} \in Z$ holds at time k, it follows $x_{N-1|k+1} \in Z$ which ensures the convergence).

2.2.5 Singular value decomposition (SVD)

SVD is a powerful linear algebra technique used to analyze and decompose matrices. It is widely employed in various fields, such as data science, machine learning, signal processing, and image compression. SVD provides insights into the structure of a matrix, enabling dimensionality reduction, noise filtering, and the identification of patterns [115].

Definition 2.17. *(Singular value and singular vectors). ([116], chapter 45). Suppose a complex matrix A with m rows and n columns. If σ is a nonnegative scalar, and $\mathbf{u} \in \mathbb{R}^m$ and $\mathbf{v} \in \mathbb{R}^n$ are non-zero vectors, respectively, such that*

$$A\mathbf{v} = \sigma\mathbf{u} \quad \text{and} \quad A^*\mathbf{u} = \sigma\mathbf{v},$$

*then σ is a **singular value** of A, and $\mathbf{u}$ and $\mathbf{v}$ are corresponding left and right **singular vectors**, respectively.*

This definition indicates the relationship between the matrix with a singular value and a singular vector. Then, a matrix can be decomposed by its singular values and singular vectors.

Theorem 2.1. *([115], Chapter 4) Suppose a complex matrix A which has m rows and n columns with right singular vectors $\mathbf{v}_1, \mathbf{v}_2, \ldots, \mathbf{v_r}$, right singular vectors $\mathbf{u}_1, \mathbf{u}_2, \ldots, \mathbf{u_r}$, and corresponding singular values $\sigma_1, \sigma_2, \ldots, \sigma_r$. Then*

$$A = \sum_{i=1}^{r} \sigma_i \mathbf{u_i} \mathbf{v_i}^{\mathrm{T}}. \tag{2.14}$$

As a result, from the view of the matrix, another definition is given.

Definition 2.18. *(SVD) ([116], chapter 45). Suppose a complex matrix A which has m rows and n columns, the matrix product $U\Sigma V^*$ is a SVD for the matrix A if*

- *U and V, respectively, have orthonormal columns,*
- *Σ has nonnegative elements on its principal diagonal and zeros elsewhere,*
- *$A = U\Sigma V^*$.*

Let p and q be the number of rows and columns of Σ, where U is $m \times p, p \leq m$, and V is $n \times q, q \leq n$. If $p = q = r$, the matrix Σ is square. This form is called **reduced SVD** and denoted by $\hat{U}\hat{\Sigma}\hat{V}^*$.

2.2.6 Dynamic mode decomposition (DMD)

The Koopman operator is a mathematical framework that provides a linear perspective on nonlinear dynamic systems. It is an infinite-dimensional linear operator that acts on functions of the system state, rather than on the state variables themselves directly. This shift in perspective enables the use of powerful linear analysis tools to study nonlinear dynamics. Figure 2.1 shows the idea of the mapping of the Koopman operator [117].

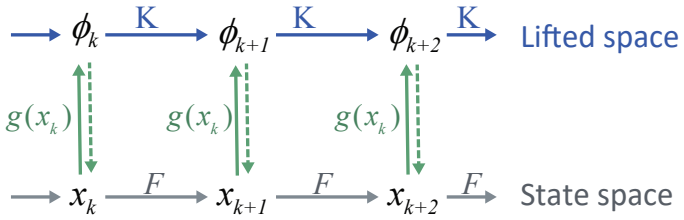

Figure 2.1: Projection mapping of the Koopman operator.

Inspired by the Koopman operator, a lightweight data-driven model identification technique called DMD is developed for characterizing system dynamics into a linear form in real time [118]. The essential idea therein is to use online measured input-output data to regress a linear mapping. This method has been applied to handle the fluid dynamic problem, such as the helium jet system [119]. Compared to other indirect approaches, DMD has a very concise algorithmic framework that is appropriate to time-sensitive applications, and is capable of performing dimensionality reduction of high-dimensional systems with sparse data [120].

Due to these features, some works have been conducted to integrate the DMD with the data-driven MPC for complex dynamic systems, leading to the development of DMD-based MPC (DMD-MPC). For example, researchers implemented the DMD-MPC to control the hydraulic fracturing system which is of high nonlinearity and high dimensions [121]. The DMD-MPC has also been utilized to operate the two-dimensional thermal diffusion systems and residential heating systems [122, 123] whose dynamics are of pretty high dimensions. Moreover, an extended DMD (EDMD) approach is proposed as an efficient method for approximating the eigenvalues and modes of the Koopman operator, enabling a linear representation of the system dynamics [124]. In [125], the authors design the EDMD algorithm to approximate the Koopman operator and demonstrate the convergence of the algorithm, then use the MPC approach to optimize the system performance.

2.2.7 Mixed-integer nonlinear programming (MINLP)

MINLP is a crucial type of problem in the fields of mathematical optimization and operations research. This problem involves both continuous and integer variables, with objective functions or constraints that include nonlinear expressions.

Within the spectrum of optimization problems, MINLP is considered one of the more complex categories because it combines elements of both integer decision-making (as seen in mixed-integer linear programming) and nonlinear relationships (as seen in nonlinear programming). This complexity allows it to model more realistic scenarios where both discrete choices and nonlinear dynamics are present. MINLP problems are complex due to their hybrid nature of variable types and the presence of nonlinear dynamics, making them challenging yet essential for handling real-world problems that require nuanced solutions across various disciplines.

MINLP is a general modeling form in optimization including nonlinear programming (NLP) and mixed-integer linear programming as subproblems.

Definition 2.19. *(MINLP). ([126], Chapter 1). The general form of the MINLP is defined as*

$$\begin{cases} \underset{x}{\text{minimize}} & f(x,y), \\ \text{subject to} & c(x,y) \leq 0, \\ & x \in X, \\ & y \in \mathbb{Z}, \end{cases} \tag{2.15}$$

where $f : \mathbb{R}^n \to \mathbb{R}$ and $c : \mathbb{R}^n \to \mathbb{R}^m$ are twice continuously differential functions, $x \in X \subseteq \mathbb{R}^n$ are continuous variables with constraints, and $y \in \mathbb{Z}$ are integer variables.

The problem (2.15) is an NP-hard combinatorial problem that is hard to find the optimal solution, especially when the dimension of states is high. However, many control problems contain integer control inputs and are actually an MINLP problem.

Chapter 3

Asynchronous stabilization of discrete-time switched linear systems under dwell-time constraints

This chapter investigates the asynchronous stabilization problem for discrete-time switched linear systems under dwell-time constraints. In this chapter, a novel "basic pattern" concept is introduced to characterize the system. It is further adopted to establish a non-conservative convex stability criterion for the addressed system under a linear state feedback controller with adaptive feedback gain design. Comparative simulation results show the advantages of the proposed method over existing methods.

3.1 Introduction

In engineering practice, a switched systemevitably needs some time to identify the activated mode or start the corresponding controller, resulting in the undesirable time lag between system modes switching and controllers switching. This phenomenon is called "asynchronous switching". For instance, the scheduling of controllers under asynchronous switching can introduce a noticeable delay which may lead to a collision in the teleoperation [127]; other examples involving the asynchronous switching in mechanical or chemical systems can be found in [128, 129]. It is underscored that although the asynchronous switching exists in many switched systems, some of them

can be neglected when the dwell-times are far larger than asynchronous durations: The performance degradation is insignificant in this case. Thus, the interest of this work focuses on the case where the two-time scales are in the same order.

Some results have been reported on the stability analisys of synchronously switched systems [130–135]. Recently, graph-based approaches are increasingly utilized for stability analysis of switched systems in continuous-time and discrete-time domains. For instance, in [132], admissible switching paths are characterized in a graph, and finite-path dependent Lyapunov function is accordingly established for uniformly exponential stability. In [133], the authors reformulate a switched system as a graph, and then propose a set of graph-based stability conditions for dwell-time switching systems. In [134], a novel Lyapunov function for continuous-time switched systems is presented, and the sufficient stability conditions in the dwell-time setting are also derived based on the path-completed graph framework. Its generality is further proved by re-stating seminal works [133, 135].

On the other hand, the asynchronous stabilization problem of switched systems has attracted considerable research attention [136–142]. To mention a few, in [136], the authors point out the conservatism of constant-gain controllers. This inspires researchers to explore new formalisms for Lyapunov functions and controllers that are better suited to handling asynchronous features. In [137], the authors propose a class of Lyapunov functions that increase in the asynchronous intervals and decrease in the synchronous intervals. However, the derived stability criterion is conservative and only the weighted l_2-gain can be obtained; yet, the weighted form cannot meet practical requirements. To solve the open problem of determining a non-weighted l_2-gain [138], a dwell-time dependent Lyapunov function (DTDLF) is constructed in [139] which facilitates the asynchronous control and a non-weighted l_2-gain of the closed-loop system. However, the obtained stability conditions can only provide sufficiency. In [140], a quasi-time dependent Lyapunov function (QTDLF) is established to achieve a non-weighted l_2-gain by extracting the weighted coefficients. In [141], another novel Lyapunov function is established in the continuous-time domain to fit the asynchronous feature. A non-weighted l_2-gain is also obtained by using the coefficients extraction technique. However, one possible drawback of the coefficients extracting technique lies in that, the introduction of tuning parameters makes the achieved noise attenuation level very sensitive to these parameters. Moreover, as analyzed in [143], the derived stability conditions cannot guarantee the necessity. In view of this, an important question arises: How to develop a non-conservative sta-

bility criterion of asynchronously switched systems under dwell-time constraints, and the criterion preserves convex features for achieving a non-weighted l_2-gain?

To tackle this problem, we adapt the formalism of the graph-based [132–135] and virtual-clock approaches [144] to the asynchronously switched systems subject to dwell-time constraints. We present a novel conception called "basic pattern" which involves all the possible combinations of system modes and scheduled controllers under the asynchronous switching. For any concerned asynchronous conditions, we provide a method to construct a finite number of basic patterns and make post-concatenation rules for a precise characterization. Upon this idea, we propose a convex stability criterion for the closed-loop asynchronously switched linear system the discrete-time domain. The derived stability conditions depend on an integer parameter that can be possibly unbounded to reach the non-conservativeness. Moreover, a non-weighted l_2-gain of the closed-loop system can be guaranteed by extending the derived stability criterion to the disturbed systems.

3.2 Problem formulation

Consider a class of discrete-time switched linear systems:

$$x_{k+1} = A_{\sigma(k)}x_k + B_{\sigma(k)}u_k, \tag{3.1}$$

where $x_k \in \mathbb{R}^{n_x}$ denotes the system state, $u_k \in \mathbb{R}^m$ denotes the control input, $A_{\sigma(k)} \in \mathbb{R}^{n_x \times n_x}$ and $B_{\sigma(k)} \in \mathbb{R}^{n_x \times m}$ dictate the system dynamics at the kth sampling instant, $k \in \mathbb{Z}_+$, $\sigma(k) : \mathbb{Z}_+ \to \mathcal{I}_N := \mathbb{Z}[1, N]$ indicates the activated subsystem among N possible modes. Let $k_0, k_1, \ldots, k_s, \ldots$ be the switching instants, $s \in \mathbb{Z}_+$ and $x_0 \in \mathbb{R}^{n_x}$ be the initial state. Without loss of generality, we fix $k_0 = 0$ in this work for simplicity.

According to Definition 2.14, the admissible switching signals satisfy the inequalities $k_{s+1} - k_s \geq \tau$, $\forall s \in \mathbb{Z}_+$. Under the asynchronous switching, the switched system may not detect the activated subsystem or start the matched controller in time, undesirably resulting in the unmatched closed-loop systems. Let Δ_s be the asynchronous duration for the sth switching, $\Delta_s \in \mathbb{Z}_+$. We assume that Δ is bounded by $\Delta_s \leq \Delta < \tau$, which means that there must exist a synchronous interval for each switching. The assumption of $\Delta < \tau$ is reasonable; otherwise, the system may always be equipped with unmatched controllers. If $\Delta = 0$, then the switching is synchronous.

Inspired by [136, 140], we can assign $\tau + 1$ controller gains to each subsystem

for reducing the conservatism induced by the constant controller gains due to the dwell-time constraint:

$$u_k = K_{\sigma(k)}\left(\varphi(k)\right) x_k, k \in [k_s, k_{s+1}), s \in \mathbb{Z}_+, \tag{3.2}$$

where $\varphi(k)$ is a gain scheduler online calculated by

$$\varphi(k) = \begin{cases} k - k_s, & k \in [k_s, k_s + \tau) \\ \tau, & k \in [k_s + \tau, k_{s+1}) \end{cases}. \tag{3.3}$$

Under the asynchronous switching, $\sigma(k)$ and $\varphi(k)$ may be incorrectly calculated as $\tilde{\sigma}\left(k\right) = \sigma\left(k - \Delta_s\right)$ and

$$\tilde{\varphi}(k) = \begin{cases} \tau, & k \in \left[k_s, \bar{k}_s\right) \\ k - k_s, & k \in \left[\bar{k}_s, k_s + \tau\right) \\ \tau, & k \in [k_s + \tau, k_{s+1}) \end{cases}, \tag{3.4}$$

where $\bar{k}_s := k_s + \Delta_s$ denotes the end time of the asynchronous interval for the sth switching. However, the control input can always be considered proportional to the state at each sampling instant with a time-varying gain; hence, the closed-loop system can be written as

$$x_{k+1} = G_{\hat{\sigma}(k)} x_k, \tag{3.5}$$

where $G_{\hat{\sigma}(k)} \in \mathbb{R}^{n_x \times n_x}$ dictates the system dynamics, and $\hat{\sigma}$ denotes a new switching signal which is determined by τ and Δ. Let $S_{\text{p-dwell}}[\tau, \Delta]$ be the set of admissible switching signals $\hat{\sigma}$.

Fig. 3.1 shows an example to illustrate the relation between $\sigma \in S_{\text{p-dwell}}[\tau]$ and $\hat{\sigma} \in S_{\text{p-dwell}}[\tau, \Delta]$. In the interval $[k_s, k_{s+1})$, σ maintains a constant value but $\hat{\sigma}$ switches τ times since $G_{\hat{\sigma}(k)}$ evolves as $A_{\sigma(k)} + B_{\sigma(k)} K_{\sigma(k)}(\varphi(k))$, $\varphi(k) \in \mathbb{Z}[0, \tau]$. In the interval $[k_{s+1}, \bar{k}_{s+1})$, $G_{\hat{\sigma}(k)}$ is fixed to $A_{\sigma(k)} + B_{\sigma(k)} K_{\sigma(k_{s-1})}(\tau)$: no switching occurs but the closed-loop system may be unstable due to the controller mismatch. The switching recovers to be synchronous after $\bar{k}_{s+1}$.

Based on the above observations, we find out that the switching signal $\hat{\sigma}$ involves fast-switching intervals $[k_s, k_s + \tau) \cup [\bar{k}_{s+1}, k_{s+1} + \tau)$, unstable non-switching intervals $[k_{s+1}, \bar{k}_{s+1})$, and stable non-switching intervals $[k_s + \tau, k_{s+1}) \cup [k_{s+1} + \tau, k_{s+2})$, $s \in \mathbb{Z}_+$. This finding eliminates the need for subjectively constructing Lyapunov functions for stability analysis, as seen in previous literature. Instead, it motivates us to first

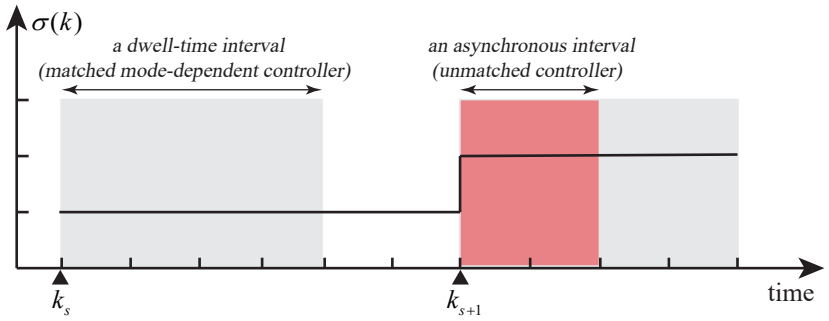

(a) The $\sigma(k)$ changes at the switching instant k_s.

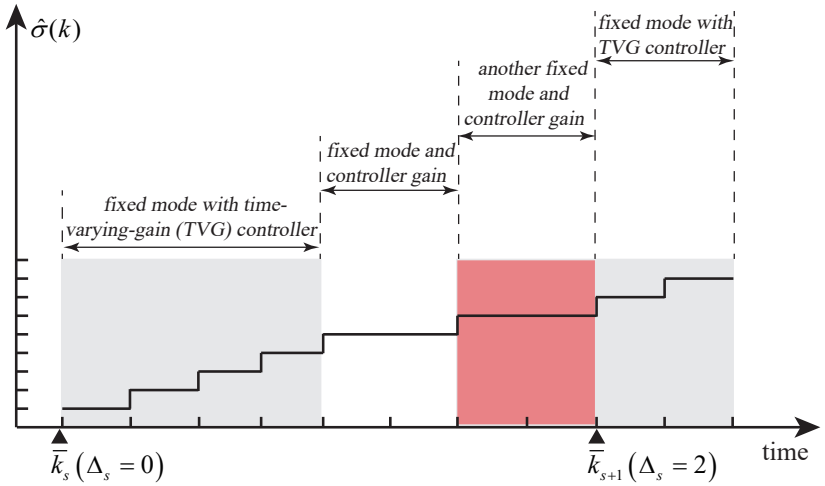

(b) The $\hat{\sigma}(k)$ varies when either $\sigma(k)$ or the controller gain changes.

Figure 3.1: An example illustrating the relation between $\sigma \in S_{\text{p-dwell}}[4]$ and $\hat{\sigma} \in S_{\text{p-dwell}}[4,3]$. k_s is the sth switching instant, and $\bar{k}_s$ is the instant when the system recovers to be synchronous. The Δ_s denotes the duration of the sth asynchronous interval.

develop a non-conservative stability criterion for the system (3.5) and subsequently extend it to address asynchronous stabilization.

3.3 Stability analysis

To list all the admissible switching signals $\hat{\sigma}$ in the interval $[k_s, k_{s+1})$, $s \in \mathbb{Z}_+$, we introduce a notation of $\{i, j, p\}$ to represent a "pattern" where i denotes the activated subsystemdex, j denotes the subsystemdex whose controller is practically used under the asynchronous switching, and p denotes the practical values of $\varphi(k)$. Then, we extract several basic patterns of the asynchronous switching (i.e., possible combinations of subsystems and controllers in $G_{\hat{\sigma}(k)}$) and make the post-concatenation rules

Table 3.1: Three classes of basic patterns that can construct any admissible switching signal $\hat{\sigma}$ under post-concatenation rules.

classes	basic patterns
asynchronous	$\underbrace{\{i,j,\tau\},\ldots,\{i,j,\tau\}}_{\text{of length } l},\{i,i,l\},\ldots,\{i,i,\tau-1\},$ $l\in\mathbb{Z}[1,\Delta], i,j\in\mathbb{Z}[1,N], i\neq j$
synchronous	$\{i,i,0\},\{i,i,1\},\ldots,\{i,i,\tau-1\},\ i\in\mathbb{Z}[1,N]$
free	$\{i,i,\tau\},\ i\in\mathbb{Z}[1,N]$

for a precise characterization of $\hat{\sigma}$.

A total of three classes of basic patterns are captured, as listed in Table I. The corresponding constrained switching rules are also reformulated as an automaton in Fig. 3.2, where each node denotes a class of patterns and the path between two nodes implies conditional connections. In [145], the authors present a novel W-path-dependent lifting technique that can merge nodes in an automaton so as to update the automation which follows the same switching rule but with new nodes. Inspired by this, we perform the W-path-dependent lifting technique to the automaton in Fig. 3.2 and define by $\mathcal{P}_W[\tau,\Delta]$ the set of all new admissible patterns. This operation makes each lifted node contain W initial nodes. In particular, $\mathcal{P}_W[\tau,0]$ is a set of admissible patterns under the synchronous switching. Let us clarify definitions of the following symbols which are crucial for understanding Theorem 3.1 before further proceeding.

- $\mathcal{P}_i$: the ith pattern in $\mathcal{P}_W[\tau,\Delta]$, $i\in\mathcal{I}_{\mathcal{P}}:=\mathbb{Z}[0,|\mathcal{P}_W[\tau,\Delta]|-1]$.
- $\mathcal{C}_i$: the index set of the admissible post-concatenation patterns after $\mathcal{P}_i$, $i\in\mathcal{I}_{\mathcal{P}}$.
- $\mathcal{C}_{i,j}$: the jth element in $\mathcal{C}_i$, which is also an index. Thus, $\mathcal{P}_{\mathcal{C}_{i,j}}$ denotes the $\mathcal{C}_{i,j}$th pattern in $\mathcal{P}_W[\tau,\Delta]$, and the sequence $\{\mathcal{P}_i,\mathcal{P}_{\mathcal{C}_{i,j}}\}$ is admissible, $i\in\mathcal{I}_{\mathcal{P}}$, $j\in\mathcal{I}_{\mathcal{C}_i}:=\mathbb{Z}[0,|\mathcal{C}_i|-1]$.
- $\hat{k}_s$: we define by $\hat{k}_0,\hat{k}_1,\ldots,\hat{k}_s,\ldots$ the switching instants of the patterns, $s\in\mathbb{Z}_+$.

Based on the proposed characterization of the asynchronous switching, we are in a position to give the convex stability conditions for the system (3.5) in the following theorem.

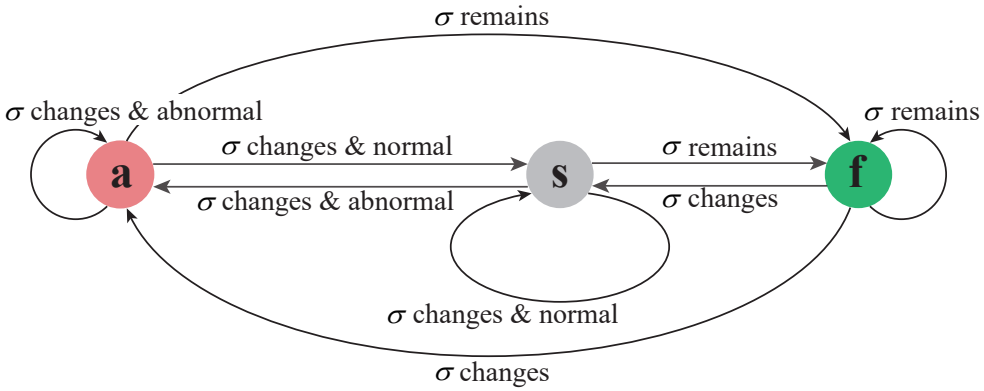

Figure 3.2: An automaton regulating the post-concatenation rules. It has three state sets: "**a**", "**s**", and "**f**" corresponding to asynchronous, synchronous, and free basic patterns. The inputs are the value of $\sigma(k)$ and whether the system is (ab)normal. The "normal" means that there is no mismatch between the activated subsystem and controller, and "abnormal" means that there is a mismatch. The initial state of the automaton is "**s**". The transition conditions among nodes are marked on lines.

Theorem 3.1. *The following statements are equivalent:*

a) The system (3.5) is GUES.

b) There exists a positive integer W*, and a matrix sequence* $L_i\,(t) \in \mathbb{S}^{n_x}_{\succ 0}$*,* $i \in \mathcal{I}_{\mathcal{P}}$*,* $t \in \mathbb{Z}\,[0, |\mathcal{P}_i|]$*, such that*

$$G^T_{\mathcal{P}_{i,t}} L_i\,(t+1)\, G_{\mathcal{P}_{i,t}} - L_i\,(t) \prec 0, \qquad \forall i \in \mathcal{I}_{\mathcal{P}}, \forall t \in \mathbb{Z}\,[0, |\mathcal{P}_i| - 1]\,, \tag{3.6}$$

$$L_{\mathcal{C}_{j,i}}\,(0) - L_j\,(|\mathcal{P}_j|) \prec 0, \forall j \in \mathcal{I}_{\mathcal{P}}, \forall i \in \mathcal{I}_{\mathcal{C}_j}. \tag{3.7}$$

Proof. **Proof of (a)⇒(b).** According to Definition 2.11, if the system (3.5) is GUES, then there must exist positive constants μ and c such that $\|x_k\| < ce^{-\mu(k)}\,\|x\,(0)\|$, $\forall \hat{\sigma} \in S_{\text{p-dwell}}\,[\tau, \Delta]$, $\forall x(0) \in \mathbb{R}^{n_x}$, $\forall k \in \mathbb{Z}_+$.

For any pattern $\mathcal{P}_i$, $i \in \mathcal{I}_{\mathcal{P}}$, we can always select a k such that the pattern sequence in the interval $[0, k)$ goes through W nodes of the automaton, i.e., the sequence of the closed-loop system (3.5) $(G_{\hat{\sigma}(0)}, G_{\hat{\sigma}(k_1)}, \ldots, G_{\hat{\sigma}(k-1)})$ exactly corresponds to the

pattern $\mathcal{P}_i \in \mathcal{P}_W[\tau, \Delta]$. Then we can obtain

$$\begin{aligned}\|x_k\| &= \left\| \prod_{t=0}^{k-1} G_{\hat{\sigma}(t)} x(0) \right\| = \left\| \prod_{t=0}^{|\mathcal{P}_i|-1} G_{\mathcal{P}_{i,t}} x(0) \right\| \\ &< c e^{-\mu(k)} \|x(0)\| = c e^{-\mu|\mathcal{P}_i|} \|x(0)\|.\end{aligned}$$

Increasing W which also implicitly increases k and $|\mathcal{P}_i|$, $i \in \mathcal{I}_{\mathcal{P}}$, we can get

$$\lim_{W\to\infty} \left\| \prod_{t=0}^{|\mathcal{P}_i|-1} G_{\mathcal{P}_{i,t}} x(0) \right\| = 0.$$

This further implies $\lim_{W\to\infty} \prod_{t=0}^{|\mathcal{P}_i|-1} G_{\mathcal{P}_{i,t}} = 0$, $\forall i \in \mathcal{I}_{\mathcal{P}}$. Then, for any arbitrarily selected $L_j(|\mathcal{P}_j|) \in \mathbb{S}^{n_x}_{\succ 0}$, $j \in \mathcal{I}_{\mathcal{P}}$, and any $\mathcal{P}_{\mathcal{C}_{j,i}}$, $i \in \mathcal{I}_{\mathcal{C}_j}$, it holds that

$$\begin{aligned}\lim_{W\to\infty} &\left(\prod_{t=0}^{|\mathcal{P}_i|-1} G_{\mathcal{P}_{i,t}} \right)^{\mathrm{T}} L_{C_{j,i}}\left(|\mathcal{P}_{C_{j,i}}|\right) \\ &\times \left(\prod_{t=0}^{|\mathcal{P}_i|-1} G_{\mathcal{P}_{i,t}} \right) - L_j(|\mathcal{P}_j|) \prec 0.\end{aligned}$$

Hence, for any arbitrarily chosen scalar $\epsilon > 0$, there exists a positive integer W^* such that for any integer $W > W^*$, $j \in \mathcal{I}_{\mathcal{P}}$, and $i \in \mathcal{I}_{\mathcal{C}_j}$, the following inequality holds

$$\begin{aligned}\left(\prod_{t=0}^{|\mathcal{P}_i|-1} G_{\mathcal{P}_{i,t}} \right)^{\mathrm{T}} &L_{C_{j,i}}\left(|\mathcal{P}_{C_{j,i}}|\right) \left(\prod_{t=0}^{|\mathcal{P}_i|-1} G_{\mathcal{P}_{i,t}} \right) \\ &- L_j(|\mathcal{P}_j|) \prec -\epsilon I. \end{aligned} \tag{3.8}$$

The rest of the proof is to transform the conditions in (3.8) to the conditions in (3.6) and (3.7) by applying the lifting technique proposed in [146].

Selecting a matrix sequence $R_i(t) \succ 0$, $i \in \mathcal{I}_{\mathcal{P}}$, $t \in \mathbb{Z}[0, |\mathcal{P}_i| - 1]$, we can define $L_i(t)$ by $L_i(t) := R_i(t) + G^{\mathrm{T}}_{\mathcal{P}_{i,t}} L_i(t+1) G_{\mathcal{P}_{i,t}}$. This definition inherently ensures the

conditions in (3.6). By basic algebraic operations, we can get

$$L_{\mathcal{C}_{j,i}}(0) = \left(\prod_{t=0}^{|\mathcal{P}_i|-1} G_{\mathcal{P}_{i,t}}\right)^{\mathrm{T}} L_{C_{j,i}}(|\mathcal{P}_{C_{j,i}}|)\left(\prod_{t=0}^{|\mathcal{P}_i|-1} G_{\mathcal{P}_{i,t}}\right) + \sum_{k=0}^{|\mathcal{P}_i|-1}\left(\prod_{t=0}^{k-1} G_{\mathcal{P}_{i,t}}\right)^{\mathrm{T}} R_i(k)\left(\prod_{t=0}^{k-1} G_{\mathcal{P}_{i,t}}\right). \tag{3.9}$$

Substituting (3.9) to (3.8), we can obtain

$$\begin{aligned} &L_{\mathcal{C}_{j,i}}(0) - L_j(|\mathcal{P}_j|) \\ &\prec -\epsilon I + \sum_{k=0}^{|\mathcal{P}_i|-1}\left(\prod_{t=0}^{k-1} G_{\mathcal{P}_{i,t}}\right)^{\mathrm{T}} R_i(k)\left(\prod_{t=0}^{k-1} G_{\mathcal{P}_{i,t}}\right). \end{aligned}$$

The second term on the right hand side of the above inequality can be sufficiently small by adjusting the matrix sequence $R_i(k)$, which further guarantees the conditions in (3.7).

Proof of (b)⇒(a). Due to the existence of the matrix sequence $L_j\ (t) \in \mathbb{S}^{n_x}_{\succ 0}$, $j \in \mathcal{I}_{\mathcal{P}}$, $t \in \mathbb{Z}[0, |\mathcal{P}_j|]$, we can establish the Lyapunov function for the system (3.5) by:

$$V_j(x_k) = x^{\mathrm{T}}(k) L_j(k - \hat{k}_s) x_k, k \in [\hat{k}_s, \hat{k}_{s+1}) \tag{3.10}$$

with $j \in \mathcal{I}_{\mathcal{P}}$, i.e., the Lyapunov function changes with the activated pattern in $\mathcal{P}_W[\tau, \Delta]$ and the activation time of the pattern. Let $\Delta V_j(x_k) := V_j(x_{k+1}) - V_j(x_k)$, $k \in [\hat{k}_s, \hat{k}_{s+1} - 1)$, $s \in \mathbb{Z}_+$, be the difference of the Lyapunov function between consecutive sampling instants inside certain patterns of $\mathcal{P}_W[\tau, \Delta]$. The conditions in (3.6) ensure

$$\begin{aligned} \Delta V_j(x_k) &= x^{\mathrm{T}}(k) G^{\mathrm{T}}_{\mathcal{P}_{j,k-\hat{k}_s}} L_j(k - \hat{k}_s + 1) G_{\mathcal{P}_{j,k-\hat{k}_s}} x_k \\ &\quad - x^{\mathrm{T}}(k) L_j(k - \hat{k}_s) x_k \\ &= x^{\mathrm{T}}(k) \left[G^{\mathrm{T}}_{\mathcal{P}_{j,t}} L_j(t+1) G_{\mathcal{P}_{j,t}} - L_j(t)\right] x_k \\ &< -\lambda_1 \|x_k\|^2 < 0 \end{aligned} \tag{3.11}$$

for $t \in \mathbb{Z}\left[0, |\mathcal{P}_j| - 2\right]$ and

$$\begin{aligned} & G^{\mathrm{T}}_{\mathcal{P}_{j,\hat{k}_{s+1}-\hat{k}_s-1}} L_j\left(p+1\right) G_{\mathcal{P}_{j,\hat{k}_{s+1}-\hat{k}_s-1}} - L_j\left(p\right) \\ = & G^{\mathrm{T}}_{\mathcal{P}_{j,\left|\mathcal{P}_j\right|-1}} L_j\left(|\mathcal{P}_j|\right) G_{\mathcal{P}_{j,\left|\mathcal{P}_j\right|-1}} - L_j\left(|\mathcal{P}_j| - 1\right) \prec 0 \end{aligned}$$

for $t = |\mathcal{P}_j| - 1$, $\forall j \in \mathcal{I}_{\mathcal{P}}$, where $p = \hat{k}_{s+1} - \hat{k}_s - 1$ and λ_1 can be selected such that

$$\begin{aligned} 0 < \lambda_1 < \max\{\bar{\sigma}\left(G^{\mathrm{T}}_{\mathcal{P}_{j,t}} L_j\left(t+1\right) G_{\mathcal{P}_{j,t}} - L_j\left(t\right)\right) \\ |j \in \mathcal{I}_{\mathcal{P}}, t \in [0, |\mathcal{P}_j| - 1)\}. \end{aligned}$$

Together with the conditions in (3.7), we can get

$$G^{\mathrm{T}}_{\mathcal{P}_{j,\left|\mathcal{P}_j\right|-1}} L_{\mathcal{C}_{j,i}}\left(0\right) G_{\mathcal{P}_{j,\left|\mathcal{P}_j\right|-1}} - L_j\left(|\mathcal{P}_j| - 1\right) \prec 0,$$

which further indicates

$$\Delta V_{j,i}\left(x_k\right) < -\lambda_2 \left\|x_k\right\|^2 \tag{3.12}$$

by letting $\Delta V_{j,i}(x_k) := V_{\mathcal{C}_{j,i}}(x_{k+1}) - V_j(x_k)$, $k = \hat{k}_{s+1} - 1$, $s \in \mathbb{Z}_+$, $i \in \mathcal{I}_{\mathcal{C}_j}$, where λ_2 can be selected such that

$$\begin{aligned} 0 < \lambda_2 < \max\Big\{\bar{\sigma}\Big(G^{\mathrm{T}}_{\mathcal{P}_{j,\left|\mathcal{P}_j\right|-1}} L_{\mathcal{C}_{j,i}}\left(0\right) G_{\mathcal{P}_{j,\left|\mathcal{P}_j\right|-1}} \\ -L_j\left(|\mathcal{P}_j| - 1\right) | j \in \mathcal{I}_{\mathcal{P}}, i \in \mathcal{I}_{\mathcal{C}_j}\Big\}. \end{aligned}$$

According to (3.10), we know

$$\rho_{\min} \left\|x_k\right\|^2 \leq V_j\left(x_k\right) \leq \rho_{\max} \left\|x_k\right\|^2, \tag{3.13}$$

where $\rho_{\min} := \min\left\{\sigma\left(L_j\left(t\right)\right) | \, j \in \mathcal{I}_{\mathcal{P}}, t \in \mathbb{Z}\left[0, |\mathcal{P}_j|\right)\right\}$ and
$\rho_{\max} := \max\left\{\bar{\sigma}\left(L_j\left(t\right)\right) | \, j \in \mathcal{I}_{\mathcal{P}}, t \in \mathbb{Z}\left[0, |\mathcal{P}_j|\right)\right\}$.

From (3.11)-(3.13), we can get $\left\|x_k\right\| \leq c e^{-\mu(k)} \left\|x\left(0\right)\right\|$ where $c = \sqrt{\frac{\rho_{\max}}{\rho_{\min}}}$, $\mu = \ln\left(1 - \frac{\lambda}{\rho_{\max}}\right)^{-\frac{1}{2}}$, and $\lambda := \min\{\lambda_1, \lambda_2, \lambda_\rho \rho_{\max}\}$, $0 < \lambda_\rho < 1$. □

Remark 3.1. *Compared to the DTDLF [139] and QTDLF methods [140, 141], Theorem 3.1 presents a stability criterion without requiring tuning parameters any more. The derived stability conditions depend on an integer parameter that can be possibly*

unbounded to reach the non-conservativeness. It also shows how we adapt graph-based approaches [145, 147] to fit asynchronous switching cases. Moreover, the convex feature of the derived conditions also facilitates extensions to the l_2-gain computation and the H_∞ control problems.

Remark 3.2. *To obtain the stability criterion under the synchronous switching, one can remove the asynchronous patterns in Table I and the node "$\boldsymbol{a}$" in Fig. 3.2. Then, Theorem 3.1 also fits the synchronous dwell-time switching and arbitrary switching by setting $\Delta = 0$ and $\tau = 1, \Delta = 0$, respectively.*

Remark 3.3. *The potential drawback of Theorem 3.1 is that the non-conservativeness is achieved by generating basic patterns of the concerned asynchronous conditions which, however, are based on a possibly unbounded positive integer W not known* a priori. *Our future work will focus on developing a numerical method to estimate W.*

Remark 3.4. *To tackle issues induced by asynchronous switching, here we make two major technical adaptations relative to [144], including the new rules for scheduling controller gains, and the basic pattern-based characterization for asynchronous switching cases.*

Table 3.2: Computational complexity of statement (b) in Theorem 3.1. $M := |\mathcal{P}_W[\tau, \Delta]| - 1$.

Statement	Number of variables	Size of LMIs
b)	$\frac{n(n+1)}{2}\sum_{i=0}^{M}(\lvert\mathcal{P}_i\rvert + 1)$	$n\sum_{i=0}^{M}(\lvert\mathcal{P}_i\rvert + \lvert\mathcal{C}_i\rvert)$

Remark 3.5. *The computational complexity of the statement b) in Theorem 3.1 is shown in Table 3.2. It is seen that the values of M, $|\mathcal{P}_i|$, and $|\mathcal{C}_i|$ are all corresponding to the number of basic patterns established in Table 3.1, which are positively correlated to τ and Δ, leading to a higher cost due to the lifting technique. This is actually the price we must pay for preserving the convexity with respect to the system data.*

3.4 Asynchronous stabilization

In this section, we extend the proposed convex stability criterion to the l_2-gain computation and H_∞ control problems for the following discrete-time switched linear

system:

$$x_{k+1} = A_{\sigma(k)}x_k + B_{\sigma(k)}u_k + E_{\sigma(k)}\omega_k, \tag{3.14a}$$

$$y_k = C_{\sigma(k)}x_k + D_{\sigma(k)}u_k + F_{\sigma(k)}\omega_k, \tag{3.14b}$$

where $u_k \in \mathbb{R}^{n_u}$ and $y_k \in \mathbb{R}^{n_y}$ are the systemput and output, $\omega_k \in \mathbb{R}^{n_\omega}$ is the exogenous noise, and $\omega \in l_2[0,\infty)$. The matrices $E_{\sigma(k)}$, $C_{\sigma(k)}$, $D_{\sigma(k)}$, $F_{\sigma(k)}$, are constant with appropriate dimensions. Equipped with the controller in (3.2), the system (3.14) can be reformulated to the following closed-loop form

$$x_{k+1} = G_{\hat{\sigma}(k)}x_k + E_{\sigma(k)}\omega_k, \tag{3.15a}$$

$$y_k = H_{\hat{\sigma}(k)}x_k + F_{\sigma(k)}\omega_k, \tag{3.15b}$$

where $\hat{\sigma} \in S_{\text{p-dwell}}[\tau,\Delta]$, $\sigma \in S_{\text{p-dwell}}[\tau]$, and $H_{\hat{\sigma}(k)} \in \mathbb{R}^{n_y\times n_x}$ dictates the output dynamics.

As in Fig. 3.1, a certain σ may be extended to multiple $\hat{\sigma}$ due to uncertain values of Δ_s; however, a certain $\hat{\sigma}$ corresponds to only one σ. Hence, for the ith pattern $\mathcal{P}_i \in \mathcal{P}_W[\tau,\Delta]$, we define $\mathcal{Q}^1_{i,t}$, $\mathcal{Q}^2_{i,t}$, and $\mathcal{Q}^3_{i,t}$ as the first, second, and third tuple of the tth term in the ith pattern in Table 3.1. For instance, $\mathcal{Q}^1_{i,t}$ and $\mathcal{Q}^2_{i,t}$ can be used to access the tth real subsystem or misconceived subsystem (induced by asynchronous switching) in the ith pattern; $\mathcal{Q}^3_{i,t}$ can be used to get the value of the scheduler when the ith pattern is activated online.

Definition 3.1. *For a scalar $\gamma > 0$, the system (3.15) is said to be GUES with an l_2 gain, if the system (3.15) is GUES with $\omega_k = 0$, and under the zero initial condition, $\sum_{s=0}^{\infty} y^T(s)y(s) \le \gamma^2 \sum_{s=0}^{\infty} \omega^T(s)\omega(s)$ holds for all $\hat{\sigma}(k) \in S_{p\text{-}dwell}[\tau,\Delta]$ and nonzero $\omega \in l_2[0,\infty)$.*

Theorem 3.2. *Consider the system (3.15) with a dwell-time τ and an upper bound of asynchronous intervals Δ. Suppose that there exists a positive integer W, a matrix sequence $L_i(t) \in \mathbb{S}^{n_x}_{\succ 0}$, $i \in \mathcal{I}_{\mathcal{P}}$, $t \in \mathbb{Z}[0,|\mathcal{P}_i|]$, and a scalar $\gamma > 0$ such that*

$$\Omega(i,t) \prec 0, \forall i \in \mathcal{I}_{\mathcal{P}}, \forall t \in \mathbb{Z}[0,|\mathcal{P}_i|-1], \tag{3.16}$$

$$L_{\mathcal{C}_{j,i}}(0) - L_j(|\mathcal{P}_j|) \prec 0, \forall j \in \mathcal{I}_{\mathcal{P}}, \forall i \in \mathcal{I}_{\mathcal{C}_j}, \tag{3.17}$$

where $\Omega(i,t)$, $i \in \mathcal{I}_{\mathcal{P}}$, $t \in \mathbb{Z}[0, |\mathcal{P}_i| - 1]$ *is defined by*

$$\begin{bmatrix} -L_i(t+1) & 0 & L_i(t+1) G_{\mathcal{P}_{i,t}} & L_i(t+1) E_{\mathcal{Q}^1_{i,t}} \\ \star & -I & H_{\mathcal{P}_{i,t}} & F_{\mathcal{Q}^1_{i,t}} \\ \star & \star & -L_i(t) & 0 \\ \star & \star & \star & -\gamma^2 I \end{bmatrix}.$$

Then the system (3.15) is GUES and has an l_2*-gain* γ.

Proof. First of all, consider $\omega = 0$. The conditions in (3.16)-(3.17) can ensure the conditions in (3.6)-(3.7). By Theorem 3.1, the system (3.15) is GUES.

Next, consider $\omega \neq 0$ and $x(0) = 0$. Let $\xi(k)$ be defined by $[\ x_k^{\mathrm{T}},\ \ \omega_k^{\mathrm{T}}\ ]^{\mathrm{T}}$. For any $k \in [\hat{k}_s, \hat{k}_{s+1})$, the conditions in (3.16) ensure that

$$\begin{aligned} &\xi^{\mathrm{T}}(k)\, \Xi\left(j, k - \hat{k}_s\right) \xi(k) \\ &= \Delta \bar{V}(x_k) + y_k^{\mathrm{T}} y_k - \gamma^2 \omega_k^{\mathrm{T}} \omega_k < 0, \end{aligned} \tag{3.18}$$

where $\Xi(j,t)$ is defined by

$$\begin{bmatrix} \bar{\Omega}(j,t) & G_{\mathcal{P}_{j,t}}^{\mathrm{T}} L_j(t+1) E_{\mathcal{Q}^1_{j,t}} + H_{\mathcal{P}_{j,t}}^{\mathrm{T}} F_{\mathcal{Q}^1_{j,t}} \\ \star & E_{\mathcal{Q}^1_{j,t}}^{\mathrm{T}} L_j(t+1) E_{\mathcal{Q}^1_{j,t}} + F_{\mathcal{Q}^1_{j,t}}^{\mathrm{T}} F_{\mathcal{Q}^1_{j,t}} - \gamma^2 I \end{bmatrix},$$

with $\bar{\Omega}(j,t) = G_{\mathcal{P}_{j,t}}^{\mathrm{T}} L_j(t+1) G_{\mathcal{P}_{j,t}} + H_{\mathcal{P}_{j,t}}^{\mathrm{T}} H_{\mathcal{P}_{j,t}} - L_j(t)$,

$$\begin{aligned} &\Delta \bar{V}(x_k) \\ &:= \begin{cases} V_j(x_{k+1}) - V_j(x_k), & k \in [\hat{k}_s, \hat{k}_{s+1} - 1) \\ \tilde{V}_j(x_{k+1}) - V_j(x_k), & k = \hat{k}_{s+1} - 1 \end{cases} \end{aligned}$$

for any $\hat{\sigma}(\hat{k}_s) = j \in \mathcal{I}_{\mathcal{P}}$, and $\tilde{V}_j(x_{\hat{k}_s})$ is defined by

$$\tilde{V}_j(x_{\hat{k}_s}) := x_{\hat{k}_s}^{\mathrm{T}} L_j(|\mathcal{P}_j|) x_{\hat{k}_s}, j \in \mathcal{I}_{\mathcal{P}}.$$

Consider the switching instants of the patterns, i.e., $k = \hat{k}_s$. The conditions in (3.17) ensure that for any $i \in \mathcal{I}_{\mathcal{C}_j}$, $s \in \mathbb{Z}_+$,

$$\Delta \tilde{V}_j(x_{\hat{k}_s}) := V_{\mathcal{C}_{j,i}}(x_{\hat{k}_s}) - \tilde{V}_j(x_{\hat{k}_s}) < 0. \tag{3.19}$$

Let J be the l_2-gain performance, then we have

$$\begin{aligned} J &= \sum_{k=0}^{\infty} \left(y_k^{\mathrm{T}} y_k - \gamma^2 \omega_k^{\mathrm{T}} \omega_k \right) \\ &= \sum_{s=0}^{\infty} \left(\sum_{k=\hat{k}_s}^{\hat{k}_s - 1} \Gamma(k) + V_{\mathcal{C}_{j,i}}(x_{\hat{k}_s}) - \tilde{V}_j(x_{\hat{k}_{s+1}}) \right) \\ &= \sum_{s=0}^{\infty} \sum_{k=\hat{k}_s}^{\hat{k}_s - 1} \Gamma(k) + \sum_{s=0}^{\infty} \Delta \tilde{V}_j(x_{\hat{k}_{s+1}}), \end{aligned}$$

where

$$\Gamma(k) := \Delta \bar{V}(x_k) + y_k^{\mathrm{T}} y_k - \gamma^2 \omega_k^{\mathrm{T}} \omega_k.$$

Hence, $J < 0$ is guaranteed by $\Gamma(k) < 0$ in (3.18) and $\Delta \tilde{V}_j(x_{\hat{k}_{s+1}}) < 0$ in (3.19). This implies that the l_2-gain performance is obtained. □

Remark 3.6. *As in stability analysis, Theorem 3.2 can also be extended for the synchronous dwell-time switching and arbitrary switching in the discrete-time domain.*

Suppose that $\hat{\sigma}(k) = i \in \mathcal{I}_{\mathcal{P}}$ without loss of generality. The closed-loop system (3.15) can be rewritten to the pattern-dependent form:

$$\begin{aligned} x_{k+1} &= G_{\mathcal{P}_{i,t}} x_k + E_{\mathcal{P}_{i,t}} \omega_k \qquad (3.20a) \\ &= (A_{\mathcal{Q}^1_{i,t}} + B_{\mathcal{Q}^1_{i,t}} K_{\mathcal{Q}^2_{i,t}}(\mathcal{Q}^3_{i,t})) x_k + E_{\mathcal{P}_{i,t}} \omega_k, \\ y_k &= H_{\mathcal{P}_{i,t}} x_k + F_{\mathcal{P}_{i,t}} \omega_k \qquad (3.20b) \\ &= (C_{\mathcal{Q}^1_{i,t}} + D_{\mathcal{Q}^1_{i,t}} K_{\mathcal{Q}^2_{i,t}}(\mathcal{Q}^3_{i,t})) x_k + F_{\mathcal{P}_{i,t}} \omega_k. \end{aligned}$$

These two conditions establish the relationships among the patterns $\mathcal{P}_i \in \mathcal{P}_W[\tau, \Delta]$, $i \in \mathcal{I}_{\mathcal{P}}$, the activated subsystem $A_{\mathcal{Q}^1_{i,t}}$, $B_{\mathcal{Q}^1_{i,t}}$, $C_{\mathcal{Q}^1_{i,t}}$, $D_{\mathcal{Q}^1_{i,t}}$, the index of the subsystem $(\mathcal{Q}^2_{i,t})$ whose controller is practically used under the asynchronous switching, and the practical value of φ $(\mathcal{Q}^3_{i,t})$ when the pattern is activated online. Then, the following theorem is given to facilitate the H_∞ controller design for asynchronous stabilization.

Theorem 3.3. *Consider the system (3.14) with a dwell-time τ and an upper bound of the asynchronous interval Δ. Suppose that there exists a positive integer W, two matrix sequences $X_m(\varphi)$, $U_m(\varphi)$, $m \in \mathcal{I}_N$, $\varphi \in \mathbb{Z}[0, \tau]$, a matrix sequence $M_i(t) \in$*

$\mathbb{S}^{n_x}_{\succ 0}$, $i \in \mathcal{I}_{\mathcal{P}}$, $t \in \mathbb{Z}\left[0, |\mathcal{P}_i|\right]$, *and a scalar* $\gamma > 0$ *such that*

$$\Psi\left(i,t\right) \prec 0, \forall i \in \mathcal{I}_{\mathcal{P}}, \forall t \in \mathbb{Z}\left[0, |\mathcal{P}_i| - 1\right] \tag{3.21}$$

$$M_j\left(|\mathcal{P}_j|\right) - M_{\mathcal{C}_{j,i}}\left(0\right) \prec 0, \forall j \in \mathcal{I}_{\mathcal{P}}, \forall i \in \mathcal{I}_{\mathcal{C}_j}, \tag{3.22}$$

where $\Psi\left(i,t\right)$ *is defined by* $\Psi(i,t) := \begin{bmatrix} \Psi_{11} & \Psi_{12} \\ \star & \Psi_{22} \end{bmatrix}$ *with*

$$\Psi_{11} := \begin{bmatrix} -M_i(t+1) & 0 \\ \star & -I \end{bmatrix},$$

$$\Psi_{12} := \begin{bmatrix} A_{\mathcal{Q}^1_{i,t}} X_{\mathcal{Q}^2_{i,t}}\left(\mathcal{Q}^3_{i,t}\right) + B_{\mathcal{Q}^1_{i,t}} U_{\mathcal{Q}^2_{i,t}}\left(\mathcal{Q}^3_{i,t}\right) & E_{\mathcal{Q}^1_{i,t}} \\ C_{\mathcal{Q}^1_{i,t},t} X_{\mathcal{Q}^2_{i,t}}\left(\mathcal{Q}^3_{i,t}\right) + D_{\mathcal{Q}^1_{i,t}} U_{\mathcal{Q}^2_{i,t}}\left(\mathcal{Q}^3_{i,t}\right) & F_{\mathcal{Q}^1_{i,t}} \end{bmatrix},$$

$$\Psi_{22} := \begin{bmatrix} M_i(t) - X_{\mathcal{Q}^2_{i,t}}\left(\mathcal{Q}^3_{i,t}\right) - X^{\mathrm{T}}_{\mathcal{Q}^2_{i,t}}\left(\mathcal{Q}^3_{i,t}\right) & 0 \\ \star & -\gamma^2 I \end{bmatrix}.$$

Then, the closed-loop system (3.15) is GUES and has an l_2*-gain* γ*. Moreover, if a feasible solution exists, then the admissible controller gains are given by*

$$K_m\left(\varphi\right) = U_m\left(\varphi\right) X_m^{-1}\left(\varphi\right), m \in \mathcal{I}_N, \varphi \in \mathbb{Z}\left[0, \tau\right]. \tag{3.23}$$

Remark 3.7. *Theorem 3.3 presents a method to offline design a group of controller gains for stabilization and noise attenuation. Each subsystem is assigned to* $\tau + 1$ *gains which are scheduled by the gain scheduler in (3.3). The proposed controller can also be reduced to the mode-dependent type or the common gain type by updating* $K_{\sigma(k)}(\varphi(k))$ *in (3.3) to* $K_{\sigma(k)}$ *and* K*, respectively.*

By setting $E_{\mathcal{P}_{i,t}}$ to zero matrix, we can obtain a set of convex conditions for designing stabilizing controllers of the switched system (3.1) based on Theorem 3.3.

Corollary 3.1. *Consider the system (3.1) with a dwell-time* τ*, and an upper bound of asynchronous intervals* Δ*. Suppose that there exists a positive integer* W*, two matrix sequences* $X_m(\varphi)$*,* $U_m(\varphi)$*,* $m \in \mathcal{I}_N$*,* $\varphi \in \mathbb{Z}[0,\tau]$*, a matrix sequence* $M_i(t) \in \mathbb{S}^{n_x}_{\succ 0}$*,*

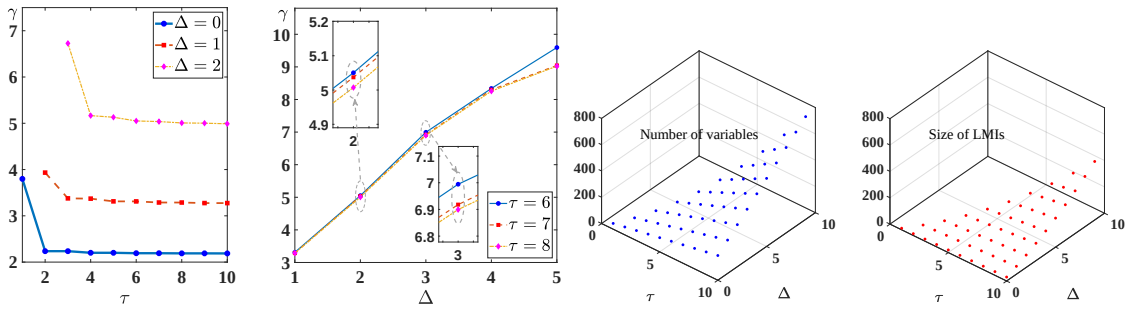

(a) (b) (c) (d)

Figure 3.3: The l_2-induced gains of the closed-loop system with varying asynchronous conditions: (a) The dwell-time τ, (b) The upper bound of the asynchronous interval Δ, and (c)-(d) The computational costs.

$i \in \mathcal{I}_{\mathcal{P}}$, $t \in \mathbb{Z}[0, |\mathcal{P}_i|]$, *such that*

$$\begin{bmatrix} -M_i(t+1) & A_{Q^1_{i,t}} X_{Q^2_{i,t}}\left(Q^3_{i,t}\right) + B_{Q^1_{i,t}} U_{Q^2_{i,t}}\left(Q^3_{i,t}\right) \\ \star & M_i(t) - X_{Q^2_{i,t}}\left(Q^3_{i,t}\right) - X^T_{Q^2_{i,t}}\left(Q^3_{i,t}\right) \end{bmatrix} \prec 0$$

and (3.22) hold. Then, the closed-loop system (3.5) is GUES and the admissible controller gains are given by (3.23).

3.5 Simulation results

In this section, we will use two examples borrowed from the previous literature to illustrate the derived theories, and make comparisons to existing methods.

Example 3.1. *[139] Consider the switched system (3.14) with two subsystems:*

$$A_1 = \begin{bmatrix} 1.08 & 0.39 \\ -0.13 & 0.09 \end{bmatrix}, B_1 = \begin{bmatrix} -0.54 \\ -1.89 \end{bmatrix}, C_1 = \begin{bmatrix} -0.67 & -0.91 \end{bmatrix}, E_1 = \begin{bmatrix} -0.56 \\ 0.18 \end{bmatrix},$$

$$A_2 = \begin{bmatrix} -0.63 & 0.44 \\ -0.56 & -0.95 \end{bmatrix}, B_2 = \begin{bmatrix} -0.11 \\ -1.31 \end{bmatrix}, C_2 = \begin{bmatrix} -0.15 & 0.95 \end{bmatrix}, E_2 = \begin{bmatrix} -0.77 \\ -0.94 \end{bmatrix},$$

$D_1 = 1.55, D_2 = 0.43, F_1 = -1.41, F_2 = -1.91.$

The l_2-gain of the closed-loop system (3.14) varies with the concerned dwell-time τ, the upper bound of the asynchronous intervals Δ, and the positive integer W for paths lifting. In the first example, we will mainly analyze the relationship between

the achieved l_2-gain and these parameters.

Table 3.3: The l_2-induced gains of the closed-loop system with different W.

(Δ, W)	$(1,1)$	$(1,2)$	$(2,1)$	$(2,2)$
γ	3.3772	3.3767	6.7275	6.7216

Applying Theorem 3.3 to Example 3.1 by increasing Δ from 0 (i.e., the synchronous switching) to 2, and setting τ to $\mathbb{Z}[\Delta+1, 10]$, we can obtain the optimal index γ of the l_2-gain performance under different asynchronous conditions, as depicted in Fig. 3.3a. It is seen that γ monotonically decreases as τ increases. This is reasonable since frequent switching among stable subsystems may lower the noise attenuation level and even induce instability [140]. On the other hand, γ increases as Δ increases for fixed dwell-times (Fig. 3.3b), from which we can see that the asynchronous switching significantly degrades the performance of the closed-loop system, and one of the effective solutions is to increase the dwell-time. Here we fix W to 1 in these two trials for a fair comparison. Fig. 3.3c and Fig. 3.3d show the computational cost. We can find out that both the number of variables and size of LMIs increase with the increase of dwell-time τ and the asynchronous time Δ. This is reasonable since the number of basic patterns and the number of controller gains positively correlate with τ and Δ.

In Table 3.3, we compare the l_2-induced gains with different W. The fact that γ decreases as W increases correlates well with the results in [145] where the conservativeness can be significantly reduced by increasing the number of the dependent paths after the lifting operation.

Example 3.2. *[144] Consider the switched system (3.14) with two subsystems:*

$$A_1 = \begin{bmatrix} -0.92 & -0.34 \\ 1.0350 & -0.31 \end{bmatrix}, B_1 = \begin{bmatrix} -0.52 \\ 0.40 \end{bmatrix}, C_1 = \begin{bmatrix} -0.49 & 0.34 \end{bmatrix}, E_1 = \begin{bmatrix} 0.90 \\ 0.97 \end{bmatrix},$$

$$A_2 = \begin{bmatrix} -0.92 & -0.34 \\ 1.0350 & -0.31 \end{bmatrix}, B_2 = \begin{bmatrix} 0.85 \\ 0.05 \end{bmatrix}, C_2 = \begin{bmatrix} 0.67 & -0.42 \end{bmatrix}, E_2 = \begin{bmatrix} 0.06 \\ -0.08 \end{bmatrix},$$

$D_1 = 1.44, D_2 = -0.36, F_1 = F_2 = 0.$

This example is provided for comparisons between the proposed controller and some representative controllers. As verified in [144], this system can be stabilized under arbitrary switching. To show the advantage of the proposed controller, we compute the l_2-induced gains of the closed-loop system (3.15) equipped with the common-

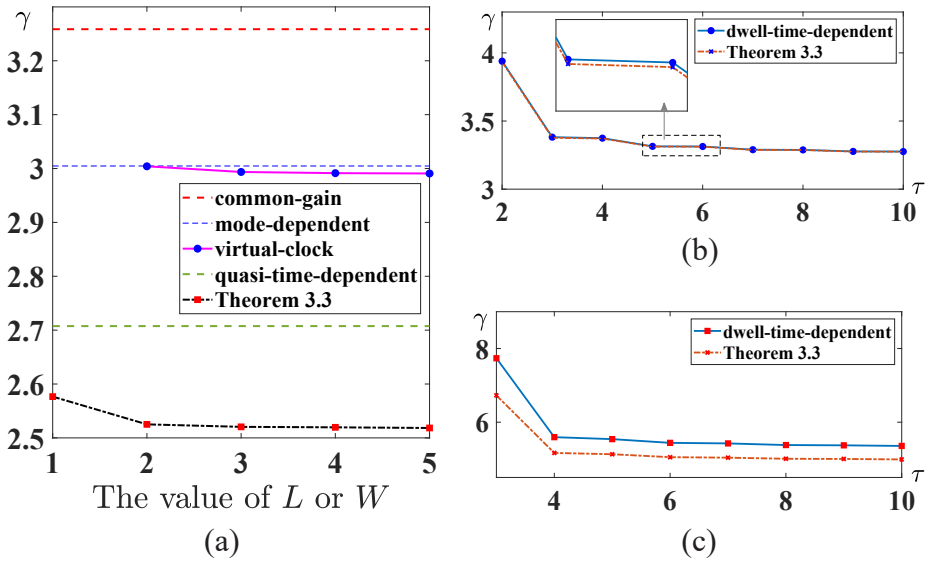

Figure 3.4: Comparisons to representative controllers. (a) The l_2-induced gains of the closed-loop system equipped with the common-gain controller, the mode-dependent controller, the virtual-clock controller, the quasi-time-dependent controller, and the proposed controller in Theorem 3.3. The switching is synchronous. (b)-(c) The l_2-induced gains of the closed-loop system equipped with the dwell-time-dependent controller and the proposed controller. The Δ is set to 1 and 2 in (b) and (c), respectively.

gain controller, the mode-dependent controller, the virtual-clock controller [144], the quasi-time-dependent controller [140], the dwell-time-dependent controller [139], and the proposed controller in Theorem 3.3. The first two controllers are obtained as indicated in Remark 3.7. For the quasi-time-dependent controller, the original controller design conditions in [140] are for the persistent dwell-time switching. Here we set the period of persistence to 0 such that the derived conditions therein also fit the dwell-time switching.

In Fig. 3.4a, we plot the l_2-induced gains under the synchronous switching. We can find out that the proposed controller outperforms the others since it yields the smallest l_2-induced gains. Particularly, it can be seen that the optimal index of the l_2-gain performance decreases as the value of L in the virtual-clock controller and the value of W in the proposed controller increase. This finding is reasonable because a larger L or W corresponds to a more precise characterization of $\hat{\sigma}$. On the other hand, the quasi-time-dependent controller needs users to select two tuning parameters: the decreasing rate $0 < \alpha < 1$ and the jump bound $\mu > 1$. Here, we set α and μ to 0.9940 and 1.0001, respectively, after searching for the best parameters at the step size of

0.0001 in the intervals $0 < \alpha < 1$ and $1 < \mu < 2$. Although the quasi-time-dependent controller achieves the second best performance, parameter tuning is laborious and time-consuming. Fig. 3.4b and Fig. 3.4c compare the l_2-induced gains between the dwell-time-dependent controller and proposed controller in Theorem 3.3 of this work. In both cases, the proposed controller performs better than the dwell-time-dependent controller, and the advantage gets bigger as Δ increases. This is because our method provides a more precise characterization of the closed-loop system, which is further highlighted when the asynchronous switching occurs more frequently.

3.6 Conclusion

In this work, we investigate the asynchronous stabilization problem of switched linear systems under dwell-time constraints. To precisely characterize the possible combinations of system modes and scheduled controllers under the asynchronous switching, we present a conception called "basic pattern", which can be constructed and concatenated for any concerned asynchronous conditions. We also present a convex stability criterion based on the established basic patterns, and the non-conservativeness of the derived stability conditions can be reached depending on an integer parameter that is possibly unbounded. The convex feature of the proposed stability criterion further facilitates the extension to the non-weighted l_2-gain computation and H_∞ controller design. The simulation results demonstrate the advantages of the proposed controller, compared to other representative controllers reported in the previous literature.

Chapter 4

Error reachable set-based stabilization of switched linear systems with bounded peak disturbances

In Chapter 3, the stability of the asynchronous switched system under DT condition is discussed. This chapter studies the error reachable set-based stabilization problem for the switched system with bounded peak disturbances under PDT constraint.

4.1 Introduction

Based on Lyapunov stability theory, a number of effective results have been reported for the stability analysis of the switched systems with those three kinds of switching signals mentioned in Chapter 1 [148]. In [146, 149], an improved method called the lifting technique is presented that can convert the well-known non-convex stability conditions [135] to equivalent convex ones for DT switched systems. This technique further facilitates the study of non-conservative stability criteria for switched systems under DT constraints [144] or even arbitrary switching [150]. Some attempts have also been performed to lift the existing non-convex stability conditions, e.g., [21, 22], for ADT and PDT switched systems to convex conditions, but still fail to achieve the convexification of the conditions due to the complexity and exibility of these two switching signals [151]. Among others, the widely-used quasi-time-dependent (QTD)

technique presents the QTD Lyapunov function approach. Its main idea is to confine the Lyapunov function to descend in the non-switching intervals, and have a bound in the arbitrary-switching intervals. Some tuning parameters are necessary to shape the Lyapunov function. As a result, the QTD technique can only obtain non-convex stability conditions in the form of a bilinear matrix inequality (BMI) which are known to be NP-hard. Some other results about dynamics with PDT switching features also suffer from the nonconvexity [10,152,153]. Till now, to the best of authors' knowledge, necessary and sufficient convex stability conditions for PDT switched linear systems have not been addressed, which motivates the first interest of this work.

As a crucial issue in control discipline, the stabilization problem of systems with disturbances has been broadly investigated [7, 154–157]. For the switched systems under various types of time constraints, lots of significant results are reported for the systems with energy-bounded disturbance [158–160], but relatively seldom for the amplitude-bounded disturbances. Recently, a study on characterizing the robust invariant set for the switched system with bounded additive disturbance under DT constraint has been carried out [161]. This method is further extended to the PDT case for the uniform tube-based stabilization [162]. However, it only presents a method to compute the robust invariant set for PDT switched systems, and the so-called stabilization controller is unreasonably considered the same as the linear quadratic optimal regulator. On the other hand, the reachable set estimation problem for the switched systems has received increasing attention in recent years by the so-called ellipsoidal technique [163–166], which aims to determine a set of ellipsoids tightly containing the concerned reachable set. An important problem therein is to design a controller such that the reachable set of the closed-loop system is over-approximated by some bounding ellipsoids that are as small as possible [167, 168]. However, existing results only cover the cases of switched systems with arbitrary switching and dwell-time switching [166, 168], and the controller synthesis to "minimize" the reachable set approximation for PDT switched systems has not been addressed. Thus, the second interest of this work arises: How to stabilize the PDT switched system with bounded peak disturbances and simultaneously "minimize" the effect caused by the disturbances?

Motivated by the above issues, this work considers the error reachable set-based stabilization problem of switched systems with bounded peak disturbances under PDT constraint. The main contributions of this work are summarized as follows:

- We present a double clock-dependent control scheme for PDT switched systems

by splitting the disturbed switched system into a nominal system and an error system. Each system is assigned a controller scheduled by its own clock.

- We present a necessary and sufficient convex global exponential stability criterion for PDT switched systems, and accordingly design the stabilization controller for the nominal system.
- We present a virtual-sequence-dependent reachable set estimation method, and further design the stabilization controller to minimize the reachable set of the error system by ellipsoidal technique.
- The closed-loop switched systems integrated with the two controllers are proved to be globally exponentially stable in the sense of converging to a set which is also regarded as the cross section of a tube containing the practical trajectories of the disturbed system.

4.2 Problem formulation

Consider a class of discrete-time switched linear systems with bounded peak disturbances:

$$x_{k+1} = A_{\sigma(k)}x_k + B_{\sigma(k)}u_k + D_{\sigma(k)}\omega_k, \tag{4.1}$$

where $x_k \in \mathbb{R}^{n_x}$ and $u_k \in \mathbb{R}^{n_u}$ are the system state and control input, respectively; $\omega_k \in \mathbb{R}^{n_\omega}$ denotes the bounded peak disturbance satisfying:

$$\omega_k^{\mathrm{T}}\omega_k \leq \bar{\omega}^2, k \in \mathbb{Z}_+, \tag{4.2}$$

where $\bar{\omega} > 0$ is a known constant. The switching signal $\sigma(k) : \mathbb{Z}_+ \to \mathcal{I}_N := \{1, 2, \ldots, N\}$ indicates the activated subsystem among N possible modes. The switching instants of subsystem modes are denoted by $k_s, s \in \mathbb{Z}_+$. It should be noted that another kind of disturbances widely discussed in literature is energy-bounded, which has the form of $\sum_{k=0}^{\infty}\omega_k^{\mathrm{T}}\omega_k \leq \bar{\omega}^2$. Compared to energy-bounded disturbances, bounded peak disturbances are a kind of uncertainties that persistently influence the system evolution over time, and they will not degrade with time.

According to Definition 2.15, any admissible PDT switching sequences can be segmented into two kinds of intervals, denoted by τ-portion and T-portion, which correspond to the non-switching intervals and the arbitrary switching intervals [22, 169],

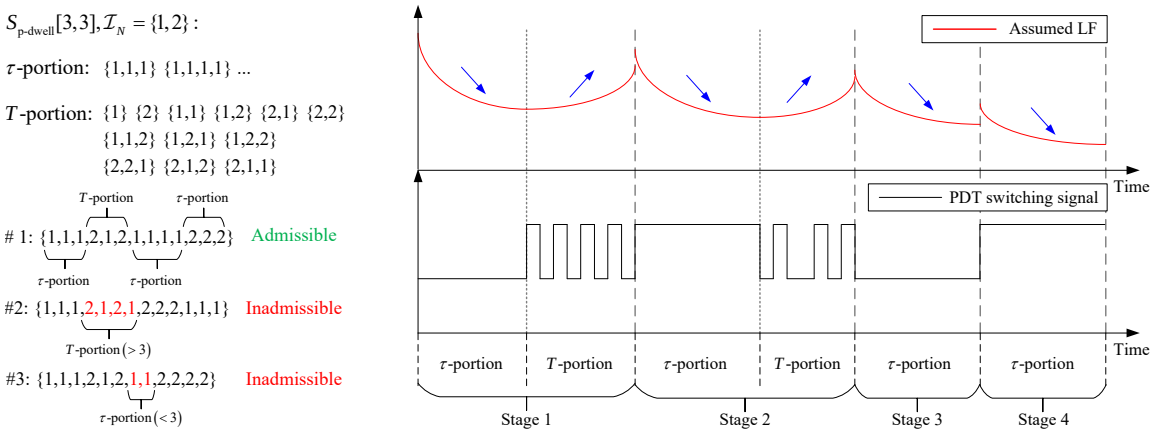

Figure 4.1: Illustration of PDT signal set and the widely-used stage partition framework. (a) τ-portions, T-portions, and three illustrative PDT switching sequences for $S_{\text{p-dwell}}[3,3]$ with $\mathcal{I}_N = \{1,2\}$. (b) Evolution of Lyapunov function in the framework of stage partition. Blue arrows indicate the variation trend of the assumed Lyapunov function.

respectively. For example, consider the PDT signal set $S_{\text{p-dwell}}[3,3]$. Figure 4.1(a) gives three switching sequences, where the first switching sequence is an admissible PDT switching sequence since the running time for each τ-portion is no less than τ, and for each T-portion is no more than T. The other two sequences are inadmissible because they violate the time constraints of T-portion and τ-portion, respectively.

It splits the disturbed system (4.1) into a nominal system and an error system. The nominal system (4.1) is denoted by:

$$z_{k+1} = A_{\sigma(k)} z_k + B_{\sigma(k)} v_k, \tag{4.3}$$

where $z_k \in \mathbb{R}^{n_x}$ and $v_k \in \mathbb{R}^{n_u}$ are the nominal system state and control input, respectively; $A_{\sigma(k)} \in \mathbb{R}^{n_x \times n_x}$ and $B_{\sigma(k)} \in \mathbb{R}^{n_x \times m}$ dictate the system dynamics at the kth sampling instant, $k \in \mathbb{Z}_+$, $\sigma(k) : \mathbb{Z}_+ \to \mathcal{I}_N := \mathbb{Z}[1,N]$ indicates the activated subsystem among N possible modes. Define the system error $e_k = x_k - z_k$, then by (4.1) and (4.3) we can obtain the error system dynamics of the disturbed system (4.1) in form of:

$$\begin{aligned} e_{k+1} &= A_{\sigma(k)} e_k + B_{\sigma(k)}(u_k - v_k) + D_{\sigma(k)} \omega_k, \\ e_0 &= x_0 - z_0 = 0. \end{aligned} \tag{4.4}$$

The main idea of the tube-based MPC is to control the trajectory of the nominal system (4.3) to converge to the origin by optimizing v_k at each sampling instant, and keep the trajectory of the error system (4.4) within a robust positive invariant set. However, in this work, the concept of the invariant set is not suitable because:

- The invariant set requires all trajectories originating from the set always stay within the set, but in fact, the initial state of the error system (4.4) is $e_0 = 0$, so the invariant set contains unnecessary initial states.
- Generally, the invariant set is iteratively generated with a given controller gain, and the synthesis problem still yet remains open: How to design a controller such that the invariant set of the switched system is as "small" as possible under certain switching signals?

For the purpose of "minimizing" the effect of ω_k in the system(4.1), we replace the invariant set by the reachable set of the error system (4.4), which is defined by:

$$\mathcal{R}_e := \{e_k \in \mathbb{R}^{n_x} \mid e_k, e_0 \text{ satisfy } (4.4), k \in \mathbb{Z}_+\}, \tag{4.5}$$

and employ ellipsoidal techniques to estimate the reachable set [6, 7]. The estimated reachable set $\hat{\mathcal{R}}_e$ satisfies $\mathcal{R}_e \subseteq \hat{\mathcal{R}}_e$, and is denoted by a union of some bounding ellipsoids in form of:

$$\mathcal{E}(P) := \left\{e_k \in \mathbb{R}^{n_x} \mid e_k^{\mathrm{T}} P e_k \leq 1, P \in \mathbb{S}^{n_x}_{\succ 0}\right\}. \tag{4.6}$$

The main advantages of using ellipsoidal techniques are three-fold: 1)The attenuation of bounded peak disturbances can be achieved by minimizing the reachable set via an optimization-based approach, which is mathematically tractable, 2) By embedding our non-conservative stability conditions in Theorem 4.1, the reachable set can be further minimized compared to other existing methods, and 3) By introducing the virtual-sequence-dependent control scheme, operations on the error system do not affect the nominal system.

In the framework of double clock-dependent control scheme, we use the following

controllers for the systems in (4.1), (4.3), and (4.4):

$$u_k = v_k + g_k, \tag{4.7}$$

$$v_k = F_{\sigma(k)}\left(\theta_z(k)\right) z_k, \tag{4.8}$$

$$g_k = K_{\sigma(k)}\left(\theta_e(k)\right) e_k, \tag{4.9}$$

where $F_{\sigma(k)}\left(\theta_z(k)\right)$ and $K_{\sigma(k)}\left(\theta_e(k)\right)$ are the controller gains for the nominal system (4.3) and the error system (4.4), respectively. $\theta_z(k)$ and $\theta_e(k)$ are online scheduled controller clocks which can be simply calculated by

$$\theta_z(k) = \begin{cases} k - k_s, & k \in [k_s, k_s + \tau_z) \\ \tau_z, & k \in [k_s + \tau_z, k_{s+1}) \end{cases}, \tag{4.10}$$

and

$$\theta_e(k) = \begin{cases} k - k_s, & k \in [k_s, k_s + \tau_e) \\ \tau_e, & k \in [k_s + \tau_e, k_{s+1}) \end{cases}, \tag{4.11}$$

where τ_z and τ_e denote persistent dwell time to ensure the stability of the system (4.3), and minimize the reachable set of the system (4.4), respectively.

Definition 4.1. *The equilibrium $z = 0$ of the system (4.3) is said to be GES with a decay rate $\mu > 0$ if $\|z_k\| \leq ce^{-\mu(k-k_0)} \|z_{k_0}\|$ holds for any initial condition $z_{k_0} \in \mathbb{R}^{n_x}$, any $k \geq k_0$ and a constant $c > 0$.*

Consider the composite system (4.1) and (4.3) with the composite state (x_k, z_k) [51]. Define its norm by $\|(x_k, z_k)\| := \|x_k\| + \|z_k\|$.

Definition 4.2. *A set $\mathcal{R}$ is said to be GES for the composite system (4.1) and(4.3) with a decay rate $\mu > 0$, if $\|(x_k, z_k)\|_{\mathcal{R}} \leq ce^{-\mu(k-k_0)} \|(x_{k_0}, z_{k_0})\|_{\mathcal{R}}$ for any composite initial state (x_{k_0}, z_{k_0}), any $k \geq k_0$ and a constant $c > 0$.*

Then, for a given period of persistence T, the objectives of this work are:

- Design the controller gains $F_{\sigma(k)}\left(\theta_z(k)\right)$ in (4.8) with minimal τ_z such that the closed-loop nominal system is GES.
- Design the controller gains $K_{\sigma(k)}\left(\theta_e(k)\right)$ in (4.9) with minimal τ_e such that the reachable set $\mathcal{R}_e$ bounded by $\hat{\mathcal{R}}_e$ is as small as possible.
- Determine a set $\mathcal{R}$ and admissible switching signal sets for the closed-loop composite system (4.1) and (4.3) such that it is GES in the sense of Definition 4.2.

4.3 Switching sequence list with admissible concatenation list

Existing results about PDT switched systems are based on the same framework, named "stage partition" [10, 22, 152, 153, 160, 169]. In this framework, PDT switching sequences are segmented to stages, and each stage consists of a τ-portion, or a τ-portion followed by a T-portion. The Lyapunov function under this framework is required to satisfy the following conditions:

- decreases in the τ-portion;
- has a bound in the T-portion;
- decreases at the starting instant of each stage.

Figure 4.1b illustrates the evolution of the Lyapunov function under the framework of the stage partition. Some tuning parameters, like the descending rate α and jump bound μ, have to be introduced to ensure the associated Lyapunov function satisfies the above conditions and thus to guarantee the closed-loop stability.s, which yields that no matter what stability analysis or control synthesis is in the form of BMIs. The main reason lies in that the stage partition may generate uncertain intervals, e.g., τ-portion contains an infinite number of switching sequences, and the finite switching sequences in the T-portion are not fully used under this framework. To solve this problem and obtain non-conservative convex stability conditions, we need to develop a novel approach that can represent the infinite number of admissible PDT switching sequences by a finite number of certain switching subsequences. To address this, some novel concepts are given as follows.

Definition 4.3. *A switching sequence list* $\mathcal{A} := \{\mathcal{A}_0, \mathcal{A}_1, \ldots, \mathcal{A}_{M-1}\}$ *is a list that consists of* M *certain switching subsequences,* $M \in \mathbb{Z}_{\geq 1}$. *The concatenation list* $\mathcal{C} := \{\mathcal{C}_0, \mathcal{C}_1, \ldots, \mathcal{C}_{M-1}\}$ *of* $\mathcal{A}$ *is a list where* $\mathcal{C}_i$ *is an index list that consists of all the indices of admissible elements in* $\mathcal{A}$*, which can follow* $\mathcal{A}_i, i \in \mathbb{Z}_{[0,M-1]}$. *Here, "admissible" means that the switching sequence* $\{\mathcal{A}_i, \mathcal{A}_j\}, j \in \mathcal{C}_i$ *is an admissible PDT switching sequence.*

Example 4.1. *Consider a PDT signal set* $S_{\text{p-dwell}}[2, 1]$ *with* $\mathcal{I}_N = \{1, 2\}$. *We can construct a switching sequence list* $\mathcal{A} = \{\mathcal{A}_0, \mathcal{A}_1\} = \{\{1, 1, 1\}, \{2, 1\}\}$, *and assume its concatenation list* $\mathcal{C}$ *as* $\mathcal{C} = \{\mathcal{C}_0, \mathcal{C}_1\} = \{\{0, 1\}, \{0, 1\}\}$.

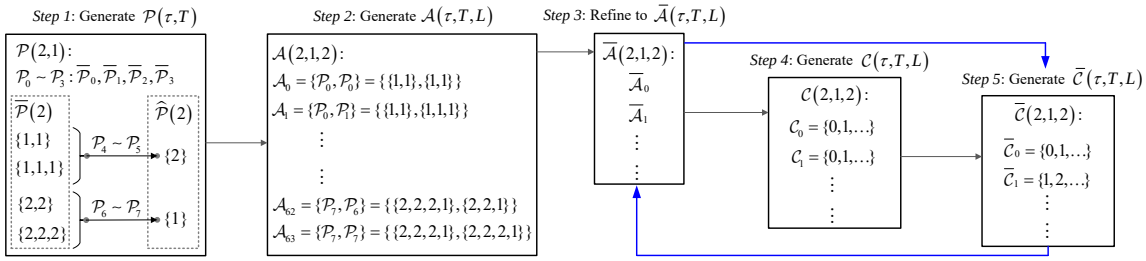

Figure 4.2: Procedures of generating switching sequence list and its concatenation list for a given PDT signal set $S_{\text{p-dwell}}[\tau, T]$.

Definition 4.4. *A PDT signal set $S_{\text{p-dwell}}[\tau, T]$ is said to be equivalent to a switching sequence list $\mathcal{A}$ with its concatenation list $\mathcal{C}$, if it follows:*

- *Any admissible PDT switching sequence can be denoted by concatenations of elements in $\mathcal{A}$ with $\mathcal{C}$, e.g., $\{\mathcal{A}_i, \mathcal{A}_j, \mathcal{A}_k, \ldots\}$, where $j \in \mathcal{C}_i, k \in \mathcal{C}_j, \forall \mathcal{A}_i \in \mathcal{A}$.*
- *Any element of $\mathcal{A}$ with concatenation list $\mathcal{C}$, denoted by $\{\mathcal{A}_i, \mathcal{A}_j, \mathcal{A}_k, \ldots\}$, can generate an admissible PDT switching sequence, where $j \in \mathcal{C}_i, k \in \mathcal{C}_j, \forall \mathcal{A}_i \in \mathcal{A}$.*
- *If $\mathcal{A}_i \in \mathcal{A}$, then $\mathcal{A}_j \in \mathcal{A}, \forall j \in \mathcal{C}_i, \forall i \in \mathbb{Z}_{[0,|\mathcal{A}|-1]}$.*
- *"$\mathcal{A}$ with $\mathcal{C}$ " means that any concatenations of elements in $\mathcal{A}$ comply with the concatenation list $\mathcal{C}$.*

In Example 4.1, it can be checked that the switching sequence list $\mathcal{A}$ with its concatenation list $\mathcal{C}$ is not equivalent to $S_{\text{p-dwell}}[2,1]$ because: i) $\{2,2,1\}$ is an admissible PDT switching sequence but cannot be denoted by $\mathcal{A}$ with $\mathcal{C}$, ii) $\{\mathcal{A}_1, \mathcal{A}_1\} = \{\{2,1\},\{2,1\}\}$ is a switching sequence generated by $\mathcal{A}$ with $\mathcal{C}$ (because $1 \in \mathcal{C}_1$), but it is not an admissible PDT switching sequence due to the violation of constraints in the T-portion. Thus, a problem to be addressed in this section arises: How to construct a switching sequence list $\mathcal{A}$ with its concatenation list $\mathcal{C}$ that is equivalent to a given PDT signal set $S_{\text{p-dwell}}[\tau, T]$? If this problem can be solved, then we can only focus on a finite number of certain switching subsequences for further convex conditions about stability analysis and control synthesis.

Next, we will give a detailed procedures of generating $\mathcal{A}$ with $\mathcal{C}$ (equivalent to $S_{\text{p-dwell}}[\tau, T]$) by the following five steps. Figure 4.2 summarizes the process.

Step 1: We first give the concept of PDT primary sequence list, denoted by $\mathcal{P}(\tau, T)$, for a given $S_{\text{p-dwell}}[\tau, T]$. To represent all admissible sequences in τ-portion,

we define a sequence list $\bar{\mathcal{P}}(\tau) := \left\{\bar{\mathcal{P}}_0, \ldots, \bar{\mathcal{P}}_{N\tau-1}\right\}$ which is composed of sequences $\{i, i, \ldots, i\}$ with length of $\mathbb{Z}_{[\tau,2\tau-1]}, i \in \mathcal{I}_N$. It can be easily checked that any admissible τ-portion sequences can be constructed by concatenating elements in $\bar{\mathcal{P}}(\tau)$. Moreover, we define a sequence list $\hat{P}(T) := \left\{\hat{P}_0, \hat{P}_1, \ldots, \hat{P}_T\right\}$ which contains all admissible sequences in T-portion. The "admissible" here indicates the length of $\hat{\mathcal{P}}_j, j \in \mathbb{Z}_{[0,T]}$, is no more than T, and the length of consecutive same subsystem modes in $\hat{\mathcal{P}}_j$ is less than τ. Then, the PDT primary sequence list is defined as $\mathcal{P}(\tau, T) := \{\mathcal{P}_0, \mathcal{P}_1, \ldots, \mathcal{P}_{M-1}\}$ where elements from $\mathcal{P}_0$ to $\mathcal{P}_{N\tau-1}$ are same to $\bar{\mathcal{P}}(\tau)$ elements, and each element from $\mathcal{P}_{N\tau}$ to $\mathcal{P}_{M-1}$ is constructed by one element in $\bar{\mathcal{P}}(\tau)$ (denoted by $\bar{\mathcal{P}}_i$) followed by one element in $\hat{\mathcal{P}}(T)$ (denoted by $\hat{\mathcal{P}}_j$), and the subsystem mode in $\bar{\mathcal{P}}_i$ is different with the first mode in the concatenated $\hat{\mathcal{P}}_j$. Figure 4.2 also gives an example of PDT primary sequences for $S_{\text{p-dwell}}[2, 1]$. It can be checked that $S_{\text{p-dwell}}[2, 1]$ is equivalent to $\mathcal{P}(2, 1)$ with the concatenation list $\mathcal{C} = \{\mathcal{C}_0, \mathcal{C}_1, \ldots, \mathcal{C}_7\}$ where $\mathcal{C}_i = \{0, 1, \ldots, 7\}, i \in \mathbb{Z}_{[0,7]}$.

Step 2: Define $\mathcal{A}(\tau, T, L) := \{\mathcal{A}_0, \ldots, \mathcal{A}_{M^L-1}\}$ as the augmented PDT primary sequence list, which contains all possible combinations of $L\mathcal{P}(\tau, T)$ elements. Figure 4.2 shows the augmentation operation from $\mathcal{P}(2, 1)$ to $\mathcal{A}(2, 1, 2)$ by illustratively letting $L = 2$. It is concluded that $S_{\text{p-dwell}}[2, 1]$ is also equivalent to $\mathcal{A}(2, 1, 2)$ with the concatenation list $\mathcal{C} = \{\mathcal{C}_0, \mathcal{C}_1, \ldots, \mathcal{C}_{63}\}$ where $\mathcal{C}_i = \{0, 1, \ldots, 63\}, i \in \mathbb{Z}_{[0,63]}$.

Step 3: Note that $\mathcal{A}(\tau, T, L)$ may contain some same elements (for example, $\mathcal{A}_1 = \{\mathcal{P}_0, \mathcal{P}_1\}$ is same to $\mathcal{A}_9 = \{\mathcal{P}_1, \mathcal{P}_0\}$). Thus, we define $\bar{\mathcal{A}}(\tau, T, L)$ as the refined PDT sequence list, which is generated by removing the redundant same elements in $\mathcal{A}(\tau, T, L)$. The equivalence between $S_{\text{p-dwell}}[2, 1]$ and $\bar{\mathcal{A}}(2, 1, 2)$ with the concatenation list $\mathcal{C} = \left\{\mathcal{C}_0, \mathcal{C}_1, \ldots, \mathcal{C}_{|\bar{\mathcal{A}}(2,1,2)|-1}\right\}$ is also guaranteed, where $\mathcal{C}_i = \{0, 1, \ldots, |\bar{\mathcal{A}}(2, 1, 2)| - 1\}, i \in \mathcal{I}_L := \mathbb{Z}_{[0,|\bar{\mathcal{A}}(2,1,2)|-1]}$.

Step 4: Although Step 3 generates equivalent $\bar{\mathcal{A}}(\tau, T, L)$ with $\mathcal{C}$ to $S_{\text{p-dwell}}[\tau, T]$, there may exist different concatenations corresponding to same switching sequences. For example, there may exist a case of $\left\{\bar{\mathcal{A}}_{i_1}, \bar{\mathcal{A}}_{j_1}\right\} = \left\{\bar{\mathcal{A}}_{i_2}, \bar{\mathcal{A}}_{j_2}\right\}$ where $i_1, i_2 \in \mathcal{I}_L, j_1 \in \mathcal{C}_{i_1}, j_2 \in \mathcal{C}_{i_2}$. To simplify the concatenations lists, we only maintain the concatenations as the following cases (here we denote the concatenation in form of $\left\{\bar{\mathcal{A}}_i, \bar{\mathcal{A}}_j\right\}, \forall i, j \in \mathcal{I}_L$):

i) If $\bar{\mathcal{A}}_{i,\text{ last}} \neq \bar{\mathcal{A}}_{j,\text{ first}}$, then this concatenation is kept, where $\bar{\mathcal{A}}_{i,\text{ last}}$ denotes the last subsystem mode in $\bar{\mathcal{A}}_i$, and $\bar{\mathcal{A}}_{j,\text{ first}}$ denotes the first subsystem mode in $\bar{\mathcal{A}}_j$.

ii) If $\bar{\mathcal{A}}_{i,\text{ last}} = \bar{\mathcal{A}}_{j,\text{ first}}$, but the last $\mathcal{P}(\tau, T)$ element in $\bar{\mathcal{A}}_i$ belongs to $\bar{\mathcal{P}}(\tau)$, then

the concatenation is kept.

iii) If $\bar{\mathcal{A}}_{i,\text{ last}} = \bar{\mathcal{A}}_{j,\text{ first}}$, and the last $\mathcal{P}(\tau, T)$ element in $\bar{\mathcal{A}}_i$ does not belong to $\bar{\mathcal{P}}(\tau)$, then this concatenation is discarded. The reason lies in that, in this case, we can move the consecutive same subsystem modes at the end of $\bar{\mathcal{A}}_i$ to the front of $\bar{\mathcal{A}}_j$, which yields to $\bar{\mathcal{A}}_{i,\text{ last}} \neq \bar{\mathcal{A}}_{j,\text{ first}}$, so this case is converted to case i).

We use $\mathcal{C}(\tau, T, L)$ to denote the concatenation list under the above three cases. As in fact $\bar{\mathcal{A}}(\tau, T, L)$ with $\mathcal{C}(\tau, T, L)$ can also cover all admissible PDT switching sequences, the equivalence to $S_{\text{p-dwell}}[\tau, T]$ still holds.

Step 5: Note that there may still exist different concatenations corresponding to same switching sequences in case ii), such as $\{\bar{\mathcal{A}}_{i_1}, \bar{\mathcal{A}}_{j_1}\} = \{\{1,1\},\{1,1,1,2\}\}$, and $\{\bar{\mathcal{A}}_{i_2}, \bar{\mathcal{A}}_{j_2}\} = \{\{1,1,1\},\{1,1,2\}\}$, where $i_1, i_2 \in \mathcal{I}_L$, $j_1 \in \mathcal{C}_{i_1}, j_2 \in \mathcal{C}_{i_2}$. Note that $\bar{\mathcal{A}}_{i_1}, \bar{\mathcal{A}}_{i_2} \in \bar{\mathcal{P}}$ due to $\bar{\mathcal{P}}_0 = \{1,1\}, \bar{\mathcal{P}}_1 = \{1,1,1\}$, and we assume $L = 1$ for simplification. So we only keep one concatenation for the above case, and use $\bar{\mathcal{C}}(\tau, T, L)$ to represent the concatenation list of $\bar{\mathcal{A}}(\tau, T, L)$ after removal.

Thus, according to the above five steps, we can generate a switching sequence list $\bar{\mathcal{A}}(\tau, T, L)$ with the concatenation list $\bar{\mathcal{C}}(\tau, T, L)$, which is equivalent to any given PDT signal set $S_{\text{p-dwell}}[\tau, T]$. In summary, any admissible PDT switching sequences can be represented by the circle marked by blue arrows in Figure 4.2. The sequence starts from one element $\bar{\mathcal{A}}_i, i \in \mathcal{I}_L$, in $\bar{\mathcal{A}}(\tau, T, L)$, then taking one index j in $\bar{\mathcal{C}}_i$, and evolves as the sequence indicated by the element $\bar{\mathcal{A}}_j$. The above process is repeated to generate an infinite admissible PDT switching sequence.

For any admissible PDT switching sequences, denoted by $\{\bar{\mathcal{A}}_i, \bar{\mathcal{A}}_j, \ldots\}, i \in \mathcal{I}_L, j \in \bar{\mathcal{C}}_i$, without loss of generality, we define the switching instants of $\bar{\mathcal{A}}(\tau, T, L)$ elements by $\bar{k}_s, s \in \mathbb{Z}_+$, and use the symbol $\hat{\sigma}(k)$ to indicate the activated $\bar{\mathcal{A}}(\tau, T, L)$ elements at time k.

4.4 Stabilization of nominal systems

This section aims to design the stabilization controller (4.8) for the nominal system (4.3). According to the concepts of the switching sequence list and the concatenation list introduced in Section 4.3, we first give a non-conservative convex stability criterion for PDT switched systems.

Theorem 4.1. *Consider the switched system (4.3). The following two statements are equivalent.*

a) The switched system (4.3) is GES under PDT constraint for a given $S_{\text{p-dwell}}[\tau_z, T]$.

b) There exists a scalar $L \in \mathbb{Z}_{\geq 1}$ *and a symmetric matrix sequence* $R_i(p) \in \mathbb{S}^{n_x}_{\succ 0}, i \in \bar{\mathcal{I}}_L, p \in \mathbb{Z}_{[0,|\bar{\mathcal{A}}_i|]}$, *such that* $\forall i \in \mathcal{I}_L, j \in \bar{\mathcal{C}}_i$

i) $\forall i \in \mathcal{I}_L, p \in \mathbb{Z}_{[0,|\bar{\mathcal{A}}_i|-1]}$,

$$A^T_{\bar{\mathcal{A}}_{i,p}} R_i(p+1) A_{\bar{\mathcal{A}}_{i,p}} - R_i(p) \prec 0. \tag{4.12}$$

ii) $\forall i \in \mathcal{I}_L, j \in \bar{\mathcal{C}}_i$

$$R_j(0) - R_i\left(\left|\bar{\mathcal{A}}_i\right|\right) \prec 0. \tag{4.13}$$

Proof. **Proof of a) $\Rightarrow$ b).** For any arbitrarily chosen $R_i\left(\left|\bar{\mathcal{A}}_i\right|\right) \in \mathbb{S}^{n_x}_{\succ 0}, i \in \mathcal{I}_L$, we can define a matrix sequence $W_i(p) \in \mathbb{S}^{n_x}_{\succ 0}, p \in \mathbb{Z}_{[0,|\bar{\mathcal{A}}_i|-1]}$, and let

$$R_i(p) := W_i(p) + A^{\mathrm{T}}_{\bar{\mathcal{A}}_{i,p}} R_i(p+1) A_{\bar{\mathcal{A}}_{i,p}}. \tag{4.14}$$

which ensures the satisfiction of the condition (4.12). This further gives rise to $R_i(0) = \bar{W}_i(0) + \left(\prod_{k=0}^{|\bar{\mathcal{A}}_i|-1} A_{\bar{\mathcal{A}}_{i,k}}\right)^{\mathrm{T}} R_i\left(\left|\bar{\mathcal{A}}_i\right|\right) \left(\prod_{k=0}^{|\bar{\mathcal{A}}_i|-1} A_{\bar{\mathcal{A}}_{i,k}}\right)$ where

$$\bar{W}_i(0) := \sum_{k=0}^{|\bar{\mathcal{A}}_i|-1} \left(\prod_{p=0}^{k-1} A_{\bar{\mathcal{A}}_{i,p}}\right)^{\mathrm{T}} W_i(k) \left(\prod_{p=0}^{k-1} A_{\bar{\mathcal{A}}_{i,p}}\right). \tag{4.15}$$

Since the switched system in (4.3) is GES, there must exist a decay rate $\mu > 0$, and a scalar $L \in \mathbb{Z}_{\geq 1}$ to regulate the considered switching sequence length, such that $\left\|z_{\bar{k}_1}\right\| := \left\|\Phi\left(\bar{k}_1, k_0\right) z_{k_0}\right\| \leq c e^{-\mu\left(\bar{k}_1 - k_0\right)} \left\|z_{k_0}\right\|$, where $c > 0$ is a constant, $\bar{k}_1 = \left|\bar{\mathcal{A}}_i\right|, \forall i \in \mathcal{I}_L$, and

$$\Phi\left(\bar{k}_1, k_0\right) := \prod_{p=0}^{|\bar{\mathcal{A}}_i|-1} A_{\bar{\mathcal{A}}_{i,p}} = A_{\bar{\mathcal{A}}_{i,|\bar{\mathcal{A}}_i|-1}} \cdots A_{\bar{\mathcal{A}}_{i,0}}.$$

Thus, we can obtain that $\lim_{L\to\infty} \Phi\left(\bar{k}_1, k_0\right) = 0$ due to $\bar{k}_1 - k_0 \to \infty$. For arbitrarily chosen $R_j\left(\left|\bar{\mathcal{A}}_j\right|\right) \in \mathbb{S}^{n_x}_{\succ 0}, \forall j \in \mathcal{I}_L$, there exists a scalar $\varepsilon > 0$ such that

$$\lim_{L\to\infty} \Phi^{\mathrm{T}}\left(\bar{k}_1, k_0\right) R_i\left(\left|\bar{\mathcal{A}}_i\right|\right) \Phi\left(\bar{k}_1, k_0\right) - R_j\left(\left|\bar{\mathcal{A}}_j\right|\right) \prec -\varepsilon I.$$

Moreover, there exists a scalar $L^* \in \mathbb{Z}_+$such that for any $L > L^*$, it holds that

$$\Phi^{\mathrm{T}}\left(\bar{k}_1, k_0\right) R_i\left(\left|\bar{\mathcal{A}}_i\right|\right) \Phi\left(\bar{k}_1, k_0\right) - R_j\left(\left|\bar{\mathcal{A}}_j\right|\right) \prec -\varepsilon I. \tag{4.16}$$

Considering (4.16) together with (4.14), we know that

$$R_i(0) - R_j\left(\left|\bar{\mathcal{A}}_j\right|\right) \prec -\varepsilon I + \bar{W}_i(0) \tag{4.17}$$

holds for any $i, j \in \mathcal{I}_L$. Since $j \in \bar{\mathcal{C}}_i \subseteq \mathcal{I}_L, R_j(0) - R_i\left(\left|\bar{\mathcal{A}}_i\right|\right) \prec -\varepsilon I + \bar{W}_j(0)$ also holds for $i \in \mathcal{I}_L$, $j \in \bar{\mathcal{C}}_i$. Since the norm of $\bar{W}_j(0)$ can be adjusted to be sufficiently small by the matrix sequences $W_j(p)$, $R_j(0) - R_i\left(\left|\bar{\mathcal{A}}_i\right|\right) \prec 0$ is ensured.

Proof of b) $\Rightarrow$ a) Define the Lyapunov function for the system (4.3) by:

$$V_{\hat{\sigma}(k)}(z_k) := \sqrt{z^{\mathrm{T}}(k) R_{\hat{\sigma}(k)}\left(k - \bar{k}_s\right) z_k}, \tag{4.18}$$

where $k \in \left[\bar{k}_s, \bar{k}_{s+1}\right), s \in \mathbb{Z}_+$. Define $\delta_{\max}(\cdot)$ as the largest matrix singular value, and define $\delta_{\min}(\cdot)$ as the smallest matrix singular value. Moreover, define

$$\begin{aligned}
\bar{\delta}_{\max} &:= \max_{i \in \mathcal{I}_L, p \in \mathbb{Z}_{[0,|\bar{\mathcal{A}}_i|]}} \delta_{\max}\left(R_i(p)\right) \\
\bar{\delta}_{\min} &:= \min_{i \in \mathcal{I}_L, p \in \mathbb{Z}_{[0,|\bar{\mathcal{A}}_i|]}} \delta_{\min}\left(R_i(p)\right).
\end{aligned}$$

then we can obtain that

$$\sqrt{\bar{\delta}_{\min}}\|z_k\| \leq V_{\hat{\sigma}(k)}(z_k) \leq \sqrt{\bar{\delta}_{\max}}\|z_k\|, \tag{4.19}$$

and

$$\begin{aligned}
&V_{\hat{\sigma}(k+1)}(z_{k+1}) - V_{\hat{\sigma}(k)}(z_k) \\
=&\sqrt{z^{\mathrm{T}}(k+1) R_{\hat{\sigma}(k+1)}\left(k+1-\bar{k}_s\right) z_{k+1}} - \sqrt{z^{\mathrm{T}}(k) R_{\hat{\sigma}(k)}\left(k-\bar{k}_s\right) z_k} \\
=&\frac{z^{\mathrm{T}}(k+1) R_{\hat{\sigma}(k+1)}\left(k+1-\bar{k}_s\right) z_{k+1} - z^{\mathrm{T}}(k) R_{\hat{\sigma}(k)}\left(k-\bar{k}_s\right) z_k}{\sqrt{z^{\mathrm{T}}(k+1) R_{\hat{\sigma}(k+1)}\left(k+1-\bar{k}_s\right) z_{k+1}} + \sqrt{z^{\mathrm{T}}(k) R_{\hat{\sigma}(k)}\left(k-\bar{k}_s\right) z_k}} < 0.
\end{aligned} \tag{4.20}$$

According to (4.12), we can obtain (4.20), where $k \in \left[\bar{k}_s, \bar{k}_{s+1} - 1\right), \hat{\sigma}(k) = \hat{\sigma}(k+$

$1) = i \in \mathcal{I}_L$ without loss of generality, and positive scalars $\varepsilon_1, \rho_1, \lambda_1$ are defined by

$$\begin{aligned}
\varepsilon_1 &:= \min_{i\in\mathcal{I}_L, p\in\left[0,\left|\bar{\mathcal{A}}_i\right|-2\right]} \delta_{\min}\left(R_i(p) - A_{\bar{\mathcal{A}}_{i,p}}^{\mathrm{T}} R_i(p+1) A_{\bar{\mathcal{A}}_{i,p}}\right), \\
\rho_1 &:= \max_{i\in\mathcal{I}_L, p\in[0,|\mathcal{A}_i|-2]} \delta_{\max}\left(A_{\mathcal{A}_{i,p}}^{\mathrm{T}} R_i(p+1) A_{\bar{\mathcal{A}}_{i,p}}\right), \\
\lambda_1 &:= \varepsilon_1 / \left(\sqrt{\rho_1} + \sqrt{\bar{\delta}_{\max}}\right).
\end{aligned}$$

It is seen that (4.20) indicates the decrease of Lyapunov function for any $\bar{\mathcal{A}}_i, i \in \mathcal{I}_L$, in $\bar{\mathcal{A}}(\tau, T, L)$.

Next, consider the switching instants between two consecutive $\bar{\mathcal{A}}(\tau, T, L)$ elements. Let us define

$$\bar{V}_{\hat{\sigma}\left(\bar{k}_s\right)}\left(z_{\bar{k}_{s+1}}\right) := \sqrt{z_{\bar{k}_{s+1}}^{\mathrm{T}} R_{\hat{\sigma}\left(\bar{k}_s\right)}\left(\left|\bar{\mathcal{A}}_i\right|\right) z_{\bar{k}_{s+1}}},$$

then from (4.12) we can also obtain that

$$\begin{aligned}
&\bar{V}_{\hat{\sigma}\left(\bar{k}_s\right)}\left(z_{\bar{k}_{s+1}}\right) - V_{\hat{\sigma}\left(\bar{k}_s\right)}\left(z_{\bar{k}_{s+1}-1}\right) \\
=&\sqrt{z_{\bar{k}_{s+1}}^{\mathrm{T}} R_{\hat{\sigma}\left(\bar{k}_s\right)}\left(\bar{k}_{s+1} - \bar{k}_s\right) z_{\bar{k}_{s+1}}} \\
&-\sqrt{z^{\mathrm{T}}\left(\bar{k}_{s+1}-1\right) R_{\hat{\sigma}\left(\bar{k}_s\right)}\left(\bar{k}_{s+1} - \bar{k}_s - 1\right) z_{\bar{k}_{s+1}-1}} \\
<&-\frac{\varepsilon_2 \left\|z_{\bar{k}_{s+1}-1}\right\|^2}{\sqrt{\rho_2}\left\|z_{\bar{k}_{s+1}-1}\right\| + \sqrt{\bar{\delta}_{\max}}\left\|z_{\bar{k}_{s+1}-1}\right\|} \\
:=&-\lambda_2 \left\|z_{\bar{k}_{s+1}-1}\right\|,
\end{aligned} \tag{4.21}$$

where positive scalars $\varepsilon_2, \rho_2, \lambda_2$ are defined by

$$\begin{aligned}
\varepsilon_2 =& \min_{i\in\mathcal{I}_L} \delta_{\min}\left(R_i\left(\left|\bar{\mathcal{A}}_i\right| - 1\right)\right. \\
&\left. - A_{\bar{\mathcal{A}}_{i,\left|\bar{\mathcal{A}}_i\right|-1}^{\mathrm{T}}} R_i\left(\left|\bar{\mathcal{A}}_i\right|\right) A_{\bar{\mathcal{A}}_{i,\left|\bar{\mathcal{A}}_i\right|-1}}\right) \\
\rho_2 :=& \max_{i\in\mathcal{I}_L} \delta_{\max}\left(A_{\bar{\mathcal{A}}_{i,\left|\bar{\mathcal{A}}_i\right|-1}}^{\mathrm{T}} R_i\left(\left|\bar{\mathcal{A}}_i\right|\right) A_{\bar{\mathcal{A}}_{i,\left|\bar{\mathcal{A}}_i\right|-1}}\right) \\
\lambda_2 :=& \varepsilon_2 / \left(\sqrt{\rho_2} + \sqrt{\bar{\delta}_{\max}}\right),
\end{aligned}$$

.

According to (4.13), we can obtain that

$$\begin{aligned}
&V_{\hat{\sigma}\left(\bar{k}_{s+1}\right)}\left(z_{\bar{k}_{s+1}}\right)-\bar{V}_{\hat{\sigma}\left(\bar{k}_{s}\right)}\left(z_{\bar{k}_{s+1}}\right)\\
=&\sqrt{z_{\bar{k}_{s+1}}^{\mathrm{T}} R_{\hat{\sigma}\left(\bar{k}_{s+1}\right)}(0) z_{\bar{k}_{s+1}}}\\
-&\sqrt{z_{\bar{k}_{s+1}}^{\mathrm{T}} R_{\hat{\sigma}\left(\bar{k}_{s}\right)}\left(\bar{k}_{s+1}-\bar{k}_{s}\right) z_{\bar{k}_{s+1}}}\\
<&-\frac{\varepsilon_{3}\left\|z_{\bar{k}_{s+1}}\right\|^{2}}{2\sqrt{\bar{\delta}_{\max}}\left\|z_{\bar{k}_{s+1}}\right\|}:=-\lambda_{3}\left\|z_{\bar{k}_{s+1}}\right\|,
\end{aligned} \tag{4.22}$$

where positive scalars ε_3 and λ_3 are defined by

$$\begin{aligned}
\varepsilon_{3}&:=\min_{i\in\mathcal{I}_{L}, j\in\bar{\mathcal{C}}_{i}}\delta_{\min}\left(R_{i}\left(\left|\bar{\mathcal{A}}_{i}\right|\right)-R_{j}(0)\right)\\
\lambda_{3}&:=\varepsilon_{3}/\left(2\sqrt{\bar{\delta}_{\max}}\right).
\end{aligned}$$

From (4.21) and (4.22), we know that

$$\begin{aligned}
&V_{\hat{\sigma}\left(\bar{k}_{s+1}\right)}\left(z_{\bar{k}_{s+1}}\right)-V_{\hat{\sigma}\left(\bar{k}_{s}\right)}\left(z_{\bar{k}_{s+1}-1}\right)\\
=&-\lambda_{2}\left\|z_{\bar{k}_{s+1}-1}\right\|-\lambda_{3}\left\|z_{\bar{k}_{s+1}}\right\|\\
<&-\lambda_{2}\left\|z_{\bar{k}_{s+1}-1}\right\|.
\end{aligned} \tag{4.23}$$

According to (4.20) and (4.23), it holds that

$$\begin{aligned}
\Delta v_{k}:&=V_{\hat{\sigma}(k+1)}(z_{k+1})-V_{\hat{\sigma}(k)}(z_{k})\\
&<\begin{cases}-\lambda_{1}\|z_{k}\| & k\in\left[\bar{k}_{s},\bar{k}_{s+1}-1\right)\\ -\lambda_{2}\|z_{k}\| & k=\bar{k}_{s+1}-1\end{cases},
\end{aligned}$$

and thus

$$\Delta v_{k}<-\lambda\|z_{k}\|, \tag{4.24}$$

where $\lambda:=\max\left(\lambda_{1},\lambda_{2},\sqrt{\bar{\delta}_{\max}}-\varepsilon\right)$ and $0<\varepsilon<\sqrt{\bar{\delta}_{\max}}$ is a constant.

According to (4.19) and (4.24), we can obtain that

$$V_{\hat{\sigma}(k+1)}(z_{k+1})<\left(1-\frac{\lambda}{\sqrt{\bar{\delta}_{\max}}}\right)V_{\hat{\sigma}(k)}(z_{k}),$$

where $0 < 1 - \frac{\lambda}{\sqrt{\bar{\delta}_{\max}}} < 1$ is a constant. Moreover, we can obtain that

$$V_{\hat{\sigma}(k)}(z_k) < \left(1 - \frac{\lambda}{\bar{\delta}_{\max}}\right)^k V_{\hat{\sigma}(0)}\left(z_{k_0}\right),$$

which together with (4.19) generates

$$\begin{aligned}
\|z_k\| &< \frac{1}{\sqrt{\bar{\delta}_{\min}}} V_{\hat{\sigma}(k)}(z_k) \\
&< \frac{1}{\sqrt{\bar{\delta}_{\min}}} \left(1 - \frac{\lambda}{\sqrt{\bar{\delta}_{\max}}}\right)^{k-k_0} V_{\hat{\sigma}(k_0)}\left(z_{k_0}\right) \\
&< \frac{\sqrt{\bar{\delta}_{\max}}}{\sqrt{\bar{\delta}_{\min}}} \left(1 - \frac{\lambda}{\sqrt{\bar{\delta}_{\max}}}\right)^{k-k_0} \|z_{k_0}\| \\
&:= c e^{-\mu(k-k_0)} \|z_{k_0}\|,
\end{aligned}$$

where $c := \sqrt{\bar{\delta}_{\max}}/\sqrt{\bar{\delta}_{\min}} > 0, \mu = -\ln\left(1 - \frac{\lambda}{\sqrt{\bar{\delta}_{\max}}}\right) > 0$. This completes the proof. □

Remark 4.1. *Two techniques are developed in Theorem 4.1 to obtain the nonconservative global exponential stability conditions. The first one is the novel sequence segmentation technique. It cancels the parameters that overly shape the Lyapunov function in the existing literature of PDT switched systems [10, 22, 152, 153, 169], and thus realizes the convexification. The second technique is to present the augmented PDT primary sequence list, which gives the user an additional integer L with respect to the primary sequence list. By setting $L = 1$, we actually require the Lyapunov function (4.18) to decrease at starting instants of $\mathcal{P}(\tau, T)$. Note that in this case, the stability conditions are still convex, and this is also an improvement compared to the existing nonconvex conditions.*

Remark 4.2. *The widely used QTD stability conditions, in the framework of stage partition, are nonconvex due to some tuning parameters, and are also sufficient to our conditions even if we set $L = 1$. The strict proof can be drawn according to the linear version of Lemma 4.1 in [162] and Theorem 4.1 in this work, and is omitted here.*

Remark 4.3. *As PDT signal set can cover ADT and DT signal sets, the nonconservative stability conditions in Theorem 4.1 can also be slightly modified for the*

switched linear systems under these two time constraints. For example, the non-conservative conditions for DT switched systems can be generated by setting $T = 0$ *in Theorem 4.1.*

Remark 4.4. *Theorem 4.1 gives a necessary and sufficient stability criterion for switched linear system (4.3). However, (4.12) and (4.13) correlate with the index* i *of the activated element in* $\bar{\mathcal{A}}(\tau, T, L)$ *and the activated concatenated element index* j *in* $\bar{\mathcal{C}}_i$*, respectively. A common challenge is that the system typically cannot predict the switching sequences, the indices* i *and* j*, or the control schedule clock* $\theta_z(k)$ *in advance. Thus, the general extension in the existing literature from stability conditions in LMI form a mode-dependent or quasi-time-dependent controller design approach fails.*

Note that the aforementioned Step 4 for generating $\bar{\mathcal{A}}(\tau, T, L)$ with $\mathcal{C}(\tau, T, L)$, only two kinds of concatenations, denoted by $\left\{\bar{\mathcal{A}}_i, \bar{\mathcal{A}}_j\right\}, i, j \in \mathcal{I}_L$, are kept under case i) and case ii). Among others, case i) keeps the concatenation under $\bar{\mathcal{A}}_{i,\text{ last}} \neq \bar{\mathcal{A}}_{j,\text{first}}$, and in this case $\theta_z(k)$ is reset to 0 when $\bar{\mathcal{A}}_i$ switches to $\bar{\mathcal{A}}_j$; case ii) keeps the concatenation under $\bar{\mathcal{A}}_{i,\text{ last}} = \bar{\mathcal{A}}_{j,\text{ first}}$ and the last $\mathcal{P}(\tau, T)$ element in $\bar{\mathcal{A}}_i$ belongs to $\bar{\mathcal{P}}(\tau)$. In this case, the last subsystem mode in $\bar{\mathcal{A}}_i$ has been activated for no less than τ_z at the switching instant from $\bar{\mathcal{A}}_i$ to $\bar{\mathcal{A}}_j$, so $\theta_z(k)$ is set to τ when $\bar{\mathcal{A}}_j$ starts.

Example 4.2. *Consider a PDT signal set* $S_{\text{p-dwell}}[3, 2]$ *with* $\mathcal{I}_N = \{1, 2, 3\}$ *and* L=1*. The two switching sequences* $\left\{\bar{\mathcal{A}}_{i_1}, \bar{\mathcal{A}}_{j_1}\right\} = \{\{1, 1, 1, 2\}, \{3, 3, 3\}\}$ *and* $\left\{\bar{\mathcal{A}}_{i_2}, \bar{\mathcal{A}}_{j_2}\right\} = \{\{2, 2, 2\}, \{2, 2, 2, 1\}\}$ *are admissible. Each inner brace indicates one element in* $\bar{\mathcal{A}}(3, 2, 1)$*. The clock* $\theta_z(k)$*, computed by (4.10), strikes as* $\{\{0, 1, 2, 0\}, \{0, 1, 2\}\}$ *and* $\{\{0, 1, 2\}, \{3, 3, 3, 0\}\}$*, respectively.*

We can find out that the two admissible switching sequences in Example 4.2 are constructed corresponding to case i) and case ii), respectively. If we consider the coverage of all $\bar{\mathcal{A}}(\tau, T, L)$ elements with their concatenations indicated by $\bar{\mathcal{C}}(\tau, T, L)$, the designed controller can also work for the infinite number of admissible PDT switching sequences. The controller gain $F_{\sigma(k)}(\theta_z(k))$ in (4.8) depends on the activated subsystem mode $\sigma(k)$ and its schedule clock $\theta_z(k)$, where the former one can be denoted by the switching sequence list, such as $\bar{\mathcal{A}}_{i_1,p} = 1, p = 0, 1, 2$, and $\bar{\mathcal{A}}_{i_1,3} = 2$ in Example 4.2. Thus, we aim to denote the online computed $\theta_z(k)$ by two offline calculated

variables,

$$\bar{\theta}_z(i) := \left\{\bar{\theta}_z(i,0), \bar{\theta}_z(i,1), \ldots, \bar{\theta}_z\left(i, \left|\bar{\mathcal{A}}_i\right| - 1\right)\right\}, \tag{4.25}$$

$$\hat{\theta}_z(i) := \left\{\hat{\theta}_z(i,0), \hat{\theta}_z(i,1), \ldots, \hat{\theta}_z\left(i, \left|\hat{\mathcal{A}}_i\right| - 1\right)\right\}, \tag{4.26}$$

where

$$\bar{\theta}_z(i,p) = \min_{s\in\mathbb{Z}_+} (p - p_s, \tau_z) \tag{4.27}$$

and

$$\hat{\theta}_z(i,p) = \begin{cases} \tau_z, & s = 0 \\ \bar{\theta}_z(i,p), & s \in \mathbb{Z}_{\geq 1} \end{cases}, \tag{4.28}$$

where p_s denotes the position of the last switching instant of subsystem modes in $\bar{\mathcal{A}}_i$ before $p, s \in \mathbb{Z}_+, p \in \mathbb{Z}_{[0,|\mathcal{A}_i|-1]}$. It is seen that $\bar{\theta}_z(i)$ and $\hat{\theta}_z(i)$ cover all possible $\theta_z(k)$ for $\bar{\mathcal{A}}_i, i \in \mathcal{I}_L$. Consider the two switching sequences in Example 4.2. By (4.25) and (4.26), we can obtain

$$\begin{aligned}
&\bar{\theta}_z\left(i_1\right) = \{0,1,2,0\}, \bar{\theta}_z\left(j_1\right) = \{0,1,2\}, \\
&\bar{\theta}_z\left(i_2\right) = \{0,1,2\}, \bar{\theta}_z\left(j_2\right) = \{0,1,2,0\}, \\
&\hat{\theta}_z\left(i_1\right) = \{3,3,3,0\}, \hat{\theta}_z\left(j_1\right) = \{3,3,3\}, \\
&\hat{\theta}_z\left(i_2\right) = \{3,3,3\}, \hat{\theta}_z\left(j_2\right) = \{3,3,3,0\}.
\end{aligned}$$

It can be checked that $\theta_z(k)$ for the sequence $\left\{\bar{\mathcal{A}}_{i_1}, \bar{\mathcal{A}}_{j_1}\right\}$ is identical to $\left\{\bar{\theta}_z\left(i_1\right), \bar{\theta}_z\left(j_1\right)\right\}$, and $\theta_z(k)$ for the sequence $\left\{\bar{\mathcal{A}}_{i_2}, \bar{\mathcal{A}}_{j_2}\right\}$ is identical to $\left\{\bar{\theta}_z\left(i_2\right), \hat{\theta}_z\left(j_2\right)\right\}$. Thus, if the controller design conditions hold for all the sequences determined by $\bar{\mathcal{A}}(\tau, T, L)$ with $\bar{\mathcal{C}}(\tau, T, L)$, where $\theta_z(k)$ is set equal to $\bar{\theta}_z(i)$ or $\hat{\theta}_z(i)$ for each $\bar{\mathcal{A}}_i$, the designed controller also works for the infinite number of admissible PDT switching sequences. This is called "virtual-sequence-dependent" controller design method.

Theorem 4.2. *Consider the switched system (4.3) with a given PDT signal set $S_{\text{p-dwell}}[\tau_z, T]$. Suppose that there exists a matrix sequence $S_i(p) \in \mathbb{S}^{n_x}_{\succ 0}, i \in \mathcal{I}_L$, $p \in \mathbb{Z}_{[0,|\bar{\mathcal{A}}_i|]}$, and matrix sequences $W_n(\theta), U_n(\theta)$, $n \in \mathcal{I}_N, \theta \in \mathbb{Z}_{[0,\tau_z]}$, such that*

i) $\forall i \in \mathcal{I}_L, p \in \mathbb{Z}_{[0,|\bar{\mathcal{A}}_i|-1]}, \theta = \bar{\theta}_z(i,p)$ or $\theta = \hat{\theta}_z(i,p)$,

$$\begin{bmatrix} -S_i(p+1) & A_{\bar{\mathcal{A}}_{i,p}} W_{\bar{\mathcal{A}}_{i,p}}(\theta) + B_{\bar{\mathcal{A}}_{i,p}} U_{\bar{\mathcal{A}}_{i,p}}(\theta) \\ \star & S_i(p) - W_{\bar{\mathcal{A}}_{i,p}}(\theta) - W^T_{\bar{\mathcal{A}}_{i,p}}(\theta) \end{bmatrix} \prec 0, \tag{4.29}$$

ii) $\forall i \in \mathcal{I}_L, j \in \bar{\mathcal{C}}_i$

$$S_i\left(\left|\bar{\mathcal{A}}_i\right|\right) - S_j(0) \prec 0. \tag{4.30}$$

Then the nominal system (4.3) *under controller* (4.8) *is GES. Moreover, the stabilizing controller gains are given by,* $\forall n \in \mathcal{I}_N, \theta \in \mathbb{Z}_{[0,\tau_z]}$

$$F_n(\theta) = U_n(\theta) W_n^{-1}(\theta). \tag{4.31}$$

Proof. Due to the fact that $\left(S_i(p) - W_{\bar{\mathcal{A}}_{i,p}}(\theta)\right)^{\mathrm{T}} S_i^{-1}(p) \left(S_i(p) - W_{\bar{\mathcal{A}}_{i,p}}(\theta)\right) \succeq 0$, one has $S_i(p) - W_{\bar{\mathcal{A}}_{i,p}}(\theta) - W_{\bar{\mathcal{A}}_{i,p}}^{\mathrm{T}}(\theta) \succeq -W_{\bar{\mathcal{A}}_{i,p}}^{\mathrm{T}}(\theta) S_i^{-1}(p) W_{\bar{\mathcal{A}}_{i,p}}(\theta)$, where $\bar{\mathcal{A}}_{i,p}$ denotes the p-th activated subsystem mode in $\bar{\mathcal{A}}_i$. Thus, (29) ensures that

$$\begin{bmatrix} -S_i(p+1) & A_{\bar{\mathcal{A}}_{i,p}} W_{\bar{\mathcal{A}}_{i,p}}(\theta) + B_{\bar{\mathcal{A}}_{i,p}} U_{\bar{\mathcal{A}}_{i,p}}(\theta) \\ \star & -W_{\bar{\mathcal{A}}_{i,p}}^{\mathrm{T}}(\theta) S_i^{-1}(p) W_{\bar{\mathcal{A}}_{i,p}}(\theta) \end{bmatrix} \prec 0. \tag{4.32}$$

According to (4.31), we know that

$$F_n(\theta) W_n(\theta) = U_n(\theta),$$

where $n \in \mathcal{I}_N$, and $\theta \in \mathbb{Z}_{[0,\tau_z]}$. Then (4.32) is equivalent to

$$\begin{bmatrix} -S_i(p+1) & \bar{A}_{\bar{\mathcal{A}}_{i,p}}(\theta) W_{\bar{\mathcal{A}}_{i,p}}(\theta) \\ \star & -W_{\bar{\mathcal{A}}_{i,p}}^{\mathrm{T}}(\theta) S_i^{-1}(p) W_{\bar{\mathcal{A}}_{i,p}}(\theta) \end{bmatrix} \prec 0, \tag{4.33}$$

where $\bar{A}_{\bar{\mathcal{A}}_{i,p}}(\theta) := A_{\bar{\mathcal{A}}_{i,p}} + B_{\bar{\mathcal{A}}_{i,p}} F_{\bar{\mathcal{A}}_{i,p}}(\theta)$.

Performing congruence transformations to (4.33) by diag $\left\{ S_i^{-1}(p+1), W_{\mathcal{A}_{i,p}^{-\mathrm{T}}}^{-\mathrm{T}}(\theta) \right\}$, we can obtain

$$\begin{bmatrix} -S_i^{-1}(p+1) & S_i^{-1}(p+1) \bar{A}_{\bar{\mathcal{A}}_{i,p}}(\theta) \\ \star & -S_i^{-1}(p) \end{bmatrix} \prec 0.$$

Letting $R_i(p) := S_i^{-1}(p)$ and $\bar{A}_{\bar{\mathcal{A}}_{i,p}}(\theta) := A_{\bar{\mathcal{A}}_{i,p}}$, we can get (4.12). Moreover, (4.30) ensures (4.13). By Theorem 4.1, the nominal switched system (4.3) with controller gains (4.31) is GES under PDT switching signal for $S_{\mathrm{p-\ dwell}}\,[\tau, T]$.

□

4.5 Systems with bounded peak disturbances

In this section, the estimated reachable set $\hat{\mathcal{R}}_e$ that contains the practical reachable set $\mathcal{R}_e$ of the error system (4.4) is designed as small as possible to minimize the effect caused by the bounded peak disturbances ω_k. A set $\mathcal{R}$ with admissible switching signal set is also determined to address the global exponential stability of the composite system (4.1) and (4.3) in the sense of Definition 4.3. The following lemma introduces the basic idea of generating $\hat{\mathcal{R}}_e$ for PDT switched systems by ellipsoidal techniques.

Lemma 4.1. *Consider the switched system (4) with a given PDT signal set* $S_{\text{p-dwell}}[\tau_e, T]$. *If there exists a set of functions* $V_i : \mathbb{R}^{n_x} \to \mathbb{R}_+$ *satisfying* $V_i(0) = 0$ *and* $V_i(x) > 0$, $\forall x \neq 0, \forall i \in \mathcal{I}_L$, *and a scalar* $0 < \alpha < 1$, *such that*

i) $\forall k \in \left[\bar{k}_s, \bar{k}_{s+1}\right), s \in \mathbb{Z}_+, \forall \hat{\sigma}(k) = i \in \mathcal{I}_L$

$$V_i(e_{k+1}) - \alpha V_i(e_k) - \frac{1-\alpha}{\bar{\omega}^2}\omega^T(k)\omega_k < 0, \tag{4.34}$$

ii) $\forall k = \bar{k}_{s+1}, s \in \mathbb{Z}_+, \forall \hat{\sigma}\left(\bar{k}_s\right) = i \in \mathcal{I}_L, \forall \hat{\sigma}\left(\bar{k}_{s+1}\right) = j \in \bar{C}_i$

$$V_j(e_k) - V_i(e_k) < 0, \tag{4.35}$$

then it holds that $V_{\hat{\sigma}(k)}(e_k) < 1$ *for all* e_{k_0} *satisfying* $V_{\hat{\sigma}(k_0)}(e_{k_0}) < 1$.

Proof. According to (4.34), we can obtain that

$$\begin{aligned} V_i(e_{k+1}) - \alpha V_i(e_k) &< \frac{1-\alpha}{\bar{\omega}^2}\omega^{\mathrm{T}}(k)\omega_k \\ &< 1-\alpha, \end{aligned}$$

which further implies that

$$V_i(e_{k+1}) - 1 < \alpha\left(V_i(e_k) - 1\right) \tag{4.36}$$

holds for $k \in \left[\bar{k}_s, \bar{k}_{s+1}\right)$. Moreover, (4.35) guarantees

$$V_j\left(e_{\bar{k}_{s+1}}\right) - 1 < V_i\left(e_{\bar{k}_{s+1}}\right) - 1. \tag{4.37}$$

Thus, for any $k \in \mathbb{Z}_+$, by (4.36) and (4.37), it follows that

$$\begin{aligned} V_{\hat{\sigma}(k)}(e_k) - 1 &< V_{\hat{\sigma}(k-1)}(e(k-1)) - 1 \\ &< \cdots \\ &< V_{\hat{\sigma}(k_0)}(e_{k_0}) - 1 < 0 \end{aligned}$$

due to $0 < \alpha < 1$. This completes the proof. □

Considering the error system (4.4) together with controllers (4.7) and (4.8), we can obtain the following closed-loop error system:

$$e_{k+1} = E_{\sigma(k)}(\theta_e(k))\, e_k + D_{\sigma(k)}\omega_k, \tag{4.38}$$

where $E_{\sigma(k)}(\theta_e(k)) := A_{\sigma(k)} + B_{\sigma(k)}K_{\sigma(k)}(\theta_e(k))$. The following theorem gives the linear version of Lemma 4.1 by employing the ellipsoidal techniques and multiple Lyapunov function approach [166–168].

Theorem 4.3. *Consider the switched system (4.4) with a given PDT signal set $S_{\text{p-dwell}}[\tau_e, T]$. If there exists a matrix $O_i(p) \in \mathbb{S}^{n_x}_{\succ 0}, i \in \mathcal{I}_L, p \in \mathbb{Z}_{[0,|\bar{\mathcal{A}}_i|]}$, and a scalar $0 < \alpha < 1$, such that*

i) $\forall i \in \mathcal{I}_L, p \in \mathbb{Z}_{[0,|\bar{\mathcal{A}}_i|-1]}$,

$$\begin{bmatrix} -O_i(p+1) & O_i(p+1)E_{\bar{\mathcal{A}}_{i,p}}(\theta) & O_i(p+1)D_{\bar{\mathcal{A}}_{i,p}} \\ \star & -\alpha O_i(p) & 0 \\ \star & \star & -\frac{1-\alpha}{\bar{\omega}^2} I \end{bmatrix} \prec 0, \tag{4.39}$$

ii) $\forall i \in \mathcal{I}_L, j \in \bar{\mathcal{C}}_i$,

$$O_j(0) - O_i(|\mathcal{A}_i|) \prec 0, \tag{4.40}$$

then the reachable set of the error system (4.4) satisfies $\mathcal{R}_e \subseteq \hat{\mathcal{R}}_e$, and $\hat{\mathcal{R}}_e$ can be over approximated by

$$\hat{\mathcal{R}}_e := \bigcup_{i \in \mathcal{I}_L, p \in \mathbb{Z}_{[0,|\bar{\mathcal{A}}_i|]}} \mathcal{E}(O_i(p)). \tag{4.41}$$

Proof. Define the Lyapunov function for the system (4.4) by

$$V_{\hat{\sigma}(k)}(e_k) := e^{\mathrm{T}}(k) O_{\hat{\sigma}(k)}\left(k - \bar{k}_s\right) e_k,$$

where $k \in \left[\bar{k}_s, \bar{k}_{s+1}\right), s \in \mathbb{Z}_+$. By Schur complement, (4.39) guarantees

$$\Omega := \begin{bmatrix} \Omega_{11} & \Omega_{12} \\ \star & \Omega_{22} \end{bmatrix} \prec 0 \tag{4.42}$$

with $\Omega_{11} = E^{\mathrm{T}}_{\bar{\mathcal{A}}_{i,p}}(\theta) O_i(p+1) E_{\bar{\mathcal{A}}_{i,p}}(\theta) - \alpha O_i(p)$, $\Omega_{12} = E^{\mathrm{T}}_{\bar{\mathcal{A}}_{i,p}}(\theta) O_i(p+1) D_{\bar{\mathcal{A}}_{i,p}}$, and $\Omega_{22} = D^{\mathrm{T}}_{\bar{\mathcal{A}}_{i,p}} \times O_i(p+1) D_{\bar{\mathcal{A}}_{i,p}} - \frac{1-\alpha}{\bar{\omega}^2} I$.

Let $\xi(k) := \left[e^{\mathrm{T}}(k) \omega^{\mathrm{T}}(k)\right]^{\mathrm{T}}$. From (4.42), we can obtain that

$$\begin{aligned}
&\xi^{\mathrm{T}}(k) \Omega \xi(k) \\
&= e^{\mathrm{T}}(k) \left(E^{\mathrm{T}}_{\bar{\mathcal{A}}_{i,p}}(\theta) O_i(p+1) E_{\bar{\mathcal{A}}_{i,p}}(\theta) - \alpha O_i(p) \right) e_k \\
&\quad + 2 e^{\mathrm{T}}(k) \left(E^{\mathrm{T}}_{\bar{\mathcal{A}}_{i,p}}(\theta) O_i(p+1) D_{\bar{\mathcal{A}}_{i,p}} \right) \omega_k \\
&\quad + \omega^{\mathrm{T}}(k) \left(D^{\mathrm{T}}_{\bar{\mathcal{A}}_{i,p}} O_i(p+1) D_{\bar{\mathcal{A}}_{i,p}} - \frac{1-\alpha}{\bar{\omega}^2} I \right) \omega_k \\
&= V_{\hat{\sigma}(k+1)}(e_{k+1}) - \alpha V_{\hat{\sigma}(k)}(e_k) - \frac{1-\alpha}{\bar{\omega}^2} \omega^{\mathrm{T}}(k) \omega_k \\
&< 0,
\end{aligned}$$

which ensures (4.34). Moreover, (4.40) ensures (4.35). According to Theorem 4.3, we can have

$$\begin{aligned}
e_k &\in \left\{ e \mid e^{\mathrm{T}} O_i(p) e < 1, i \in \mathcal{I}_L, p \in \mathbb{Z}_{[0, |\mathcal{A}_i|]} \right\} \\
&:= \bigcup_{i \in \mathcal{I}_L, p \in \mathbb{Z}_{[0, |\bar{\mathcal{A}}_i|]}} \mathcal{E}\left(O_i(p)\right),
\end{aligned}$$

which proofs (4.41). This completes the proof. □

Similar to the stabilization problem for the nominal system (4.3), the mismatch between the stability analysis and controller design for the error system (4.4) also exists. The stability conditions (4.39)-(4.40) depend on the index of the activated $\bar{\mathcal{A}}(\tau, T, L)$ elements, but the controller gain $K_{\sigma(k)}\left(\theta_e(k)\right)$ in (4.9) varies with the activated subsystem mode $\sigma(k)$ and the schedule clock $\theta_e(k)$. To solve this problem, here we also define two offline variables $\bar{\theta}_e(i)$ and $\hat{\theta}_e(i)$ by revising the subscripts "z" to "e" in (4.25)-(4.28).

Theorem 4.4. *Consider the switched system (4.4) with a given PDT signal set* $S_{\mathrm{p-dwell}}[\tau_e, T]$. *If there exist a matrix sequence* $Q_i(p) \in \mathbb{S}^{n_x^x}_{\succ 0}, i \in \mathcal{I}_L, p \in \mathbb{Z}_{[0, |\bar{\mathcal{A}}_i|]}$,

matrix sequences $W_n(\theta), U_n(\theta), n \in \mathcal{I}_N, \theta \in \mathbb{Z}_{[0,\tau_e]}$, *and a scalar* $0 < \alpha < 1$, *such that*

i) $\forall i \in \mathcal{I}_L, p \in \mathbb{Z}_{\left[0,|\bar{\mathcal{A}}_i|-1\right]}, \theta = \bar{\theta}_e(i,p)$ *or* $\theta = \hat{\theta}_e(i,p)$,

$$\Psi = \begin{bmatrix} \Psi_{11} & \Psi_{12} & \Psi_{13} \\ \star & \Psi_{22} & 0 \\ \star & \star & \Psi_{33} \end{bmatrix} \prec 0, \tag{4.43}$$

where $\Psi_{11} = -Q_i(p+1), \Psi_{12} = A_{\bar{\mathcal{A}}_{i,p}} W_{\bar{\mathcal{A}}_{i,p}}(\theta) + B_{\bar{\mathcal{A}}_{i,p}} U_{\bar{\mathcal{A}}_{i,p}}(\theta)$, $\Psi_{13} = D_{\bar{\mathcal{A}}_{i,p}}, \Psi_{22} = \alpha \left(Q_i(p) - W^T_{\mathcal{A}_{i,p}}(\theta) - W_{\bar{\mathcal{A}}_{i,p}}(\theta)\right)$, *and* $\Psi_{33} = -\frac{1-\alpha}{\bar{\omega}^2} I$.

ii) $\forall i \in \mathcal{I}_L, j \in \bar{\mathcal{C}}_i$,

$$Q_i\left(\left|\bar{\mathcal{A}}_i\right|\right) - Q_j(0) \prec 0. \tag{4.44}$$

Then the reachable set of the error system (4.4) *satisfies* $\mathcal{R}_e \subseteq \hat{\mathcal{R}}_e$, *and* $\hat{\mathcal{R}}_e$ *can be outer approximated by*

$$\hat{\mathcal{R}}_e := \bigcup_{i \in \mathcal{I}_L, p \in \mathbb{Z}_{[0,|\bar{\mathcal{A}}_i|]}} \mathcal{E}\left(Q_i^{-1}(p)\right). \tag{4.45}$$

Moreover, the controller gains are given by, $\forall n \in \mathcal{I}_N$, $\theta \in \mathbb{Z}_{[0,\tau_e]}$,

$$K_n(\theta) = U_n(\theta) W_n^{-1}(\theta). \tag{4.46}$$

Proof. From (4.46), we can obtain that

$$U_n(\theta) = K_n(\theta) W_n(\theta)$$

holds, $\forall n \in \mathcal{I}_N, \theta \in \mathbb{Z}_{[0,\tau_e]}$. Then, (4.43) is equivalent to

$$\Upsilon_1 = \begin{bmatrix} \Upsilon_{11} & \Upsilon_{12} & \Upsilon_{13} \\ \star & \Upsilon_{14} & 0 \\ \star & \star & \Upsilon_{15} \end{bmatrix} \prec 0, \tag{4.47}$$

where $\Upsilon_{11} = -Q_i(p+1), \Upsilon_{12} = E_{\bar{\mathcal{A}}_{i,p}}(\theta) W_{\bar{\mathcal{A}}_{i,p}}(\theta)$, $\Upsilon_{13} = D_{\bar{\mathcal{A}}_{i,p}}$,
$\Upsilon_{14} = \alpha \left(Q_i(p) - W^{\mathrm{T}}_{\mathcal{A}_{i,p}}(\theta) - W_{\bar{\mathcal{A}}_{i,p}}(\theta)\right)$, and $\Upsilon_{15} = -\frac{1-\alpha}{\bar{\omega}^2} I$.

Due to the fact that $\left(Q_i(p) - W_{\bar{\mathcal{A}}_{i,p}}(\theta)\right)^{\mathrm{T}} Q_i^{-1}(p) \left(Q_i(p) - W_{\bar{\mathcal{A}}_{i,p}}(\theta)\right) \succeq 0$, we know that $Q_i(p) - W_{\bar{\mathcal{A}}_{i,p}}(\theta) - W^{\mathrm{T}}_{\mathcal{A}_{i,p}}(\theta) \succeq -W^{\mathrm{T}}_{\mathcal{A}_{i,p}}(\theta) Q_i^{-1}(p) W_{\bar{\mathcal{A}}_{i,p}}(\theta)$. Thus, from (47) we can

obtain that

$$\Upsilon_2 = \begin{bmatrix} \Upsilon_{21} & \Upsilon_{22} & \Upsilon_{23} \\ \star & \Upsilon_{24} & 0 \\ \star & \star & \Upsilon_{25} \end{bmatrix} \prec 0, \tag{4.48}$$

where $\Upsilon_{21} = -Q_i(p+1), \Upsilon_{22} = E_{\bar{\mathcal{A}}_{i,p}}(\theta)W_{\bar{\mathcal{A}}_{i,p}}(\theta)$, $\Upsilon_{23} = D_{\bar{\mathcal{A}}_{i,p}}, \Upsilon_{25} = -\frac{1-\alpha}{\bar{\omega}^2}I$, and $\Upsilon_{24} = -\alpha W^{\mathrm{T}}_{\bar{\mathcal{A}}_{i,p}}(\theta)Q_i^{-1}(p)W_{\bar{\mathcal{A}}_{i,p}}(\theta)$.

Performing congruence transformations to (4.48) by diag $\left\{Q_i^{-1}(p+1), W^{-\mathrm{T}}_{\bar{\mathcal{A}}^{-\mathrm{T}}_{i,p}}(\theta), I\right\}$, we can obtain

$$\Upsilon_3 = \begin{bmatrix} \Upsilon_{31} & \Upsilon_{32} & \Upsilon_{33} \\ \star & \Upsilon_{34} & 0 \\ \star & \star & \Upsilon_{35} \end{bmatrix} \prec 0, \tag{4.49}$$

where $\Upsilon_{31} = -Q_i^{-1}(p+1), \Upsilon_{32} = Q_i^{-1}(p+1)E_{\bar{\mathcal{A}}_{i,p}}(\theta)$, $\Upsilon_{33} = Q_i^{-1}(p+1)D_{\bar{\mathcal{A}}_{i,p}}, \Upsilon_{34} = -\alpha Q_i^{-1}(p)$, and $\Upsilon_{35} = -\frac{1-\alpha}{\bar{\omega}^2}I$.

Letting $O_i(p) := Q_i^{-1}(p)$ and $E_{\bar{\mathcal{A}}_{i,p}} := E_{\bar{\mathcal{A}}_{i,p}}(\theta)$ in (4.49), we can get (4.39). Moreover, (4.44) ensures (4.40). By Theorem 4.3, $e_k \in \hat{\mathcal{R}}_e$ which is given by (4.45). This completes the proof.

□

Remark 4.5. *The set $\hat{\mathcal{R}}_e$ needs to be minimized to resist the effect from the external disturbance. Based on Theorem 4.4, we use the following additional constraints to $\hat{\mathcal{R}}_e$:*

$$Q_i(p) \prec \epsilon I, \epsilon > 0, p \in \mathbb{Z}_{[0,|\bar{\mathcal{A}}_i|]}, \forall i \in \mathcal{I}_L. \tag{4.50}$$

This generates $\frac{1}{\epsilon}e^T(k)e_k \leq e^T(k)Q_i^{-1}(p)e_k \leq 1$. So it holds that $e_k \in \hat{\mathcal{R}}_e \subseteq \mathcal{B}(0, \sqrt{\epsilon}) := \{e \in \mathbb{R}^{n_x} \mid \|e\| \leq \sqrt{\epsilon}\}, k \in \mathbb{Z}_+$.

To design $\hat{\mathcal{R}}_e$ as small as possible, an optimization problem can be formulated by incorporating (4.43), (4.44), and (4.50) as constraints

$$\min \epsilon \text{ s.t. } (4.43), (4.44), \text{ and } (4.50). \tag{4.51}$$

Theorem 4.5. *Consider the composite system (4.1) and (4.3). Suppose that the controllers (4.7) and (4.8) exist for the nominal system (4.3) and the error system (4.4) with $S_{p\text{-}dwell}\,[\tau_z, T]$ and $S_{p\text{-}dwell}\,[\tau_e, T]$, respectively. Then the set $\mathcal{R} := \hat{\mathcal{R}}_e \times \{0\}$ is GES for the composite system (4.1) and (4.3) with $S_{\mathrm{p-dwell}}\left[\max\left(\tau_z, \tau_e\right), T\right]$.*

Proof. If the controller (4.7) exists for the nominal system (4.3), then the closed-loop

nominal system is GES by Theorem 4.2, so there must exist scalars $c > 0, \mu > 0$, such that

$$\|z_k\| \leq ce^{-\mu(k-k_0)} \|z_{k_0}\| \tag{4.52}$$

with $S_{\text{p-dwell}}\ [\tau_z, T]$. Moreover, we can obtain that

$$\begin{aligned} \|x_k\|_{\hat{\mathcal{R}}_e} &= d\left(z_k + e_k, \hat{\mathcal{R}}_e\right) \\ &\leq d(z_k + e_k, e_k) \\ &= \|z_k\| \leq ce^{-\mu(k-k_0)} \|z_{k_0}\|, \end{aligned} \tag{4.53}$$

where the first " $\leq$ " holds due to $e_k \in \mathcal{R}_e \subseteq \hat{\mathcal{R}}_e$. Then, it follows that

$$\begin{aligned} \|(x_k, z_k)\|_{\mathcal{R}} &= \|x_k\|_{\mathcal{R}_e} + \|z_k\|_{\{0\}} \\ &\leq 2ce^{-\mu(k-k_0)} \|z_{k_0}\| \\ &\leq 2ce^{-\mu(k-k_0)} \left(\|z_{k_0}\| + \|x_{k_0}\|_{\hat{\mathcal{R}}_e}\right) \\ &= 2ce^{-\mu(k-k_0)} \|(x_{k_0}, z_{k_0})\|_{\mathcal{R}} \end{aligned}$$

for given $S_{\text{p-dwell}}\,[\tau_e, T]$ and $S_{\text{p-dwell}}\,[\tau_z, T]$. As (4.52) and (4.53) require the minimal persistent dwell-time τ for the composite system (4.1) and (4.3) satisfy $\tau \geq \tau_z$ and $\tau \geq \tau_e$, respectively, the set $\mathcal{R}$ is GES for the composite system (4.1) and (4.3) with $S_{\text{p-dwell}}\,[\max(\tau_z, \tau_e), T]$. □

4.6 Simulation results

In this section, two examples demonstrate the validity of the obtained outcomes. The first example is to determine the admissible PDT signal set $S_{\text{p-dwell}}[\tau, T]$. This is an pure numerical example of switched system that contains two discrete-time linear subsystems with a PDT signal.

Example 4.3. *Consider the following discrete-time switched linear system with two subsystems given by:*

$$A_1 = \begin{bmatrix} 0.9680 & 0.0760 \\ -0.7599 & 0.8920 \end{bmatrix}, A_2 = \begin{bmatrix} 0.9987 & 0.0684 \\ -0.0068 & 0.7252 \end{bmatrix}.$$

Solving linear matrix inequalities (4.12)-(4.13) in Theorem 4.1, we can find out

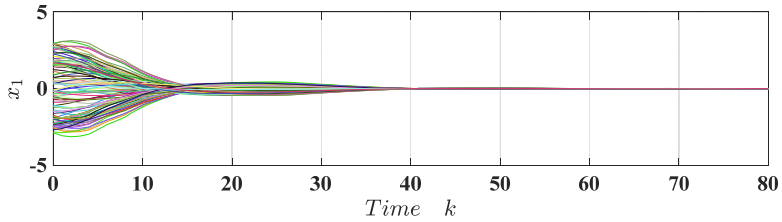

(a) Evolution of x_1

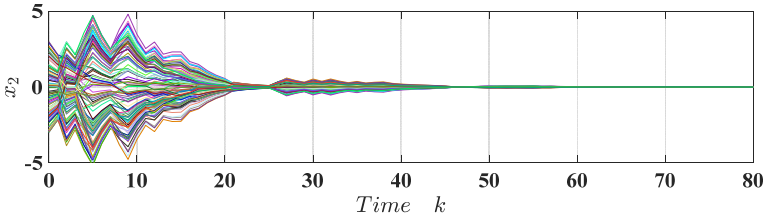

(b) Evolution of x_2

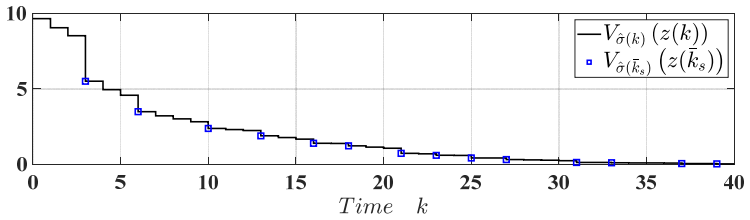

(c) Lyapunov function

Figure 4.3: Verification of the non-conservative global exponential stability conditions of the nominal system (4.3). (a)-(b) State trajectories with 100 randomly generated admissible PDT switching sequences. (c) The Lyapunov function $V_{\hat{\sigma}(k)}(z_k)$ along one sequence.

that they are infeasible in the case of $\tau = T = L = 1$, but feasible in the case of $\tau = T = 1, L \geq 2$. This demonstrates that the considered switched system is GES under arbitrary switching, which is obviously non-conservative in Example 4.3. However, it is always infeasible to solve the widely-used QTD stability conditions, whatever the tuning parameters are. This also verifies Remark 4.2, i.e., the QTD stability conditions are sufficient to this example even if we set $L = 1$.

Figure 4.3a and 4.3b show the system state trajectories with 100 randomly generated arbitrary switching sequences. The convergence demonstrates the system stability for $S_{\text{p-dwell}}[1, 1]$. Figure 4.3c shows one scenario of the 100 randomly generated cases, where the Lyapunov function (4.18) monotonously decreases with time instant k which is identical to (4.24).

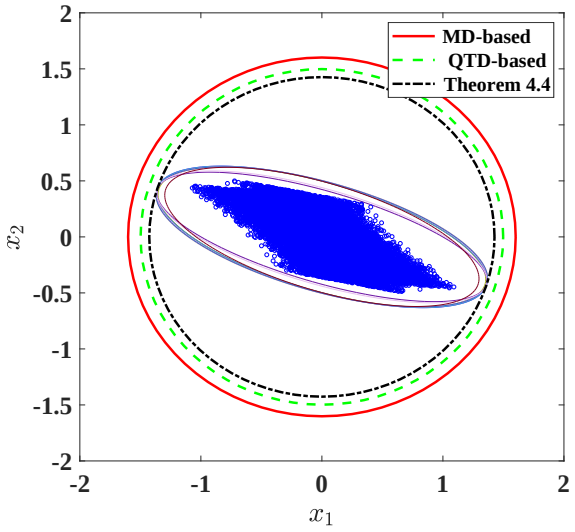

Figure 4.4: Reachable set estimated by MD, QTD methods, and Theorem 4.4. The union of all the ellipsoids is $\hat{\mathcal{R}}_e$. Blue circles denote the states of the closed-loop error system (4.4) with 50 randomly generated admissible PDT switching sequences.

Example 4.4. *Consider the switched linear system* (4.1) *with the following parameters [168]:*

$$A_1 = \begin{bmatrix} 1.5 & 1.2 \\ 0.8 & -0.6 \end{bmatrix}, A_2 = \begin{bmatrix} -0.3 & 1.3 \\ -1.1 & 1.2 \end{bmatrix},$$
$$B_1 = \begin{bmatrix} 0.2 & 0.3 \end{bmatrix}^T, B_2 = \begin{bmatrix} 0.1 & 0.7 \end{bmatrix}^T,$$
$$D_1 = \begin{bmatrix} 0.2 & -0.4 \end{bmatrix}^T, D_2 = \begin{bmatrix} -0.5 & 0.4 \end{bmatrix}^T, \bar{\omega} = 1.$$

Our objective here is to design controller gains (4.8) *and* (4.9) *and explore admissible* $S_{\text{p-dwell}}[\tau, T]$ *such that the composite system* (4.1) *and* (4.3) *is GES with a given set* $\mathcal{R} := \hat{\mathcal{R}}_e \times \{0\}$*, where* $\hat{\mathcal{R}}_e$ *containing all trajectories of error system* (4.4) *is the optimized solution.*

To address this problem, we split the disturbed system into the nominal and error systems in the forms of (4.3) and (4.4). Since the admissible PDT signal set for the composite system (4.1) and (4.3) is $S_{\text{p-dwell}}\left[\max\left(\tau_z, \tau_e\right), T\right]$, and the stabilization conditions (4.43)-(4.44) for the error system are more conservative with tuning parameter α than the conditions (4.29)-(4.30) for the nominal system, we will consider the error system first.

All the existing controller design conditions based on Lyapunov function approach

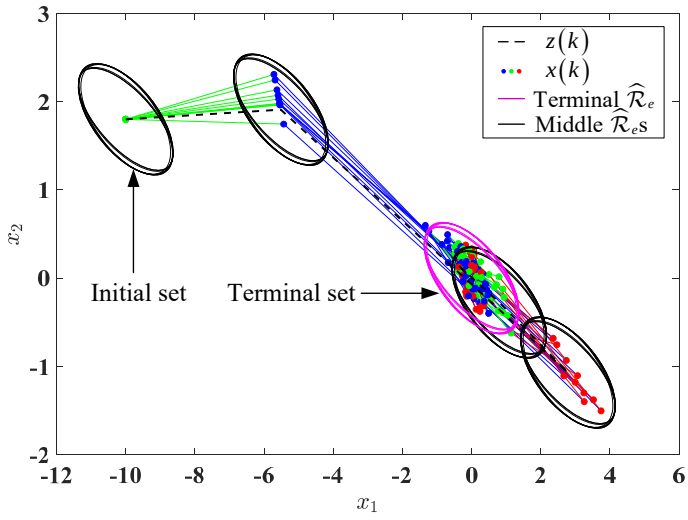

Figure 4.5: Stabilization of switched linear system (4.1) with bounded peak disturbances by the double clock-dependent control scheme.

for reachable set estimation, e.g., the mode-dependent and QTD ones, as well as Theorem 4.4 presented in this work, are nonconvex and in the form of BMIs [163–166,168]. Some efficient methods have been developed for BMIs optimization, such as iterative linear matrix inequality (LMI) approach or some numerical optimization algorithms like genetics algorithm, etc. As only one tuning parameter α is involved in Theorem 4.4, we use global searching algorithm here that repeatedly solves optimization problem (4.51) by changing α from 0.1 to 0.9 with searching step size of 0.1. For MD-based estimation approach, we use the same parameters listed in [168] which are optimized by genetics algorithm. For QTD-based estimation approach, we also use the global searching algorithm to explore the minimal ϵ by changing α from 0.1 to 0.9 and μ from 1.1 to 2.0 with searching step size of 0.1 [162, 169]. Note that the error system in Example 4.4 can be stabilized with arbitrary switching sequences. We intentionally take this example here for comparison because the MD-based method is infeasible if the switched system cannot be stabilized under arbitrary switching.

Figure 4.4 shows three $\mathcal{B}(0, \sqrt{\epsilon})$ with ϵ optimized by MD, QTD methods and Theorem 4.4, respectively. Our presented reachable set estimation method is the least conservative as it has the smallest $\mathcal{B}(0, \sqrt{\epsilon})$. Moreover, all the trajectories of the error system (4.4) always stay within $\hat{\mathcal{R}}_e$ also verifies the effectiveness of our proposed stabilization conditions in Theorem 4.4.

For the stabilization problem of the nominal system, we solve the LMI conditions (4.29)-(4.30), and further obtain the mode-dependent and clock-dependent con-

troller (4.8) under arbitrary switching. Suppose that $x_0 = [-10, 1.8]^{\mathrm{T}}$, and consider an arbitrarily admissible PDT switching sequence. Figure 4.5 shows the cluster of state trajectories of the disturbed system under 10 realizations. Three main observations and conclusions can be drawn from the figure:

i) The nominal trajectory z_k converges to the origin. This demonstrates that the presented offline clocks $\bar{\theta}_z(i)$ and $\hat{\theta}_z(i)$ can cover all cases of the online clock $\theta_z(k)$, i.e., the mismatch problem between the stability analysis and mode-activation and clock-dependent controller design is solved.

ii) All the disturbed system trajectories x_k always stay within the tube that centers at the nominal trajectory z_k with the cross section as $\hat{\mathcal{R}}_e$. This also verifies the effectiveness of the clock design among $\theta_e(k)$, $\bar{\theta}_e(i), \hat{\theta}_e(i)$. Moreover, this indicates that the double clock-dependent control scheme (the invariant set is replaced by the estimated reachable set of the error system compared to [160]) is effective.

iii) All the state trajectories of the composite system converges to the set $\mathcal{R} := \hat{\mathcal{R}}_e \times \{0\}$ under the designed controllers (4.8), (4.9) and admissible switching signal set $S_{\mathrm{p-dwell}}\left[\max\left(\tau_z, \tau_e\right), T\right]$. This solves the problem presented in Example 4.4.

To further verify the proposed design approach, we compute the values of the Lyapunov function $V_{\hat{\sigma}(k)}(z_k)$ of the closed-loop nominal system, as shown in Figure 4.6a. It monotonously decreases as the sampling time increases which verifies the effectiveness of Theorem 4.2. In addition, we also compute the values of (4.34) and (4.35) with 50 randomly generated admissible PDT switching sequences, as shown in Figure 4.6b. After we obtain the controller (4.9) by Theorem 4.4 and optimization problem (4.51), we can accordingly obtain the closed-loop error system, which is further used to compute (4.34) and (4.35). All the values in Figure 4.6b are smaller than 0, which also verifies the satisfaction of Theorem 4.4.

4.7 Conclusion

In this chapter, we investigate the stabilization problem for the PDT switched systems with bounded peak disturbances based on the error reachable set minimization. We present a novel framework, called double clock-dependent control scheme, that separates the stabilization problem of the disturbed system into two stabilization

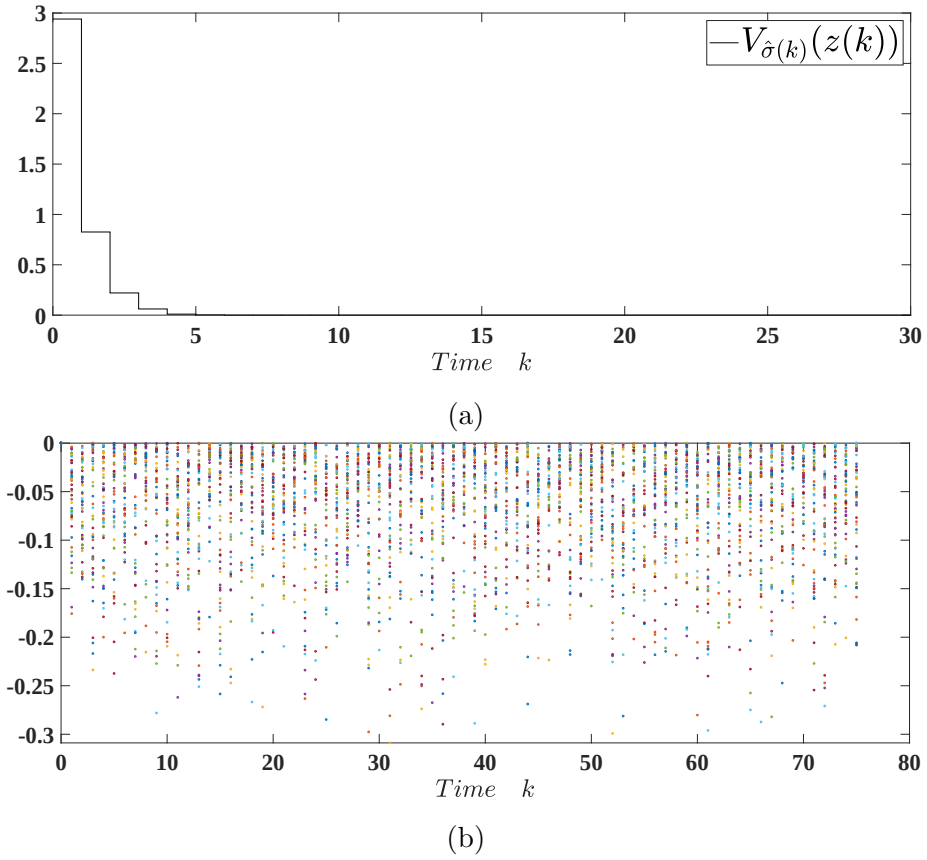

Figure 4.6: Verification of Theorem 4.2 and Theorem 4.4. (a) Evolution of Lyapunov function (4.18) for the closed-loop nominal system. (b) Values of (4.34) and (4.35) with 50 randomly generated admissible PDT switching sequences.

problems for the nominal and the error systems, respectively. A non-conservative stability criterion is presented such that the nominal system is globally exponentially stable, and a nominal-clock-dependent controller is accordingly designed. For the error system, we present the virtual-sequence-dependent reachable set minimization conditions, and also achieve an error clock-dependent controller. The disturbed system integrated with the double clock-dependent controllers are also proved to be globally exponentially stable within a tube whose cross section can be regarded as the over-approximation of the error system reachable set. Finally, the two numerical examples confirm the validity of the theoretical findings.

Chapter 5

A DMD-based MPC framework for unknown linear systems

In this chapter, a data-driven MPC framework is proposed. This framework utilizes the DMD methods as a data-driven predictor and implements the MPC to control the system. This work also guaranteed the theoretical properties of this framework, and the simulation results validate them.

5.1 Introduction

MPC has been widely deemed as a powerful model-based method to provide optimal control performance for constrained systems. Recently, a lightweight technique called DMD has been presented for characterizing system dynamics into a linear form in real-time. This section aims to develop a control framework with feasibility and stability guarantees for the first time, which embeds the DMD technique into data-driven MPC as a predictor. This framework can ensure the control properties for an unknown linear system that can handle this problem without offline data collection or calibration. Simulation examples validate the derived theoretical results and show that our data-driven method achieves comparable results to the standard tube-based robust MPC approaches.

The technical contributions of this section for addressing the above challenges are summarized as follows:

1) We develop a trimodal DMD-based MPC approach for a linear system with additive disturbances. We reformulate this system into a linear system with

multiplicative uncertainties, which well fits the DMD linear features.

2) We demonstrate the upper bound of the norm difference between the DMD-derived model and the real system, which paves a way for further control synthesis.

3) A trimodal control mechanism is developed to sufficiently utilize the DMD-induced adaptivity to the real-time measurements and reject the effect of the ill-conditioned system matrix.

4) We give a rigorous proof of the recursive feasibility and stability. Simulation examples show that the proposed trimodal DMD-based MPC (without knowing the model parameters) achieves comparable results to one of the standard tube-based RMPC (knowing the model parameters).

5.2 Problem formulation

In this section, we consider the LTI system with additive disturbances:

$$x_{k+1} = Ax_k + Bu_k + \omega_k, \tag{5.1}$$

where $x_k \in \mathbb{R}^{n_x}$ is the state vector, $u_k \in \mathbb{R}^{n_u}$ is the control vector, $w_k \in \mathbb{R}^{n_x}$ is the vector of bounded additive disturbances that satisfied $\|\omega_k\| \leq \omega_{max}$; the matrices of dynamics are $A \in \mathbb{R}^{n_x \times n_x}$, $B \in \mathbb{R}^{n_x \times n_u}$. The control objective of this problem is to drive the system to the origin point.

System (5.1) is subject to some mixed constraints

$$Fx_k + Gu_k \leq 1, \quad k = 0 \ldots \infty, \tag{5.2}$$

where $F \in \mathbb{R}^{n_x \times n_x}$ and $G \in \mathbb{R}^{n_x \times n_u}$ are the matrices of control and input constraints, respectively.

5.3 DMD-induced error analysis

A lot of significant data-driven modeling methods have been reported, such as Koopman operator [125], Gaussian process regression [170, 171], etc., but they are not suitable for the system without enough offline data. Recently, a real-time data-driven

method called DMD is developed to conquer this problem. Therefore, we implement the online DMD approach to predict the system dynamics matrices A and B in (5.1). The DMD algorithm can get the system dynamics in time by the snapshots of the states [172].

5.3.1 DMD control algorithm

The data snapshots with length m at time k ($k \geq m$) of system states and inputs are collected as:

$$\mathbf{X}_k := \begin{bmatrix} | & | & & | \\ x_{k-m}, & x_{k-m+2}, & \dots & x_{k-1} \\ | & | & & | \end{bmatrix},$$

$$\mathbf{X}'_k := \begin{bmatrix} | & | & & | \\ x_{k-m+1}, & x_{k-m+3}, & \dots & x_k \\ | & | & & | \end{bmatrix},$$

and

$$\boldsymbol{\Upsilon}_k := \begin{bmatrix} | & | & & | \\ u_{k-m}, & u_{k-m+2}, & \dots & u_{k-1} \\ | & | & & | \end{bmatrix},$$

respectively, where $\mathbf{X}'_k$ and $\mathbf{X}_k$ belongs to $\mathbb{R}^{n_x \times m}$, $\boldsymbol{\Upsilon}_k \in \mathbb{R}^{n_u \times m}$. According to the system dynamics (5.1), the snapshots of states can be expressed as $\mathbf{X}'_k = A\mathbf{X}_k + B\boldsymbol{\Upsilon}_k + \boldsymbol{\Omega}_k$, where $\boldsymbol{\Omega}_k = \begin{bmatrix} | & | & & | \\ \omega_{k-m}, & \omega_{k-m+2}, & \dots & \omega_{k-1} \\ | & | & & | \end{bmatrix}$ denotes the snapshot that collects all the disturbances. To predict the dynamic matrices, we denote the predicted models from DMD predictor as $\hat{A}_k$ and $\hat{B}_k$, and formulate them by the snapshots of system states and inputs as follows:

$$\mathbf{X}'_k = \hat{A}_k \mathbf{X}_k + \hat{B}_k \boldsymbol{\Upsilon}_k = \hat{\Pi}_k \boldsymbol{\Theta}_k,$$

where $\hat{\Pi}_k = [\hat{A}_k \;\; \hat{B}_k]$ represents the lifted dynamic matrix, and $\boldsymbol{\Theta}_k = \begin{bmatrix} \mathbf{X}_k \\ \boldsymbol{\Upsilon}_k \end{bmatrix}$ represents the corresponding data matrix.

To obtain the prediction of $\hat{\Pi}_k$, we need to calculate the pseudoinverse of $\boldsymbol{\Theta}_k$,

denoted by $\mathbf{\Theta}_k^\dagger$, which can be computed by the SVD method:

$$\mathbf{\Theta}_k \approx \hat{\mathbf{U}}_k \hat{\mathbf{\Sigma}}_k \hat{\mathbf{V}}_k^{\mathrm{T}},$$
$$\mathbf{\Theta}_k^\dagger \approx \hat{\mathbf{V}}_k \hat{\mathbf{\Sigma}}_k^{-1} \hat{\mathbf{U}}_k^{\mathrm{T}},$$

where $\hat{\mathbf{U}}_k^{\mathrm{T}} = \left[\hat{\mathbf{U}}_{k,1}^{\mathrm{T}}, \hat{\mathbf{U}}_{k,2}^{\mathrm{T}}\right]^{\mathrm{T}}$. The matrices $\hat{\mathbf{U}}_k \in \mathbb{R}^{(n_x+n_u)\times r}$ and $\hat{\mathbf{V}}_k \in \mathbb{R}^{m\times r}$ are unitary, and $\hat{\mathbf{\Sigma}}_k = \mathrm{diag}(\sigma_1, \sigma_2, \ldots, \sigma_r)$ is diagonal, where $(\sigma_1, \sigma_2, \ldots, \sigma_r)$ represents all singular values of $\mathbf{\Theta}_k$, and the scalar r is the rank of the SVD truncation. Thus, $\hat{\Pi}_k$ can be expressed as

$$\hat{\Pi}_k \approx \mathbf{X}_k' \mathbf{\Theta}_k^\dagger = \mathbf{X}_k' \hat{\mathbf{V}}_k \hat{\mathbf{\Sigma}}_k^{-1} \hat{\mathbf{U}}_k^{\mathrm{T}},$$

and the matrices of the system dynamics are estimated as

$$\hat{A}_k = \mathbf{X}_k' \hat{\mathbf{V}}_k \hat{\mathbf{\Sigma}}^{-1} \hat{\mathbf{U}}_{k,1}^{\mathrm{T}}, \ \hat{B}_k = \mathbf{X}_k' \hat{\mathbf{V}}_k \hat{\mathbf{\Sigma}}_k^{-1} \hat{\mathbf{U}}_{k,2}^{\mathrm{T}} \tag{5.3}$$

with $\hat{\mathbf{U}}_{k,1} \in \mathbb{R}^{n_x\times r}$ and $\hat{\mathbf{U}}_{k,2} \in \mathbb{R}^{n_u\times r}$. Therefore, the estimated system dynamics with DMD predictor is given as

$$x_{k+1} \approx \hat{\Pi}_k \theta_k = \hat{A}_k x_k + \hat{B}_k u_k, \tag{5.4}$$

where $\theta_k = \begin{bmatrix} x_k \\ u_k \end{bmatrix} \in \mathbb{R}^{(n_x+n_u)}$.

5.3.2 DMD regression error analysis

After a collection of m steps system data with a default system input, the controller can be designed according to $\widehat{\Pi}_k$, but it is hard to ensure the robustness of the controller under the additive disturbances. In order to design a robust controller for the system (5.1), we need to evaluate the mismatch between the DMD predictor $\widehat{\Pi}_k = [\hat{A}_k, \hat{B}_k]$ and $\Pi = [A, B]$, and represent it using a polygonal set. In this subsection, an uncertainty set is constructed to handle this problem.

Let the system run several extra steps m' controlled by a feedback control law $u_k = K_k x_k$, where K_k can be obtained by the LQR algorithm at time k from the $\widehat{\Pi}_k$. Therefore, we can gather the error between the actual system state x_{k+1} from (5.1) and the predicted one $\hat{x}_{k+1}$ from (5.4). Denote the error of the state at time k as

$$e_{k+1} = \hat{x}_{k+1} - x_{k+1} = \left(\widehat{\Pi}_k - \Pi\right) \theta_k - \omega_k. \tag{5.5}$$

Since the disturbance ω_k for all $k = 1, 2, \ldots$ are bounded, the (5.5) is induced to

$$\omega_k = \left(\widehat{\Pi}_k - \Pi\right)\theta_k - e_{k+1} \in \Omega, \tag{5.6}$$

which illustrates the bound of the difference between the mismatch of the DMD predictor and the state error. Then we can use this relationship to denote the error set Δ at time k as

$$\Delta = \left\{\Pi \mid \widehat{\Pi}_k\theta_k - e_{k+1} - \Pi\theta_k \in \Omega, \text{ for } k \in [m+1, M]\right\}, \tag{5.7}$$

where $M = m + m'$ indicates all time instants for preparation. Considering that the uncertainty set Δ in (5.7) consists of $p = n_x \times (n_x + n_u)$ elements, at least $(p+1)$ linearly independent constraints should be constructed to ensure Δ is closed. Thus, assume there are n_Ω linear constraints of Ω, and m' is at least $\lceil (p+1)/n_\Omega \rceil$ steps to ensure Δ is closed.

Then the center C of the uncertainty set Δ is defined as the nominal system for the controller design since the Chebyshev center is the most secure point we are looking for when the region is surrounded by a bunch of lines, i.e., the polyhedron. Meanwhile, the Π_k is not ensured to belong to Δ.

In order to explain how to construct the uncertainty set Δ, a numerical example is given to illustrate how to collect data and compute Δ.

Example 5.1. *Consider the following discrete-time LTI system for testing:*

$$A = \begin{bmatrix} -1.0500 & 0.2250 \\ -0.5250 & -0.9000 \end{bmatrix}, \quad B = \begin{bmatrix} 0.1 \\ 1 \end{bmatrix},$$
$$\mathcal{W} = \{\omega \mid \|\omega\|_\infty \leq \omega_{max}, \omega_{max} = 0.02\}.$$

The constraints of states and inputs are given as follows:

$$\|x_1\|_\infty \leq 10, \quad \|u\|_\infty \leq 2.$$

The weighting matrices for LQR are selected as $Q = [1, 0; 0, 1]$ *and* $R = 1$. *The system dynamics*

$$\Pi = [A, B] = \begin{bmatrix} a_{11} & a_{12} & b_1 \\ a_{21} & a_{22} & b_2 \end{bmatrix}$$

contain 6 *variables that need to be predicted and evaluated, so at least* 7 *constraints*

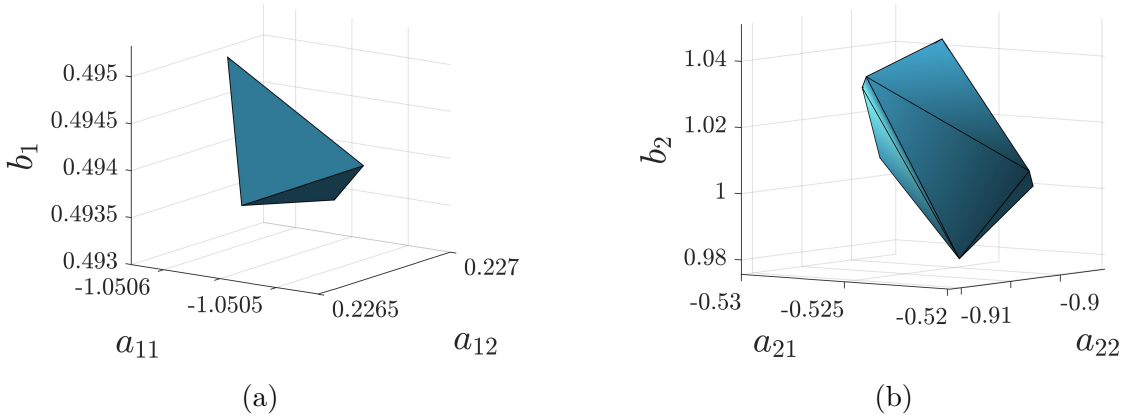

Figure 5.1: Visualization of uncertainty set Π. (a) Dimension 1 of Π: $\pi_1 = [a_{11}, a_{12}, b_1]$, (b) Dimension 2 of Π: $\pi_2 = [a_{21}, a_{22}, b_2]$.

are required. The length of snapshots is $m = 10$. *Due to* $n_x = 2, n_u = 1$, *and* $\theta_k \in \mathbb{R}^3$, *each step will generate* 3 *pairs of constraints (each pair of constraints are linear correlation, and constraints from different pairs are linearly independent), thus, it needs no less than* $m' = 3$ *more steps to bound the uncertainty set.*

Therefore, the uncertainty set of the Π *at* $M = m + m'$ *is constructed, and the projections in 3D are shown in Figure 5.1. The Figure 5.1(a) shows the first row of* Π *including* $[a_{11}, a_{12}, b_1]$ *and the Figure 5.1(b) shows the second row of* Π *including* $[a_{21}, a_{22}, b_2]$.

The proposed control scheme is shown in Figure 5.2. When the system starts, it will run m steps to collect the first snapshot for the initialization of the DMD predictor and calculation of the error set Δ. Then, the decision maker will choose the control mode according to if the $[\hat{A}_k \;\; \hat{B}_k]$ belongs to Δ and if x_k belongs to the RPI. The details about the trimodal scheme design will be introduced in Section 5.4.

5.4 DMD-based MPC algorithm

Although the considered system is an LTI system with additive disturbances, the DMD predictor cannot discriminate the disturbances and obtain explicit system dynamics. To design the robust controller for this system, we reformulate the additive disturbances as the multiplicative uncertainties, and propose a trimodal control scheme to handle this problem.

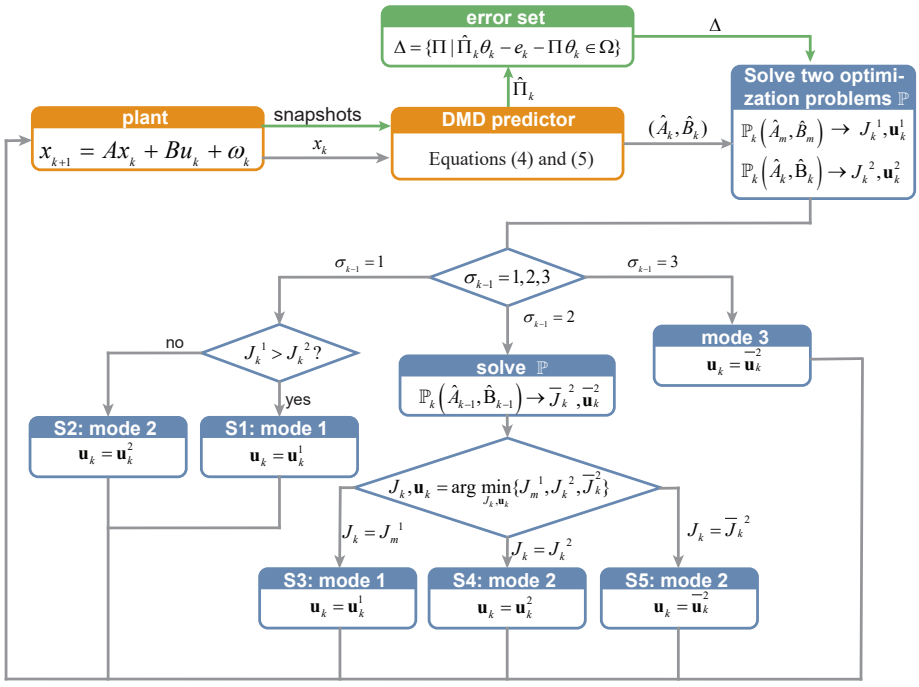

Figure 5.2: The roadmap the trimodal DMD-based MPC control scheme with the error set.

5.4.1 Tube construction

To deal with this system with constraints, a tube is constructed in this section. For mode 1, the system dynamics are

$$(\hat{A}_k, \hat{B}_k) \in (A, B) + \frac{1}{2}\mathcal{D} \in (\hat{A}_m, \hat{B}_m) + \mathcal{D}. \tag{5.8}$$

The robust MPC control law is designed in a trimodal controller as follows

$$u_k = \begin{cases} K_k x_k + c_k, & k = m \dots N-1 \text{ and } d_k \le \delta, \quad (5.9a) \\ K_m x_k + c_k, & k = m \dots N-1 \text{ and } d_k > \delta, \quad (5.9b) \\ K_m x_k, & k = N \dots \infty, \quad (5.9c) \end{cases}$$

where $c_k \in \mathbb{R}^{n_u}$ is denoted as the decision variable of the optimization problem, K_k represents the feedback control law at time k, and N is the prediction horizon of the MPC. It is supposed that the controller K can stabilize the system (5.1), and can be optimized by the linear quadratic regulator (LQR). Denote the matrix $\Phi_k = \hat{A}_k + \hat{B}_k K_k$ as the closed-loop system dynamics, so the system evolves at time

k according to

$$x_{i+1|k} = \begin{cases} \Phi_k x_{i|_k} + B_k c_{i|k}, & \text{if } \ i = 0 \dots N-1 \quad (5.10a) \\ \Phi_k x_{i|_k}, & \text{otherwise.} \quad (5.10b) \end{cases}$$

To ensure the robustness of the control scheme, the tube-based MPC is implemented. Inspired by the previous work introduced in [73, Chapter 5], we consider series of polytopic cross sections $\left\{\mathcal{X}_{0|k}, \mathcal{X}_{1|k}, \dots, \mathcal{X}_{N|k}\right\}$ as tubes, and define them by linear inequalities:

$$\mathcal{X}_{i|k} \coloneqq \{x : Vx \leq \gamma_{i|k}\}, \tag{5.11}$$

where the matrix $V \in \mathbb{R}^{n_v \times n_x}$ is a full-rank matrix chosen offline according to the system dynamics, and $\alpha_{i|k}, i = 1, \dots, N$ are vectors that will be updated in the online optimization process. To illustrate the constraints of the tube in the linear form, Farkas' lemma is introduced as follows:

Lemma 5.1. *[73] Define two sets as $S_i = \{x | F_i x \leq b_i\}, i = 1, 2$. Then we can have $S_1 \subseteq S_2$ if and only if there exists a matrix $H \succeq 0$ such that*

$$HF_1 = F_2, \quad Hb_1 \leq b_2. \tag{5.12}$$

To construct proper series of tubes, the following proposition is presented to make sure that $x_{i+1|k} \in \mathcal{X}_{i+1|k}$ for all $x_{i|k} \in \mathcal{X}_{i|k}$.

Proposition 5.1. *According to the system dynamics in Eq. (5.10) and Lemma 5.1, $x_{i+1|k} \in \mathcal{X}_{i+1|k}$ is true for all $x_{i|k} \in \mathcal{X}_{i|k}$ if there exist matrices $H^{(j)} \succeq 0$ such that*

$$H^{(j)} = V\Phi^{(j)}, \tag{5.13a}$$

$$\gamma_{i+1|k} \geq H^{(j)}\gamma_{i|k} + VB^{(j)}c_{i|k}, i = 0, \dots, N-1, \tag{5.13b}$$

$$\gamma_{i+1|k} \geq H^{(j)}\gamma_{i|k}, i = N, \dots, \infty. \tag{5.13c}$$

Proof. From (5.11), the tube cross sections are given as $\mathcal{X}_{i|k} = \{x : Vx \leq \gamma_{i|k}\}$ and $\mathcal{X}_{i+1|k} = \{x : Vx \leq \gamma_{i+1|k}\}$. Suppose that there are matrices $H^{(j)} \succeq 0$ and the $\mathcal{X}_{i|k}$ can be written as

$$\begin{aligned} S_1 : \quad & Vx_{i|k} \leq \gamma_{i|k}, \\ & H^{(j)}Vx_{i|k} \leq H^{(j)}\gamma_{i|k}. \end{aligned} \tag{5.14}$$

From (5.10a) for time instants $i = 0, \ldots, N-1$, the $\mathcal{X}_{i+1|k}$ can be expressed as

$$\begin{aligned} S_2: \quad & V(\Phi_k x_{i|_k} + B_k c_{i|k}) \leq \gamma_{i+1|k}, \\ & V\Phi_k x_{i|_k} \leq \gamma_{i+1|k} - VB_k c_{i|k}. \end{aligned} \tag{5.15}$$

As shown in Lemma 5.1, the conditions in (5.13a) and (5.13b) must hold. From (5.10b), for time $i = N, \ldots, \infty$, the set in (5.11) leads to the condition (5.13c) following the similar derivations. This completes the proof. □

In addition, we need to guarantee that all the states and inputs in the tube satisfy their constraints. Therefore, Proposition 5.2 is proposed.

Proposition 5.2. *According to the control sequence* (5.9) *and Lemma 5.1, the constraints* (5.2) *are always satisfied when* $x_{i|k} \in \mathcal{X}_{i|k}$ *there exsits a matrix* $H_c \succeq 0$ *such that*

$$H_c V = (F + GK), \tag{5.16a}$$

$$H_c \gamma_{i|k} + G c_{i|k} \leq 1, \quad i = 0, \ldots, N-1, \tag{5.16b}$$

$$H_c \gamma_{i|k} \leq 1, \quad i = N, \ldots, \infty. \tag{5.16c}$$

Proof. Suppose that there exists a matrix $H_c \succeq 0$, and we can represent the tube cross section as

$$\begin{aligned} S_3: \quad & V x_{i|k} \leq \gamma_{i|k}, \\ & H_c V x_{i|k} \leq H_c \gamma_{i|k}. \end{aligned} \tag{5.17}$$

Then the constraints (5.2) for time instants $i = 0, \ldots, N-1$ can be expressed as

$$\begin{aligned} S_4: \quad & F x_{i|_k} + G(K_m x_{i|_k} + c_{i|_k}) \leq 1, \\ & (F + GK_m) x_{i|_k} \leq 1 - G c_{i|_k}. \end{aligned} \tag{5.18}$$

using the control sequence (5.9). As shown in Lemma 5.1, to assure $S_3 \subseteq S_4$, the conditions in (5.16a), and (5.16b) need to be satisfied. For time $i = N, \ldots, \infty$, the set in (5.11) leads to the condition (5.16c) following the similar derivations. So this completes the proof. □

The matrices $H^{(j)}$ and H_c can be determined offline by solving the linear programs and the constraints depend on the variables $\gamma_{i|k}$.

5.4.2 Terminal sets construction

Denote the terminal set for the mode 3 of states as $\mathcal{X}_N = \{x : Vx \leq 1\}$ which is λ-contractive for $\lambda \in [0, 1)$. It can be chosen as the maximal RPI set for the system $x_{k+1} = (1/\lambda)\Phi_m x_k$.

Proposition 5.3. *If the $\mathcal{X}_N$ is λ-contractive for $\lambda \in [0, 1)$, then the bound*

$$\lim_{k\to\infty} \sup \|Vx_k\|_\infty \leq \frac{1}{1-\lambda} \sup_{k\geq 0} \|VB^{(j)} c^*_{0|k}\|_\infty \tag{5.19}$$

holds along the states trajectory (5.10) with the sequence of optimized results $\{c^*_{0|0}, c^*_{0|1}, \ldots, c^*_{0|k}\}$.

Proof. If $\mathcal{X}_N$ is λ-contractive for $\lambda \in [0, 1)$, it holds

$$\left\|V\Phi^{(j)}x\right\|_\infty \leq \lambda \|Vx\|_\infty, \quad j = 1, \ldots, m.$$

By Eq. (5.10a), we can obtain

$$\begin{aligned}
\|Vx_{k+1}\|_\infty &= \|V\Phi_k x_k + B_k c^*_{0|k}\|_\infty \\
&\leq \|V\Phi_k x_k\|_\infty + \|B_k c^*_{0|k}\|_\infty \\
&\leq \lambda \|Vx_k\|_\infty + \max_j \|B^{(j)} c^*_{0|k}\|_\infty \\
&\leq \lambda^{k+1} \|Vx_0\|_\infty + \sum_{i=0}^{k} \lambda^{k-i} \max_j \|B^{(j)} c^*_{0|i}\|_\infty.
\end{aligned}$$

Since $\lambda^k = 0$ when $k \to \infty$, the upper bound can be expressed as (5.19). This completes the proof. □

Inequalities (5.13c) and (5.16c) represent constraints of the terminal set. When the states enter the RPI set, the control is set as $c_{i|k} = 0,\ i \geq N$ and the tubes can be indicated by the dynamic of the parameter $\gamma_{i|k}$ as a trajectory $\{\gamma_{N|k}, \gamma_{N+1|k}, \ldots\}$. The dynamics can be formulated by a linear programming problem

$$(\gamma_{i+1|k})_l = \max_{j\in\{1,\ldots,m\}} H_l^{(j)} \gamma_{i|k}, \quad l = 1, \ldots, n_d, \tag{5.20}$$

where l indicates the number of rows of vectors and matrices. According to this equation, the invariant set of γ can be determined and its stability is ensured if the terminal set of states is λ-contractive. This is shown in the Lemma 5.2.

Lemma 5.2. *[73] If the set is λ-contractive for some $\lambda \in [0,1)$ under a specific dynamic (5.10), then $\left\|\gamma_{i+1|k}\right\|_\infty \leq \lambda \left\|\gamma_{i|k}\right\|_\infty$ is satisfied for all i under the dynamic Eq. (5.20), $i \geq N$.*

The maximal RPI set for the parameter γ is denoted as $\gamma_{N|k} \in \Gamma$. It is shown that the RPI set always exists and it can be calculated by several steps of iteration [73]. A simpler way to represent the RPI set is using the terminal constraints

$$\gamma_{N|k} \geq H^{(j)}\gamma_{N|k}, j = 1, \ldots, n_d, \tag{5.21a}$$

$$H_c\gamma_{N|k} \leq 1. \tag{5.21b}$$

5.4.3 Optimization problem

Denote the vector of decision variables as $\mathbf{c}_k = [c_0^{\mathrm{T}}, c_1^{\mathrm{T}}, \ldots, c_{N-1}^{\mathrm{T}}]^{\mathrm{T}}$ and $\mathbf{s}_k = [s_0^{\mathrm{T}}, s_1^{\mathrm{T}}, \ldots, s_{N-1}^{\mathrm{T}}]^{\mathrm{T}}$. Then the transformed matrices, denoted as E and M, satisfy $c_{0|k} = E\mathbf{c}_k$ and $\mathbf{c}_{k+1} = T\mathbf{c}_k = [c_1^{\mathrm{T}}, \ldots, c_{N-1}^{\mathrm{T}}, 0]^{\mathrm{T}}$. The prediction of the system state can be expressed as $\zeta_{i+1|k} = \Psi_k\zeta_{i|k}$ for $i = 0, 1, \ldots$ where the prediction state is denoted as $\zeta_{0|k}^{\mathrm{T}} = [s_{0|k}^{\mathrm{T}}, \mathbf{c}_k^{\mathrm{T}}]^{\mathrm{T}}$, and the transition matrix is given by $\Psi_k = \begin{bmatrix} \Phi_k & BE \\ 0 & M \end{bmatrix}$.

The cost function of the optimization problem for MPC is denoted as

$$J_k = \sum_{i=0}^{\infty} (\|s_{i|k}\|_Q^2 + \|v_{i|k}\|_R^2), \tag{5.22}$$

where $Q \succeq 0$ and $R \succeq 0$ are predesigned penalty matrices. By the control policy (5.9), we can reformulate the cost function by the matrix

$$\hat{Q} = \begin{bmatrix} Q + K_k^{\mathrm{T}} R K_k & K_k^{\mathrm{T}} R E \\ E^{\mathrm{T}} R K_k & E^{\mathrm{T}} R E \end{bmatrix}$$

as

$$J_k = \sum_{i=0}^{\infty} \zeta_{i|k}^{\mathrm{T}} \hat{Q}_k \zeta_{i|k} = \zeta_{0|k}^{\mathrm{T}} W_k \zeta_{0|k},$$

where W_k is the solution of the Lyapunov equation

$$W_k = \Psi_k^{\mathrm{T}} W \Psi_k + \hat{Q}. \tag{5.23}$$

As a result, the optimization problem of the DMD-based MPC can be formulated

as

$$\mathbb{P}_k: \quad \min_{s_{0|k},\mathbf{c}_k} \; J_k = \zeta_{0|k}^{\mathrm{T}} W_k \zeta_{0|k} \tag{5.24a}$$

$$\text{s.t.} \quad V s_{0|k} \leq \gamma_{0|k}, \tag{5.24b}$$

$$V x_k \leq \gamma_{0|k}, \tag{5.24c}$$

$$(5.13b), (5.16b), (5.21a), (5.21b).$$

The constraint (5.24c) introduces the initial condition, and constraints (5.21a) and (5.21b) guarantee the terminal condition. The constraint (5.13b) guarantees the existence of the tube, and (5.16b) guarantees state and input constraints.

5.4.4 Trimodal DMD-based MPC algorithm

Firstly, the system will run $m-1$ steps in advance to collect the snapshots of states. From the m-th step, it will update the system dynamics by the DMD predictor. Then it will calculate the control input based on current mode and implement it to the system. This trimodal DMD-based MPC algorithm is summarized in Algorithm 1, and the corresponding control scheme is shown in Figure 5.2.

5.5 Theoretical analysis

Theorem 5.1. *Algorithm 1 is recursive feasible if there exists a feasible solution at the initial time instant.*

Proof. Note that the optimization problem in Algorithm 1 is convex, the constraints in (5.2) are compact and contain the origin.

Suppose system is at mode 1 at time k. Thus, if the problem $\mathbb{P}_k(\hat{A}_m, \hat{B}_m)$ has a feasible solution, then there must exist an optimal solution, which further implies that there exists an optimal trajectory $\boldsymbol{\gamma}_k^*$, $\mathbf{c}_k^*$, and $s_{0|k}^*$ as follows:

$$\boldsymbol{\gamma}_k^* = \{\gamma_{0|k}^*, \gamma_{1|k}^*, \ldots, \gamma_{N|k}^*\},$$
$$\mathbf{c}_k^* = \{c_{0|k}^*, c_{1|k}^*, \ldots, c_{N-1|k}^*\}.$$

To demonstrate the recursive feasibility of Algorithm 1, we first construct a set of

feasible solutions for the optimization problem $\mathbb{P}_{k+1}(\hat{A}_m, \hat{B}_m)$ by:

$$\begin{aligned}\tilde{\boldsymbol{\gamma}}_{k+1} &= \{\tilde{\gamma}_{0|k+1}, \tilde{\gamma}_{1|k+1}, \ldots, \tilde{\gamma}_{N|k+1}\} \\ &:= \{\gamma^*_{1|k}, \ldots, \gamma^*_{N|k}, \tilde{\gamma}_{N|k+1}\}, \qquad (5.25a)\\ \tilde{\mathbf{c}}_{k+1} &= \{\tilde{c}_{0|k+1}, \tilde{c}_{1|k+1}, \ldots, \tilde{c}_{N-1|k+1}\} \\ &:= \{c^*_{1|k}, \ldots, c^*_{N-1|k}, \tilde{c}_{N-1|k+1}\}, \qquad (5.25b)\end{aligned}$$

where $\tilde{\gamma}_{N|k+1}$ and $\tilde{c}_{N-1|k+1}$ must satisfy:

$$\begin{aligned}\tilde{\gamma}_{N|k+1} &\geq H^{(j)}\tilde{\gamma}_{N-1|k+1} + VB^{(j)}\tilde{c}_{N-1|k+1}, \\ &\qquad j = 0, \ldots, m, \qquad (5.26a)\\ H^{(j)}\tilde{\gamma}_{N|k+1} &\leq \tilde{\gamma}_{N|k+1}, \qquad (5.26b)\\ H_c\tilde{\gamma}_{N|k+1} &\leq 1. \qquad (5.26c)\end{aligned}$$

Here, we set $\tilde{c}_{N-1|k+1}$ to 0 because the $(N-1)$th state at $k+1$ must belong to RPI set. Hence, the constraint in (5.26a) becomes $\tilde{\gamma}_{N|k+1} \geq H^{(j)}\tilde{\gamma}_{N-1|k+1}$ which holds by selecting $\tilde{\gamma}_{N|k+1} = \max_{j=1,2,\ldots,m} H^{(j)}\gamma^*_{N|k}$. According to Lemma 2, it follows $\tilde{\gamma}_{N|k+1} \in \Gamma$ and thus constraints in (5.26b)-(5.26c) naturally hold.

On the other hand, at time k, the system is at mode 2 and the problem $\mathbb{P}_k(\hat{A}_k, \hat{B}_k)$ has a feasible solution. Then, similarly to the previous condition, we can find a set of feasible solutions for the optimization problem for $\mathbb{P}_{k+1}(\hat{A}_k, \hat{B}_k)$

Hence, the recursive feasibility of Algorithm 1 is guaranteed. This completes the proof. □

Theorem 5.2. *The system (5.1) is asymptotically stable if the Algorithm 1 has a feasible solution at time* 0.

Proof. According to the system dynamics (5.9) and the system mode changing principles presented in Algorithm 1, the stability of the control scheme is proved in two folds and five scenarios.

Suppose the current time instant is k, and the system mode at $k-1$ is $\sigma_{k-1} = 1$,and the system matrices are $(\hat{A}_m, \hat{B}_m)$. Then, two kinds of scenarios are discussed.

S1: In S1, the system dynamics are kept in mode 1 from $k-1$ to k, and the weighting matrix remains $W_k = W_{k-1}$. when the system evolves, the system cost

decreases since

$$\begin{aligned} J_k^1 - J_{k-1}^1 &= \zeta_{0|k}^{\mathrm{T}} W_k \zeta_{0|k} - \zeta_{0|k-1}^{\mathrm{T}} W_{k-1} \zeta_{0|k-1} \\ &= \zeta_{0|k-1}^{\mathrm{T}} \left(\Psi_{k-1}^{\mathrm{T}} W_k \Psi_{k-1} - W_k \right) \zeta_{0|k-1}. \end{aligned}$$

As a result, Eq. (5.23) guarantees that

$$J_k^1 < J_{k-1}^1. \tag{5.27}$$

S2: In S2, the system dynamics varies to mode 2 from $k-1$ to k. In Algorithm 1, it is satisfied that $J_k^2 < J_k^1$, and considering (5.27), we can have $J_k^2 < J_{k-1}^1$, which means the system cost decreases in S2.

On contrary, when the system mode at $k-1$ is $\sigma_{k-1} = 2$, then three other kinds of scenarios are discussed. Since the system is at mode 2 in last time instant, the system cost of system $(\hat{A}_{k-1}, \hat{B}_{k-1})$ satisfies $\bar{J}_k^2 < \bar{J}_{k-1}^2$ due to

$$\begin{aligned} \bar{J}_k^2 - \bar{J}_{k-1}^2 &= \zeta_{0|k}^{\mathrm{T}} W_k \zeta_{0|k} - \zeta_{0|k-1}^{\mathrm{T}} W_{k-1} \zeta_{0|k-1} \\ &= \zeta_{0|k-1}^{\mathrm{T}} \left(\Psi_{k-1}^{\mathrm{T}} W_k \Psi_{k-1} - W_{k-1} \right) \zeta_{0|k-1}, \end{aligned}$$

where $W_k = W_{k-1}$ because they have the same system dynamics. Then, according to Eq. (5.23), we can have

$$\bar{J}_k^2 - \bar{J}_{k-1}^2 < 0. \tag{5.28}$$

S3: In S3, the relationship $J_k^1 < \bar{J}_k^2$ holds because in the algorithm the J_k^1 is the minimal cost. Due to (5.28), the cost relationship is $J_k^1 < \bar{J}_{k-1}^2$, which means it is decreasing from $k-1$ to k.

S4: In S4, the relationship $J_k^2 < \bar{J}_k^2$ holds. Similarly to S3, according to (5.28), the cost also decreases since $J_k^2 < \bar{J}_{k-1}^2$.

S5: In S5, the system dynamics does not change and Eq. (5.28) ensures the decreasing of the cost from $k-1$ to k.

Hence the system in (5.1) is asymptotically stable. This completes the proof. □

Remark 5.1. *The proof of Theorem 5.2 is considered in two cases according to the condition of mode 1 and mode 2. When the system state switches between these two modes, the convergence will not be influenced.*

5.6 Simulation results

A numerical example is presented in this section to validate the derived algorithm and make comparisons to existing results.

Consider the following discrete-time LTI system for testing:

$$A = \begin{bmatrix} -1.0500 & 0.2250 \\ -0.5250 & -0.9000 \end{bmatrix}, \quad B = \begin{bmatrix} 0.1 \\ 1 \end{bmatrix}, \quad \omega_{max} = 0.02.$$

The constraints of states and inputs are $\|x\|_\infty \leq 10, \quad \|u\|_\infty \leq 2$. The weighting matrices are selected as $Q = [1, 0; 0, 1]$ and $R = 1$. The prediction horizon N is set to 15. The length of snapshots m is set to 10. The predefined inputs for the first m steps are $u_1 = u_2 = \ldots = u_m = 1.5$, and we find out that this control sequence does not violate any constraints. Set the λ-contractive parameter as $\lambda = 0.95$ and the tuning parameter μ of threshold δ as 1.

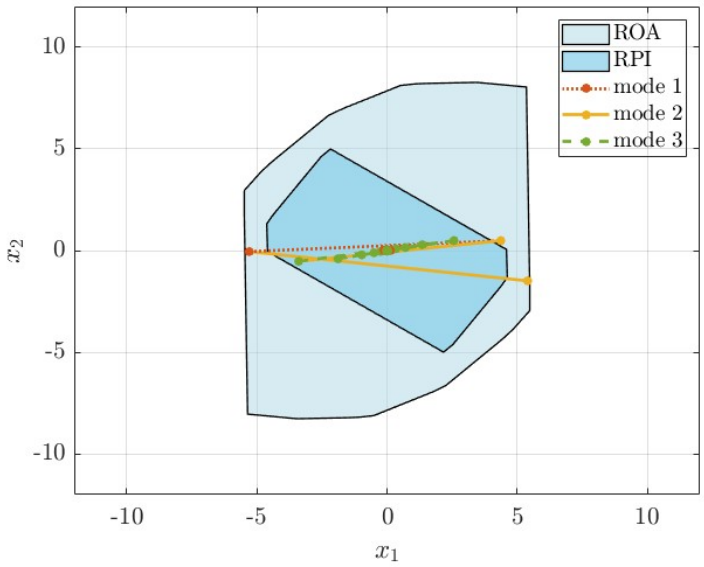

Figure 5.3: The ROA and RPI sets of the system under the trimodal control policy.

As shown in Figure 5.3, we depict the region of attraction (ROA) and RPI sets of the system identified at the m step (i.e., the dynamics described by A_m and B_m). It is checked that any state trajectory originating from ROA can enter RPI set within 18 steps. The initial state is chosen as $[5, 7]^{\mathrm{T}}$. We mark the open-loop operations, mode 1, mode 2, and mode 3 by blue, orange, yellow, green lines. We find out that the state trajectory enters RPI at the 16-th step (meeting the requirement of ROA

property) and thereafter always stays within RPI before finally converging to the equilibrium. This demonstrates the validity of our algorithm. Figure 5.4 displays the states and control inputs, which shows that both of the two trajectories satisfy the desired constraints.

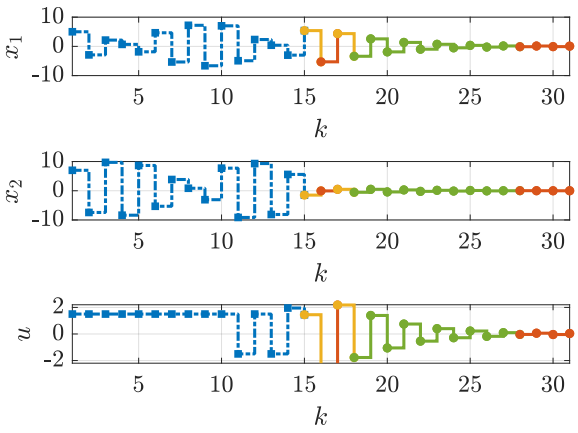

Figure 5.4: The state and input trajectories of the system starting from the preparation stage.

5.7 Conclusion

In this chapter, we present a novel data-driven MPC scheme based on the DMD predictor for the constrained LTI system with additive disturbances. The DMD predictor is applied to transfer the data of system states and inputs into a linear system dynamics. By evaluating the error of the DMD predictor, the additive disturbances are considered as multiplicative uncertainties, and a trimodal MPC framework is proposed to deal with this control problem. We have proved that the recursive feasibility of this DMD-based MPC scheme is ensured and the asymptotic stability is guaranteed. The numerical simulation is provided to demonstrate the efficacy of this control scheme and a comparison with the classical RMPC is made. The future research will concentrate on designing a control scheme for high-dimensional systems by the DMD-based MPC, fully releasing the dimensionality reduction power of the DMD predictor.

Algorithm 1 Trimodal DMD-based MPC algorithm

Input: The initial condition x_0, the bound of disturbance ω_{max}, and the state and input constraint matrices F and G. Weighting matrices Q and R, a proper input sequence $\boldsymbol{\Upsilon}_m$ and contractiveness number λ.

DMD preparation: Collect the first m steps snapshot of states $\mathbf{X}_m$, $\mathbf{X}'_m$ by $\boldsymbol{\Upsilon}_m$. Compute the initial system dynamics $\hat{A}_m$ and $\hat{B}_m$ by (5.3).

Uncertainty set: Collect m' steps of x_k and u_k and construct the error set Δ by (5.7), and the center of the error set Π_c.

Parameters setup: Calculate the mode 2 feedback gain K_c, the λ-contractive RPI set $\mathcal{Z}_\lambda$ and weighting matrix W_c. Construct the matrices H_c and $H^{(j)}$. Initialize system mode $\sigma_M = 1$.

while each time instant $k = M+1, \ldots$ **do**

  Compute the DMD regression system dynamics $\hat{A}_k$ and $\hat{B}_k$ by (5.3).

  Solve $\mathbb{P}_k\left(\hat{A}_m, \hat{B}_m\right)$ and $\mathbb{P}_k\left(\hat{A}_k, \hat{B}_k\right)$ to get $(J_k^1, \mathbf{u}_{\boldsymbol{k}}^1)$ and $(J_k^2, \mathbf{u}_{\boldsymbol{k}}^2)$, respectively.

  if $\mathbb{P}_k\left(\hat{A}_m, \hat{B}_m\right)$ and $\mathbb{P}_k\left(\hat{A}_k, \hat{B}_t\right)$ are solvable **then**

    if $\sigma_{k-1} = 1$ **then**

      if $J_k^1 \leq J_k^2$ **then**

        Let $\sigma_k = 1$, $\mathbf{u}_{\boldsymbol{k}}^* = \mathbf{u}_{\boldsymbol{k}}^1$, and remark this scenario as S1.

      else Let $\sigma_k = 2$, $\mathbf{u}_{\boldsymbol{k}}^* = \mathbf{u}_{\boldsymbol{k}}^2$, and remark this scenario as S2.

      end if

    else if $\sigma_{k-1} = 2$ **then**

      Solve $\mathbb{P}_k\left(\hat{A}_{k-1}, \hat{B}_{k-1}\right)$ to get $(\bar{J}_k^2, \bar{\mathbf{u}}_{\boldsymbol{k}}^2)$

      if $\arg_{J_k} \min\left(\bar{J}_t^2, J_t^1, J_t^2\right) = J_t^1$ **then**

        Let $\sigma_k = 1$, $\mathbf{u}_{\boldsymbol{k}}^* = \mathbf{u}_{\boldsymbol{k}}^1$, and remark this scenario as S3.

      else if $\arg_{J_k} \min\left(\bar{J}_t^2, J_t^1, J_t^2\right) = J_t^2$ **then**

        Let $\sigma_k = 2$, $\mathbf{u}_{\boldsymbol{k}}^* = \mathbf{u}_{\boldsymbol{k}}^1$, and remark this scenario as S4.

      else if $\arg_{J_k} \min\left(\bar{J}_t^2, J_t^1, J_t^2\right) = \bar{J}_t^2$ **then**

        Let $\sigma_k = 2$, $\mathbf{u}_{\boldsymbol{k}}^* = \bar{\mathbf{u}}_{\boldsymbol{k}}^2$, and remark this scenario as S5.

      end if

    end if

  end if

  Reformulate and solve the optimization problem $\mathbb{P}_k$

  Calculate the control input u_k by (5.9) and implement the first item into the system.

end while

Chapter 6

Scenario-based MPC (SCMPC) for obstacles avoidance

In previous chapters, some theoretical analyses about the stabilization and stability of switched systems, and the robustness of a data-driven hybrid system are discussed. In this chapter, a practical path planning problem for a stochastic system is considered and resolved by a novel SCMPC framework.

6.1 Introduction

Cyber physical system (CPS) represents a new generation of systems with computational and physical capabilities that also have connections with human beings [173]. A typical scenario in CPSs, such as autonomous path planning for multi vehicles [174–177], is to endow the physical vehicles intelligence so that they can operate in a more efficient manner.

One basic problem therein is how to regulate a collision-free path for the purpose of minimizing a cost function of interest. This problem can be classified into global and local planning. Several techniques have been reported for the path planning problem from a global perspective, such as Dijkstra's algorithm [178], A* algorithm [179], artificial potential field method [180], just to name a few. The flexibility of the global methods is limited due to the lack of real-time detection of the topography. On the other hand, the local methods, such as fuzzy logic [181] and particle swarm optimization algorithm [182], are applied to the path planning. Additionally, sampling-based methods such as Rapidly-exploring Random Trees (RRT) [183] and

Probabilistic Roadmaps (PRM) [184] are effective in high-dimensional spaces, allowing for dynamic obstacle avoidance by continuously updating the path in response to environmental changes. Furthermore, optimization-based techniques, such as the potential field method [185], enable real-time adjustments to the planned path, ensuring safety and efficiency in navigating around obstacles. However, these methods will lead to input saturation in practice since they often ignore the constraints of the model dynamics [186].

Among these techniques, MPC is a promising approach because it can explicitly handle constraints, take the model dynamics into consideration, and improve the performance by a large number of numerical optimization algorithms [187]. One typical method is to plan a path without consideration of system dynamics at first, and then use MPC to steer the vehicle to track the desired path [188]. In [189], a modified C/GMERS algorithm for fast nonlinear MPC is developed for an autonomous underwater vehicle, but a basic assumption of this kind of applications requires the planned path is appropriate that does not violate the physical limits of the vehicle. Another method that investigates model-based path planning by either using the nominal model [190] or disturbed model [191]. The constraints in these situations are commonly non-convex which need to be formulated to mixed-integer programming [190], linear polygonic case [191], or optimized by some other non-convex optimization algorithms [192].

On the other hand, probabilistic constraints are introduced to MPC on many practical applications, e.g., building climate control [193], energy management microgrids [194], autonomous vehicles [195], where the cost function of interest can be further minimized if some constraints are allowed to be violated with a guaranteed probability, i.e., a trade-off between the performance and the constraint satisfaction. Two typical methods to handle the probability constraints include tube-based SMPC [57] and SCMPC [69]. However, no researches have been targeting the path planning problem with probabilistic constraints to date. The main reason that prevents SMPC from working in path planning is that this algorithm requires the constraints to be linear, but constraints for obstacle avoidance cannot be simply formulated in a linear form. The obstacle avoidance is also challenging for SCMPC since a basic requirement of it is that the constraints must be convex, which, however, cannot be fulfilled in many cases.

Based on the above considerations, we investigate the path planning problem constrained by the obstacles with probabilistic safe distance. Different from the previous

literature, obstacle avoidance can be ensured with a predefined probability. The main contributions of this chapter are summarized as follows:

- We introduce a novel concept of candidate path that is used to describe possible paths of all the binary variables in the traditional MINLP optimization problem.
- We present a conditional scenario algorithm that can convert a non-convex MINLP optimization problem to a group of convex optimization problems and select the optimal one as the solution.
- We tackle the path planning problem with a guaranteed probability of obstacle avoidance. Simulation results verify the proposed theories and show how the target probability regulates the path.

6.2 Preliminaries and problem formulation

Consider a class of discrete-time linear stochastic system:

$$z_{k+1} = A(\delta_k) z_k + B(\delta_k) u_k + w(\delta_k), \tag{6.1}$$

where $z_k \in \mathbb{R}^n$ is the state vector and $u_k \in \mathbb{R}^m$ is the control input. The system is assumed initially at a known state z_0. The system is under additive disturbances $\omega(\delta_k)$ and multiplicative disturbances on state matrix $A(\delta_k) \in \mathbb{R}^{n\times n}$ and input matrix $B(\delta_k) \in \mathbb{R}^{m\times n}$. The matrices $A(\delta_k)$ and $B(\delta_k)$ are functions of a random uncertainty δ_k which satisfies the following Assumption 6.1. The constraints for the system state and the control input are as follows:

$$z_k \in \mathcal{X}, u_k \in \mathcal{U}, k = 0, 1, 2, \ldots \tag{6.2}$$

where $\mathcal{X}$ and $\mathcal{U}$ are convex sets.

Assumption 6.1. *[69] (Uncertainty)*

(a) The uncertainties $\delta_k \in \{\delta_0, \delta_1, \ldots\}$ are independent and identically distributed (i.i.d) random variables on a probability space $(\Delta, \mathbf{P})$.

(b) A "sufficient number" of δ_k can be obtained.

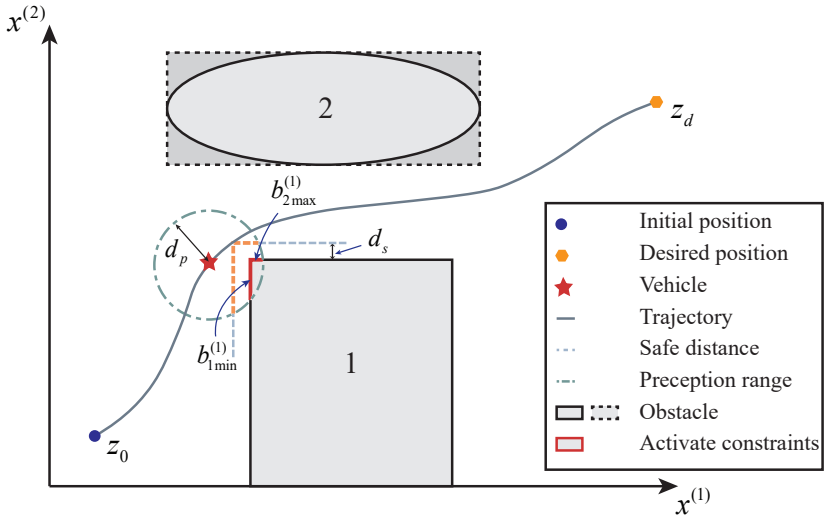

Figure 6.1: An illustration of the path planning problem with a probability of safe distance constraint violations.

Remark 6.1. *In Assumption 6.1, Δ is a support set of δ_k, and $\mathbf{P}$ is a probability measure on Δ. Assumption 6.1 also regulates that sufficient scenarios must be captured to fully reflect the true distribution of the uncertainties. Thus, an obvious advantage of the scenario-based uncertainty model is that it does not need to know the distribution information of δ_k a priori.*

Remark 6.2. *The "sufficient number" indicates twofold. It not only requires that we have the capability of repeatedly performing sufficient experiments to measure the unknown distribution information of the uncertainty, but also implies that the upper bound of constraints violation can be ensured only under condition of the sufficient numbers.*

The problem of interest in this section is illustrated in Figure 6.1. It shows a scenario in which a vehicle moves from the initial position z_0 to a desired position z_d and avoids crushing on obstacles 1 and 2. The vehicle has a circular perception range so that all the obstacles enter this range can be sensed by the vehicle. Denote the perception range of the vehicle as d_p. We also denote the minimum safe distance between the vehicle and the obstacles by d_s. It should be underscored that the "minimum" safe distance can be violated, i.e., the vehicle may regulate a "better" path (which has a lower cost function), but the price to pay is slight violation of the "minimum" safe distance. So we call this kind of constraints (that can be violated) as the probabilistic constraints. The term "slight" indicates that we can use the

probability to make a trade-off between path optimality and constraint satisfaction

Generally, the cost function of the vehicle is given as $\min_{u_k} \frac{1}{T} \sum_{k=0}^{T-1} \mathbb{E}\left[\ell\left(z_k, u_k\right)\right]$, where T denotes the running time of the vehicle; $\ell\left(z_t, u_t\right) = \|z_k - z_d\|_Q^2 + \|u_k\|_R^2$; Q and R are weighting matrices with appropriate dimensions. In the MPC scheme, the infinite horizon of cost function is reformulated over a small predicted time horizon $N \ll T$ and the cost function is shown as follows:

$$\min_{u_k} \sum_{k=0}^{N} \mathbb{E}\left[\ell\left(z_k, u_k\right)\right]. \tag{6.3}$$

For the simplicity of the analysis, we only consider the position and the velocity of the vehicle. Suppose that the state vector is $z_k = [x_k^{(1)}, x_k^{(2)}, \ldots, x_k^{(n)}, v_k^{(1)}, v_k^{(2)}, \ldots, v_k^{(n)}]^{\mathrm{T}}$ which represents the position and velocity of the vehicle, and the input vector is $u_k = [u_k^{(1)}, u_k^{(2)}, \ldots, u_k^{(m)}]^{\mathrm{T}}$ which means that we can directly control the velocity of the vehicle.

Conventionally, the constraints for obstacle avoidance on the path planning problem is formulated as a quadratic form like

$$\|z_k - o_i\|^2 \geq r + d_s, k = 0, 1, 2, \ldots; i = 0, 1, 2, \ldots$$

where o_i and r denote the center and the radius of the ith obstacle [192], respectively. This kind of obstacle formulation ignores the graphical shape of the obstacles and further yields a non-convex constraint to the optimization problem, which cannot guarantee the violation bound of SCMPC approach. Another approach is the MINLP [190]. The main idea of this approach is to take the graphic shape into consideration by the introduction of several binary variables. For the ith obstacle, denote its boundary as $b^{(i)}$, e.g., the term $b^{(1)}$ in Figure 6.1 is used to denote the obstacle 1. If it is not a rectangle, then we can use a polygon to cover it. However, for simplicity and without loss of generality, we use the minimum bounding rectangle of the non-rectangular obstacle as its boundaries, e.g., the dashed line of obstacle $b^{(2)}$ in Figure 6.1. Accordingly, we can construct the obstacle avoidance constraints as

follows:

$$
\begin{aligned}
x^{(1)} &\leq (b^i_{1\,\min} - d_s) + Mt_1 && \text{(6.4a)}\\
-x^{(1)} &\leq -(b^i_{1\,\max} - d_s) + Mt_2 && \text{(6.4b)}\\
x^{(2)} &\leq (b^i_{2\,\min} - d_s) + Mt_3 && \text{(6.4c)}\\
-x^{(2)} &\leq -(b^i_{2\,\max} - d_s) + Mt_4 && \text{(6.4d)}\\
&\vdots\\
x^{(n)} &\leq (b^{(i)}_{n\,\min} - d_s) + Mt_{2n-1} && \text{(6.4e)}\\
-x^{(n)} &\leq -(b^{(i)}_{n\,\max} - d_s) + Mt_{2n} && \text{(6.4f)}\\
\sum_{q=1}^{2n} t_q &\leq n-1, \quad t_q \in \{0,1\},\\
q &= 1,2,\ldots,2n;\ i = 0,1,2,\ldots,O
\end{aligned}
$$

where $(b^{(i)}_{1\,\min}-d_s)$, $(b^{(i)}_{1\,\max}+d_s)$, ... are the boundaries of the obstacles in its perception range d_s. Let M be a sufficiently large arbitrary positive number. The inequalities constraints (6.4a)-(6.4f) construct the state constraint $\mathcal{X}$. These constraints are non-convex since the binary variables t_q are not continuous, which results in the non-convexity of the optimization problem as well. To perform the convexification of constraints (6.4a)-(6.4d), we propose the following new concepts.

Definition 6.1. *A path $P_j := \{p_{1,j},\ldots,p_{N,j}\}$ is said to be the jth candidate path with $p_{i,j} := \{q_1,\ldots,q_O\}$ at the ith predicted step. $q_o \in \mathbb{Z}[0,4]$ denotes the activated constraint of the oth obstacle where $q_o \in \mathbb{Z}[1,4]$ means $t_{q_o} = 0$ and $q_o = 0$ represents none of the constraints of the oth obstacle is sensed.*

Definition 6.2. *Define $\mathcal{A}$ as the set of all the candidate paths, and $\mathcal{A}_F$ as the set of the candidate paths along which the optimization problem is feasible.*

To illustrate the definitions, we present an example as follows.

Example 6.1. *Consider a kind of situations shown in Figure 6.1 where the vehicle locates at the top left corner side of the obstacle 1. The prediction horizon N is assumed to 2. Either $x^{(1)}_{i|k} \leq b^{(1)}_{1\,\min} - d_s$ or $-x^{(2)}_{i|k} \leq -(b^{(1)}_{2\,\max} - d_s)$ needs to be satisfied at the ith predicted step at time k, $i = 1,2$: respectively corresponding to the two cases $t_1 = 0$, $t_2 = t_3 = t_4 = 1$ and $t_4 = 0$, $t_1 = t_2 = t_3 = 1$ in (6.4a)-(6.4d). According to*

Definition 6.1 and 6.2, all the candidate paths are as follows:

$$
\begin{aligned}
P_1 &= \{p_{1,1}, p_{2,1}\} = \{\{1,0\},\{1,0\}\}, \\
P_2 &= \{p_{1,2}, p_{2,2}\} = \{\{1,0\},\{4,0\}\}, \\
P_3 &= \{p_{1,3}, p_{2,3}\} = \{\{4,0\},\{1,0\}\}, \\
P_4 &= \{p_{1,4}, p_{2,4}\} = \{\{4,0\},\{4,0\}\},
\end{aligned}
$$

where $P_j, j \in \mathbb{Z}[1,4]$ *represents* 4 *candidate paths, and at each predicted step* i, $p_{i,j}$ *indicates all the activated constraints, e.g.,* $p_{2,3} = \{1,0\}$ *shows that for the* 3*rd path at the* 2*nd predicted step, only the first constraint of obstacle* 1 *is activated.* $\mathcal{A} = \{P_1, P_2, P_3, P_4\}$ *with the total number of* $C_2^1 \times C_2^1$. *Assume that* $\mathcal{A}_F = \{P_1, P_2\}$, *then it means that finite horizon conditional scenario program (FHCSCP) is feasible with* P_1 *and* P_2, *and is infeasible with* P_3 *and* P_4.

6.3 Finite horizon conditional scenario program (FHCSCP) and the algorithm for path planning

The widely-used constraints (6.4a)-(6.4d) yield a non-convex MINLP optimization problem, and further prevent the use of the SCMPC algorithms which require the optimization problem to be convex. To tackle this problem, we propose a novel conditional-scenario strategy which can discriminate an optimal path $P_j^\star$ from all the candidate paths set $\mathcal{A}$.

The main idea of the conditional-scenario strategy is to directly apply the SCMPC approach [69] to optimize each candidate path P_j from the candidate path set $\mathcal{A}$. The "conditional" indicates that the SCMPC can work only under condition of a particular path P_j. Once a path P_j is considered, the non-convex MINLP optimization problem becomes convex and thus the SCMPC approach can start to work.

Let $\Omega_k^{(s)}|P_j = \{\delta_{0|k}^{(s)}|P_j, \ldots, \delta_{N-1|k}^{(s)}|P_j\}$ denote i.i.d. samples of the sth scenario $\Omega_k^{(s)}|P_j$ ($s \in [1,S]$) under a certain path P_j at time k for predicted steps $i = 0, \ldots, N-$

Algorithm 2 Conditional-scenario algorithm

1: Initialize the parameters: z_d, z_0, $\mathcal{X}$, $\mathcal{U}$, N, Q, R, S, d_s, d_p, and the map of interest.
2: At each time step k, perform the following procedures:
3: Measure the current state z_k.
4: Determine which obstacles b^is are within the range of d_p (i.e., are sensed by the vehicle).
5: Generate the obstacle avoidance constraints (6.4a)-(6.4d) by b^i and d_s.
6: Generate the set $\mathcal{A}$ of candidate paths and set the feasible path set $\mathcal{A}_F = \mathcal{A}$.
7: **for** $j = 1$ to the size of $\mathcal{A}$ **do**
8: Solve the FHCSCP problem for path P_j at time k.
9: **if** The FHCSCP problem is feasible **then**
10: Record the cost value $c_{j,k}$ and first element $u_k|P_j$ of the control input sequence.
11: **else**
12: Remove P_j from $\mathcal{A}_F$.
13: **end if**
14: **end for**
15: Find the minimal cost $c_{\min,k}$ among all the computed $c_{j,k}$ and the corresponding optimal path $P_{\min}$, control input $u_k|P_{\min}$.
16: Apply the control input $u_k|P_{\min}$ to the system and **Return** to Step 3.

1. Then, for a specific path P_j, the FHCSCP reads as follows:

$$\min_{\mathbf{u}_k^\star} \sum_{s=1}^{S} \sum_{i=0}^{N-1} \ell\left(z_{i|k}^{(s)}, u_{i|k}\right) \tag{6.5a}$$

$$s.t. \quad z_{i+1|k}^{(s)} = A(\delta_{i|k}^{(s)}|P_j) z_{i|k}^{(s)} + B(\delta_{i|k}^{(s)}|P_j) u_{i|k} + w(\delta_{i|k}^{(s)}|P_j), \tag{6.5b}$$

$$z_{0|k}^{(s)} = z_0, \forall s = 1, \ldots, S \tag{6.5c}$$

$$u_{i|k} \in \mathcal{U}, \ \forall i = 0, \ldots, N-1, \tag{6.5d}$$

Constraints (6.4a)-(6.4f) under the path P_j.

Denote the optimized control input sequence as $\mathbf{u}_k|P_j = \{u_{0|k}|P_j, \ldots, u_{N-1|k}|P_j\}$. Here, we only select the first element of $\mathbf{u}_k$ and apply it to the system, i.e., $u_k := u_{0|k}$. Based on the FHCSCP, the conditional scenario algorithm is given in Algorithm 1.

Remark 6.3. *There always exists a feasible solution on the path generator algorithm. This is a widely-used almost-sure assumption in the field of SCMPC since this algorithm does not yield theoretically proved feasibility [69].*

Definition 6.3. *Define as $V_k|x_k$ the violation probability, i.e., the first state violates*

the state constraints $\mathcal{X}$ after applying the optimized control input $u_{0|k}|P_j$ to the system:

$$V_k|x_k = \mathbf{P}\left[A(\delta_k)x_k + B(\delta_k)u_{0|k}|P_j + \omega(\delta_k) \notin \mathcal{X}|x_k\right].$$

Remark 6.4. *Definition 6.3 is used to build the relationships between the scenario numbers and the state violation of the first step.*

Denote the violation level $\varepsilon \in (0, 1)$ as the upper bound of the expected time-average of constraint violations, and the violation expectation can be represented as

$$\mathbb{E}\left[V_k|x_k\right] \leq \varepsilon.$$

Theorem 6.1. *(Safe distance violation bound) Let 6.1 hold. Then for time k, the upper bound of state violation probability of next step can be expressed as*

$$\mathbf{P}[z_{k+1} \notin \mathcal{X}] \leq \frac{2}{1+S}. \tag{6.6}$$

In other words, if the sample size S satisfies $S \geq (2/\varepsilon) - 1$, the violation expectation can be guaranteed.

Proof: Since the cost function (6.5a) is convex and the input and state constraints are convex, under the Assumptions 6.1, the upper bound on distribution is ensured by [69].

Remark 6.5. *A posteriori scenario removal strategy is introduced in [69] aiming to remove the "bad" scenarios from the algorithm. In SCMPC with S scenarios, the control input may sometimes be insecure because some scenarios impact the algorithm with a large fluctuation. The removal algorithm will observe the influences of all the chosen scenarios and remove R scenarios from them according to some criteria. There are three main approaches: optimal removal, greedy removal, and marginal removal. The simplest approach still requires solving S times the optimization problem for one time instant. In this section, the computational complexity of the FHCSCP algorithm is high, so the scenario removal scheme is not appropriate. Our future work will focus on the reduction of the computational complexity with removal scenarios.*

6.4 Simulations and discussions

In this section, we consider a stochastic linear second-order vehicle. This model represents a stochastic linear second-order vehicle system, typically used in control or estimation studies involving motion in two spatial dimensions. This is a standard kinematic model (Euler discretization with constant acceleration assumption). It is formulated by (6.1) with z_k and u_k defined by:

$$z_k = [x_k^{(1)}, x_k^{(2)}, v_k^{(1)}, v_k^{(2)}]^{\mathrm{T}}, u_k = [u_k^{(1)}, u_k^{(2)}]^{\mathrm{T}},$$

where $x_k^{(1)}$ and $x_k^{(2)}$ represent the position of the vehicle at time k; $v_k^{(1)}$ and $v_k^{(2)}$ represent the velocity; $z_0 = [0\ 0\ 0\ 0]^{\mathrm{T}}$. The system matrices are as follows:

$$A(\delta_k) = \begin{bmatrix} 1+\theta_k & 0 & 1 & 0 \\ 0 & 1 & 0 & 1 \\ 0 & 0 & 1 & 0 \\ 0 & 0 & 0 & 1 \end{bmatrix}, B(\delta_k) = \begin{bmatrix} 0.5000 & 0 \\ 0 & 0.5000 \\ 1.0000 & 0 \\ 0 & 1.0000 \end{bmatrix},$$
$$\omega(\delta_k) = \left[w_k^{(1)}, w_k^{(2)}, 0, 0\right]^{\mathrm{T}}.$$

The uncertainty of the system comes from the external disturbances $\omega_k^{(1)}$, $\omega_k^{(2)}$ and the coupled model identification error θ_k in $A(\delta_k)$. θ_k follows the uniform distribution which can be represented as $\theta_k \sim \mathcal{U}([0,1])$.

The additive disturbance follows the normal distribution which is denoted by $w_k^{(1)}, w_k^{(2)} \sim \mathcal{N}(0, 0.1)$. The system state and the control input are constrained by

$$\begin{aligned} \mathcal{X} := \big\{ & z \in \mathbb{R}^4 : 0 \le x^{(1)} \le 320, 0 \le x^{(2)} \le 320, \\ & |v^{(1)}| \le 20, |v^{(2)}| \le 20 \big\}, \end{aligned} \tag{6.7}$$
$$\mathcal{U} := \big\{ u \in \mathbb{R}^2 : |u^{(1)}| \le 10, |u^{(2)}| \le 10 \big\}. \tag{6.8}$$

In the simulation, we define a rectangular map of 320×320 unit length as a planar space, and regulate a collision-free path for the vehicle. A total of two obstacles are considered in the map. The first obstacle has a rectangular shape, formulated by:

$$\mathcal{X}_1 = \{100 \le x^{(1)} \le 200, 0 \le x^{(2)} \le 200\},$$

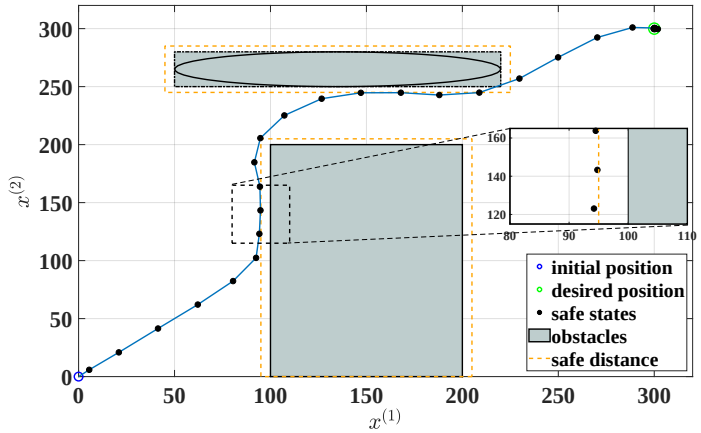

(a) Planned path with $S = 19$.

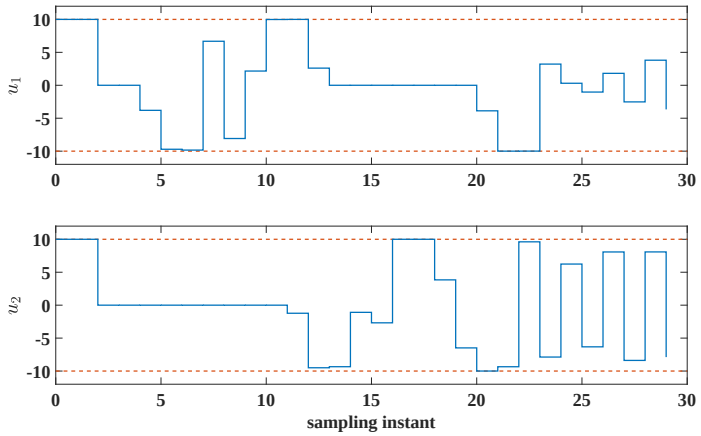

(b) Input sequence with $S = 19$.

Figure 6.2: Results of regulating a path with 90% probability of obstacle avoidance.

and the second obstacle has an ellipsoidal shape, formulated by:

$$\mathcal{X}_2 = \left\{ \frac{(x^{(1)} - 135)^2}{85^2} + \frac{(x^{(2)} - 265)^2}{15^2} \leq 1 \right\},$$

and further covered by a rectangular shape:

$$\mathcal{X}_2' = \{50 \leq x^{(1)} \leq 220, 250 \leq x^{(2)} \leq 280\}.$$

A fundamental setup for the conditional-scenario algorithm includes $z_d = [300, 300]^{\mathrm{T}}$, $z_0 0 = [0, 0]^{\mathrm{T}}$, $N = 3$, $Q = 0.5I$, $R = 3I$, $d_s = 5$, $d_p = 20$, $\mathcal{X}$ in (6.7), and $\mathcal{U}$ in (6.8). By (6.6), we know that more than 90% constraints satisfaction corresponds to $S = 19$, which is the number of scenarios for each P_j.

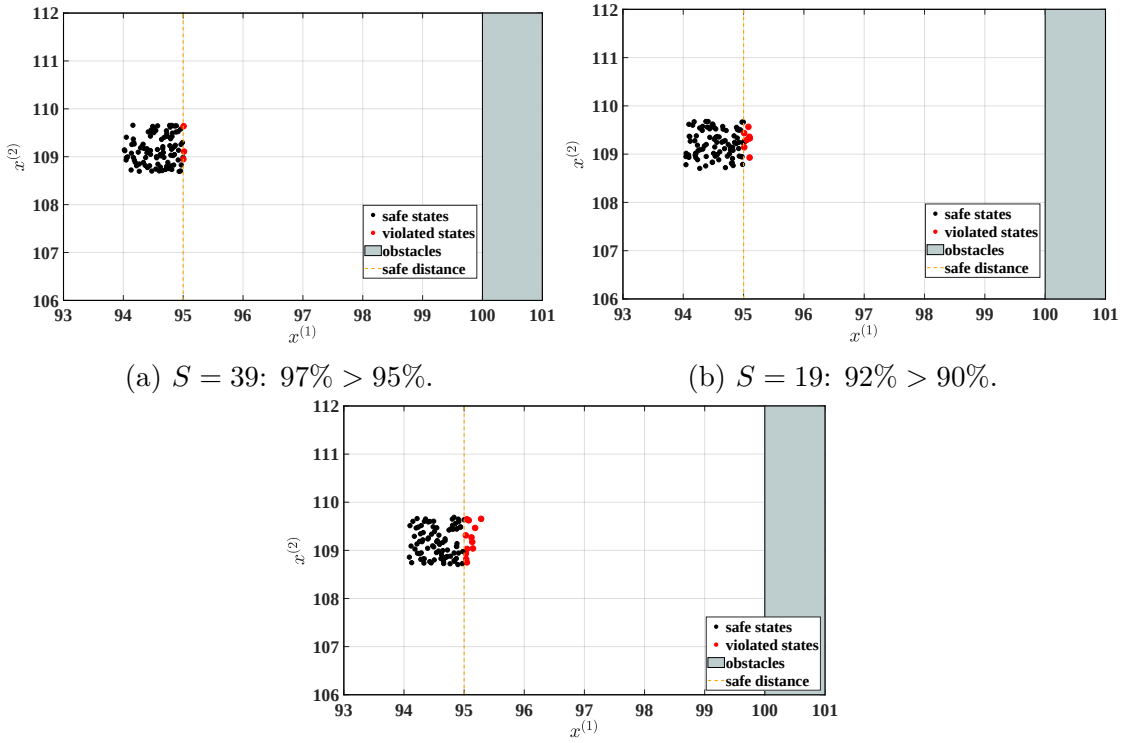

(a) $S = 39$: $97\% > 95\%$.

(b) $S = 19$: $92\% > 90\%$.

(c) $S = 9$: $84\% > 80\%$.

Figure 6.3: State violations after one-step optimization of the conditional scenario algorithm. The format of each subcaption is "scenario numbers: practical constraints satisfaction, expected constraints satisfaction."

Figure 6.2a shows the planned path for the vehicle with $S = 19$. It is seen that no constraint violation occurs during the whole process. One important position bounded by a rectangle is zoomed in for a better observation. The proposed conditional scenario algorithm successfully regulates a path from z_0 to z_d with the practical constraint satisfaction of 100% larger than the required one 90%. For the purpose of minimizing the cost function (6.5a), the vehicle states approach the two obstacles at the time interval $[7, 9]$ for obstacle 1 and the time interval $[14, 17]$ for obstacle 2. The blue line is the sketch map of the path. Since it is a discrete-time control system, the cross line between the blue line and the safe distance does not indicate the failure of the control strategy. The corresponding optimized control input $u_k|P_{\min}$ is also shown in Figure 6.2b. All the optimized control input satisfies the input constraint $\mathcal{U}$. On the other hand, $u^{(1)}$ tends to be 0 when the vehicle approaches the obstacle 1 on the time interval $[13, 20]$, since large value of $u^{(1)}$ will violate the constraints. Same observation can also be made in $u^{(2)}$ on the time interval $[3, 10]$.

To further verify the validity of the guaranteed probability of constraint satisfaction, we perform three groups of trials where each trial starts from the same initial state (the seventh step in Figure 6.2a and then just runs for one step. The only difference among the three groups is the probability of the required constraint satisfaction. The total scenarios of $S = 39$ (95%), $S = 19$ (90%), and $S = 9$ (80%) are simulated. In each group, the vehicle optimizes 100 possible scenarios for the next step, and the practical probabilities of constraint satisfaction are 97%, 92%, and 84%, respectively, larger than the expected probabilities, as shown in Figure 6.3. This result indicates that the practical probability of constraint satisfaction is guaranteed and can be conducted by manually revising the number of S, as given in (6.6).

Although the presented FHCSCP algorithm can effectively turn the original non-convex optimization problem into several convex ones, the price to pay is the relatively large computational burden. The total number of the candidate paths is

$$\text{Number of } \mathcal{A} \ : (\prod_{o=1}^{O} C_{n_o}^{1})^{N},$$

where n_o denotes the number of activated constraints of the oth obstacle. This number increases with the prediction horizon N and the number of obstacles O. In our future work, we will focus on reducing the computational complexity of the algorithm so that it can be used in large-scale path planning, such as multi-agent systems, complex shipping lanes, etc.

6.5 Conclusion

This chapter investigates the path planning problem with a guaranteed probability of obstacle avoidance. A novel concept of candidate path is proposed, which can cover all the possible non-convex constraints in the future predicted steps. A conditional SCMPC approach is presented, which turns the original non-convex optimization problem into several convex subproblems by the introduction of the concept of candidate paths. The feasible one that has the minimal cost function value among all the candidate paths decides the optimal control input. Simulation results show that the proposed algorithm can successfully regulate a path with an ideal probability of constraint satisfaction. In future work, the main performance metricssuch as path efficiency, computational time, collision avoidance rate, and robustnesswill be con-

sidered to systematically evaluate the effectiveness of the proposed path planning method for a more convincing statement.

Chapter 7

Optimal Scheduling and Control of hydrogen refueling station (HRS)

In this chapter, I will give an example of the HRS energy-saving problem. This work aims to develop innovative modeling and optimization techniques for HRSs to enhance their efficiency, reduce operational costs, and support the transition to a sustainable hydrogen-based transportation system.

7.1 Introduction

Global efforts to combat climate change have underscored the urgent need for reducing carbon emissions, with transportation being one of the largest contributors to greenhouse gas emissions. Transitioning to sustainable energy is essential to reducing carbon emissions. Hydrogen, as one of the key sustainable energies, has emerged as a promising solution to decarbonize the transportation sector. Hydrogen stands out due to its high energy density and ability to produce zero-emission energy through fuel cell technology. These characteristics have driven significant advancements in hydrogen-powered mobility, with the fuel cell electric vehicle (FCEV) emerging as a leading application. As FCEVs gain traction globally, the development of hydrogen refueling stations has become critical [196]. Consequently, Canada, along with many other countries, is actively developing HRSs to ensure efficient and reliable hydrogen supply.

In the following, we will briefly present the system configuration of hydrogen refueling stations. Then, the objective of this work is introduced.

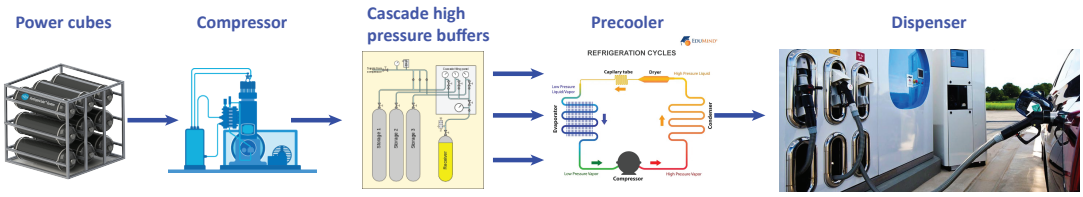

Figure 7.1: Hardware configuration of the HRS.

HRS An HRS consists of power cubes (low pressure storage), a compressor, cascade high pressure buffers, a precooler, and a dispenser. The schematic diagram of the HRS with components and their connections is shown in Figure 7.1.

- **Power cubes:** Power cubes are used to store hydrogen produced by electrolyzers. Commonly, they are designed to be modular and scalable. This design allows for flexible installation and expansion of HRSs to meet increasing demand.
- **Compressor:** A compressor is responsible for compressing the low pressure hydrogen in the power cubes into high pressure hydrogen. Hydrogen is compressed in order to be at the required pressure for fast and efficient refueling for vehicles.
- **Cascade high pressure buffers:** Cascade high pressure buffers, also known as high-pressure storage tanks, are used to store hydrogen at high pressures. These buffers store hydrogen at different pressure levels, which can deliver hydrogen at various flow rates. By coordinating the hydrogen from different buffers, HRSs ensure a stable and consistent supply during the hydrogenation process to meet different needs while maintaining the pressure required for efficient operation.
- **Precooler:** A precooler is used to decrease the temperature of hydrogen before it is dispensed into vehicles. It is necessary because the rapid compression and expansion of hydrogen lead to significant temperature increases due to the Joule-Thomson effect and adiabatic compression [197], potentially causing safety concerns and reducing the fueling efficiency.
- **Dispenser:** The dispenser is the interface between HRSs and FCEVs. It is responsible for transferring hydrogen from cascade high pressure buffers to the vehicle's onboard storage tank. The dispenser typically includes a nozzle, pressure sensors, flow meters, and safety shutoff valves to ensure that hydrogen is

dispensed accurately, efficiently, and safely. It is designed to handle the high pressure hydrogen and ensure that the refueling process is completed quickly, usually within a few minutes, to provide the vehicle with sufficient fuel for extended travel.

Objectives This work aims to develop optimization and control strategies to minimize the energy consumption of the HRS. To achieve this goal, we list the main objectives in the following.

- To build a customized simulator that can imitate the dynamic state changing of the HRS, with a particular focus on simulating the fueling processes of the compressor and the charging process of the vehicle. The simulator must account for the constraints of both HRSs and FCEVs. Additionally, it should be able to simulate and characterize the real HRS, with a good performance compared to available simulators. It is underscored that such a customized simulator can conveniently implement novel optimization and control algorithms, whereas other available simulators may not provide access to change the specific modules therein.
- To implement and test the representative logic controller reported in the literature, and to perform comprehensive simulation and comparison studies on the customized simulator developed in this work.
- To propose and design an optimal controller that can optimize energy consumption. Specifically, we will evaluate its performance, conduct comparison studies with logic controllers, and perform some quantitative analysis of energy consumption reduction.

7.2 Modeling of the HRS

To optimize the energy consumption of HRSs, an optimal control problem will be formulated. Before this, the system process of the controller should be described mathematically. As seen in Figure 7.2, the main components of the HRS include a compressor, storage buffers, a precooler, and a dispenser. Optimizing the energy consumption of an HRS can be formulated as an optimal control problem with numerical and integer variables. Some assumptions are presented below.

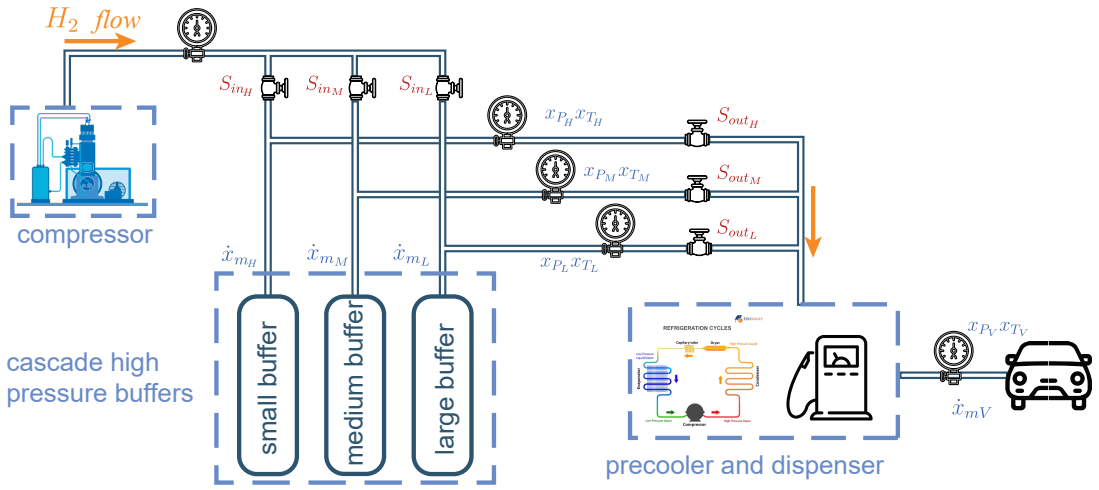

Figure 7.2: The HRS system with defined variables.

Assumption 7.1. *These assumptions are given under the consideration of the real system and the simplification for controller design.*

- *Any of the buffers can either be fueled or emptied at any given time, but not both (i.e., both operations cannot be carried out on the same buffer simultaneously).*
- *The energy consumption of the compressor and precooler are linear to the running time.*
- *Only one vehicle is fueling at each time (one dispenser is working).*
- *The remaining gas (hydrogen in the cube) is plenty enough.*
- *Suppose hydrogen is an ideal gas, which means when the temperature is stable, the pressure is proportional to the mass.*
- *The switching cost is not considered.*
- *The logic always tries to optimize hydrogen availability for dispensing. This means buffers can be switched to refuel in the HRS refueling process.*

To control HRSs more precisely, we consider the transition of the system states to build the system model characterizing the operation of HRSs. The state variables are shown in Figure 7.2. For each buffer, the sensors report the real-time data to reflect the current state. The data we use includes the pressure of buffers $x_{p_\#}$, the temperature of buffers $x_{T_\#}$, and the flow rate of buffers $x_{m_\#}$, where # represents

H, M, or L which means high, medium, or low buffer. In order to illustrate the relationship of these data, we also define some process variables which are the gas mass $x_{m_\#}$ and temperature changes $\dot{x}_{T_\#}$. Similarly, the state variables for vehicles are also defined. However, sensors in HRSs may not always communicate with vehicle tanks in real-time. As a result, these values might not be available. The variables of system states are compiled in Table 7.1.

	Unit	High buffer	Medium buffer	Low buffer	Vehicle
Gas pressure	bar	x_{p_H}	x_{p_M}	x_{p_L}	x_{p_V}
Gas mass	g	x_{m_H}	x_{m_M}	x_{m_L}	x_{m_V}
Temperature	°C	x_{T_H}	x_{T_M}	x_{T_L}	x_{T_V}
Flow rate	g/s	$\dot{x}_{m_H}$	$\dot{x}_{m_M}$	$\dot{x}_{m_L}$	$\dot{x}_{m_V}$
Temperature changes	°C/s	$\dot{x}_{T_H}$	$\dot{x}_{T_M}$	$\dot{x}_{T_L}$	$\dot{x}_{T_V}$

Table 7.1: System state variables of the HRS system.

In this control system, the decision variables are defined as binary, which can be reckoned as switches and shown in Figure 7.2 as the red valves. For each buffer, two channels are connected to them to control the inlet flow and outlet flow of hydrogen. As a result, the decision variables are defined as: Inlet and outlet valve state on each buffer: $s_{in_H}, s_{out_H}, s_{in_M}, s_{out_M}, s_{in_L}, s_{out_L}$.

7.3 MINLP controller design

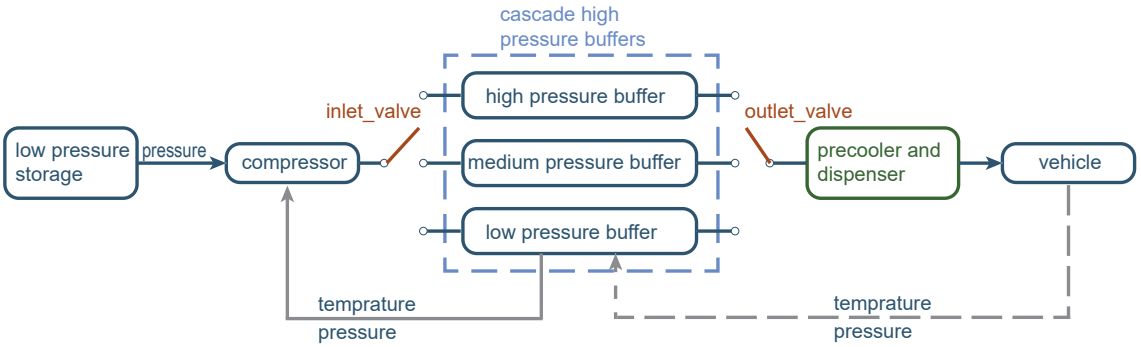

Figure 7.3: Cascade HRS structure.

The system block diagram of the HRS is shown in Figure 7.3. Hydrogen is delivered from low pressure storage (power cubes) to the compressor. The compressor delivers hydrogen to one of the cascade pressure buffers, either low pressure, medium

pressure, or high pressure, depending on the actual requirements. Once stored in the appropriate buffer, hydrogen flows through the outlet valve to precooler and dispenser. At the final stage, the dispenser fuels a vehicle.

Throughout the process, the pressure of the HRS is continuously monitored at all stages, while the temperature is measured specifically in the buffers and the vehicles. The continuous monitoring supports effective system control. The states to be monitored and controlled in the HRS simulator include: 1) The pressure of each buffer and the vehicles, 2) The delivery flow rate of each component, and 3) The temperature of hydrogen in the buffers and vehicles.

The gray solid line in Figure 7.3 represents the feedback loop between the buffers and the compressor, enabling the measured pressure and temperature data to be sent to the compressor for regulating buffer replenishment. The compressor plays a critical role in this process, replenishing the buffers whenever their pressure approaches the lower limit to maintain uninterrupted refueling. Notably, the compressor is a significant energy consumer, accounting for over 50% of the total energy consumption in the HRS. Then, the dispensing process can occur with or without communication between the vehicle and the HRS. If there is no direct communication, as indicated by the gray dashed line in Figure 7.3, the pressure and temperature of the vehicle are only monitored at the beginning of dispensing.

Finally, a controller uses the pressure and temperature data, along with the states of the inlet and outlet valves, to dynamically decide when and how to switch between three buffers, ensuring efficient hydrogen flow and safe operation. Considering three buffers located between the compressor and dispenser, the inlet and outlet valves of buffers can be designed as two three-way switches, as indicated by the red valves in Figure 7.3. In summary, the HRS simulator provides a comprehensive platform for analyzing and optimizing the replenishing and refueling processes by incorporating key components such as compressors, buffers, and dispensers. Through continuous monitoring and control of pressure, temperature, and flow rates, the simulator enables efficient system operation and enhances safety. The integration of dynamic control strategies, including buffer switching and energy management, ensures the reliable and energy-saving operation of HRSs.

In the last section, we have defined the variables of this problem. Then we need to describe all the constraints of this problem. The constraints of the MINLP can be classified into several classes.

1. System dynamics

The constraints of system dynamics reveal the model of state evolution and relationships between different states, which are always described as differential equations.

2. Condition-dependent constraints

   Constraints for the optimization problem vary according to different conditions, which means that this is a time-varying problem. In this problem, the system states change depending on whether a vehicle is refueled. If there is no vehicle, the system stays in a stable state or the compressor fuels the buffers. However, when the vehicle is refueling, system dynamics changes with the dispensing process, which needs to be considered in the MINLP problem. Simulating the process is a crucial part of the control system.

3. Limitations and requirements

   This class of constraints represents the limitations of the system or the requirements from users. They can be revised based on different conditions when we utilize the control algorithm.

System Dynamics

- **Flow rate of buffers**: The flow rate are calculated to make sure if it is beyond the constraint of the real system and to predict the the future states of buffers. When two containers have a gas exchange, the flow rate between them are proportional to the difference of their pressure. Then, in Eq. (7.1), the first item illustrates the gas exchange between buffers and the compressor, and the second item is between buffers and the vehicle. Considering different conditions, two coefficients $c_{f_{in}}$ and $c_{f_{out}}$ are assigned to them.

  However, when we solve the MINLP problem, these constrains are too strict to find a feasible solution. As a result, we separate the Eq. (7.1) into to parts: Eq. (7.2) and Eq. (7.12). It can not only increase the flexibility of the but also reduce computational burden when there is no vehicle to be refueled.

$$\dot{x}_{m_H} = c_{f_{in}}(p_{com} - x_{p_H})s_{in_H} - c_{f_{out}}(x_{p_H} - x_{p_V})s_{out_H}, \tag{7.1a}$$

$$\dot{x}_{m_M} = c_{f_{in}}(p_{com} - x_{p_M})s_{in_M} - c_{f_{out}}(x_{p_M} - x_{p_V})s_{out_M}, \tag{7.1b}$$

$$\dot{x}_{m_L} = c_{f_{in}}(p_{com} - x_{p_L})s_{in_L} - c_{f_{out}}(x_{p_L} - x_{p_V})s_{out_L}. \tag{7.1c}$$

The equality constraints are separated into two parts of inequality constraints to clamp the value of the flow rate.

$$\dot{x}_{m_H} \leq c_{f_{in}}(p_{com} - x_{p_H})s_{in_H}, \tag{7.2a}$$
$$\dot{x}_{m_M} \leq c_{f_{in}}(p_{com} - x_{p_M})s_{in_M}, \tag{7.2b}$$
$$\dot{x}_{m_L} \leq c_{f_{in}}(p_{com} - x_{p_L})s_{in_L}. \tag{7.2c}$$

- **Ideal gas relationship of buffer**: This is one of assumptions of HRSC simulator. We assume the hydrogen in our simulation obey the ideal gas rule. In Eq. (7.3), R is the gas constant, $R = 8.3145\ J \cdot K^{-1} \cdot mol^{-1}$, where pressure is expressed in pascals, volume in cubic meters, and absolute temperature in kelvin. M is the molar mass of hydrogen, which is $M = 0.002016$ in the simulator. $V_{H/M/L}$ is the volume of the buffer.

$$x_{p_H}V_H = \frac{x_{m_H}Rx_{T_H}}{M}, \qquad x_{p_M}V_M = \frac{x_{m_M}Rx_{T_M}}{M}, \qquad x_{p_L}V_L = \frac{x_{m_L}Rx_{T_L}}{M}. \tag{7.3}$$

- **Temperature changes of buffers**: In our simulator, assuming the temperature change of buffers are linear to the time, we can find proper coefficients to describe different procedures of gas changing. $c_{T_{Hin}}$, $c_{T_{Hout}}$ and c_{T_n} are the coefficients of the input valve, output valve, and environmental heat exchange respectively. In the simulator, we assume the environmental temperature is a constant value $T_{env} = 25°C$.

$$\dot{x}_{T_H} = c_{T_{Hin}}s_{in_H} - c_{T_{Hout}}s_{out_H} + c_{T_n}, \tag{7.4a}$$
$$\dot{x}_{T_M} = c_{T_{Min}}s_{in_M} - c_{T_{Mout}}s_{out_M} + c_{T_n}, \tag{7.4b}$$
$$\dot{x}_{T_L} = c_{T_{Lin}}s_{in_L} - c_{T_{Lout}}s_{out_L} + c_{T_n}. \tag{7.4c}$$

- **Temperature evolution of buffers:** The temperature of buffers evolves according to the rate calculated in Eq. (7.4). We assume this is a discrete time system, and the sampling period is one second. Then, the evolution of the

temperature can be formulated as follows.

$$x_{T_H}(k+1) = x_{T_H}(k) + \dot{x}_{T_H}(k), \tag{7.5a}$$
$$x_{T_M}(k+1) = x_{T_M}(k) + \dot{x}_{T_M}(k), \tag{7.5b}$$
$$x_{T_L}(k+1) = x_{T_L}(k) + \dot{x}_{T_L}(k). \tag{7.5c}$$

Conditions

There are two conditions or states of the HRS. One is that the vehicle has connected to the dispenser and the HRS system is under the refueling process. The other condition is that the HRS in an idle state. As a result, the constraints are considered under these two kinds of conditions:

Condition 1: At least one vehicle

Under this condition, we need to consider the states, dynamics of the fueling vehicle, and its influence to the HRS. The detailed constraints are given as following:

- **Flow rate of vehicle:** This constraint represents that the flow rate of the vehicle is proportional to the pressure difference of the vehicle and the high pressure buffers, and it depends on the valve open or close to the dispenser. $c_{f_{out}}$ is flow rate constant and its value is same as the one in Eq. (7.1).

$$\dot{x}_{m_V} = c_{f_{out}}((x_{p_H} - x_{p_V})s_{out_H} + (x_{p_M} - x_{p_V})s_{out_M} + (x_{p_L} - x_{p_V})s_{out_L}). \tag{7.6}$$

- **Flow rate of each buffer:** As we mentioned in Eq. (7.1), the second part of the buffer flow rate is only considered on Condition 1. For each buffer, if it is used to dispense, its flow rate is proportional to the difference of pressures and the value should be equal to the flow rate of vehicle. $c_{f_{out}}$ is flow rate constant and its value is same as the one in Eq. (7.1).

$$\begin{aligned} \dot{x}_{m_H} &\geq -c_{f_{out}}(x_{p_H} - x_{p_V})s_{out_H}, \\ \dot{x}_{m_M} &\geq -c_{f_{out}}(x_{p_M} - x_{p_V})s_{out_M}, \\ \dot{x}_{m_L} &\geq -c_{f_{out}}(x_{p_L} - x_{p_V})s_{out_L}. \end{aligned} \tag{7.7}$$

- **The pressure and temperature relationship of vehicle.** This relationship is considered as the ideal gas condition, which is the same as Eq. (7.3), and all

values of parameters are the same as Eq. (7.3).

$$x_{p_V} V_V = \frac{x_{m_V} R x_{T_V}}{M}. \tag{7.8}$$

- **Temperature changes of the vehicle:** The temperature changes of the vehicle is corresponding to the state of fueling. If it is in the refueling process, the temperature will increase; however, if it is pending, it will cool down due to the heat exchanges with the environment. c_{T_n} and T_{env} are the speed of temperature exchange with the environment and the environmental temperature, which are the same as in Eq. (7.4). c_{T_V} is the speed of temperature exchange when the vehicle is refueled.

$$\dot{x}_{T_V} = c_{T_V}(s_{out_H} + s_{out_M} + s_{out_L}) + c_{T_n}(T_{env} - x_{T_V}). \tag{7.9}$$

Similar to Eq. (7.5), the temperature of the vehicle follows the same rule.

$$x_{T_V}(k+1) = x_{T_V}(k) + \dot{x}_{T_V}(k). \tag{7.10}$$

- **Max/min flow rate of dispenser:** This is a bound constraint of the flow rate. For the security of the dispenser, the flow rate to fuel the vehicle should follow the limitation.

$$0 \leq \dot{x}_{m_V} \leq 60 \text{ g/s}. \tag{7.11}$$

- **Pressure threshold for fueling:** The pressure difference between buffers and vehicle during refueling process should be greater than $p_{dref} = 100$ bar. This constraint is set to guarantee the fueling efficiency since if the pressure difference is too small, the flow rate will drop fast which means it will take more time on refueling.

$$(x_{p_H} - x_{p_V} - p_{dref}) s_{out_H} \geq 0, \tag{7.12a}$$
$$(x_{p_M} - x_{p_V} - p_{dref}) s_{out_M} \geq 0, \tag{7.12b}$$
$$(x_{p_L} - x_{p_V} - p_{dref}) s_{out_L} \geq 0. \tag{7.12c}$$

- **Maximum temperature of the vehicle:** This is the bound of hydrogen temperature to keep the vehicle tank safe. The maximum temperature of the

vehicle in the simulation is set as $T_{Vmax} = 80°\text{C}$.

$$x_{T_V} \leq T_{Vmax}. \tag{7.13}$$

Condition 2: No vehicle

When there is no vehicle under the fueling process, the HRS stays in a pending state and all the dispenser valves are closed.

$$s_{out_H} = 0, \qquad s_{out_M} = 0, \qquad s_{out_L} = 0. \tag{7.14}$$

Limitations and Requirements

- This is the bound of hydrogen temperature to keep the high-pressure buffers safe.

$$x_{T_H} \leq T_{bmax}, \qquad x_{T_M} \leq T_{bmax}, \qquad x_{T_L} \leq T_{bmax}. \tag{7.15}$$

- If the pressure of a buffer is greater than the threshold 800 bar, and it is not in the fueling process, then it will not be fueled by the compressor to save more energy. The k in Eq. (7.16) represents the current time instant, so the $s_{in_H}(k-1)$ means the decision value in the last time instant, which is a constant value.

$$s_{in_H}(k) - 1 \leq s_{in_H}(k-1) - \frac{(x_{p_H}(k) - 800)}{M}, \tag{7.16a}$$

$$s_{in_M}(k) - 1 \leq s_{in_M}(k-1) - \frac{(x_{p_M}(k) - 800)}{M}, \tag{7.16b}$$

$$s_{in_L}(k) - 1 \leq s_{in_L}(k-1) - \frac{(x_{p_L}(k) - 800)}{M}. \tag{7.16c}$$

- The inlet and outlet valve cannot open simultaneously for one buffer:

$$s_{in_H} + s_{out_H} \leq 1, \qquad s_{in_M} + s_{out_M} \leq 1, \qquad s_{in_L} + s_{out_L} \leq 1. \tag{7.17}$$

- The number of compressor could be one or more which can be set by the constant n_{com}. In our simulation, we only consider the $n_{com} = 1$ condition which is same as the condition of our real stations.

$$s_{in_H} + s_{in_M} + s_{in_L} \leq n_{com}. \tag{7.18}$$

- There is only one dispenser in a set of the equipment in our simulation, so the sum of all the outlet valves of buffers should less than 1.

$$s_{out_H} + s_{out_M} + s_{out_L} \leq 1. \tag{7.19}$$

The objective function of this problem consists three parts:

1. J_1 is the sum of all energy consumption of the high pressure buffers which is defined as

$$J_1(k) = e_H(k) + e_M(k) + e_L(k). \tag{7.20}$$

Each item is also defined as follows

$$e_H(k) = c_{e_{in}} s_{in_H}(k) + c_{e_{out}} s_{out_H}(k), \tag{7.21a}$$
$$e_M(k) = c_{e_{in}} s_{in_M}(k) + c_{e_{out}} s_{out_M}(k), \tag{7.21b}$$
$$e_L(k) = c_{e_{in}} s_{in_L}(k) + c_{e_{out}} s_{out_L}(k), \tag{7.21c}$$

where c_{in} and c_{out} are the weights of cost from compressor and pre-cooling of the dispenser. Since the compressor costs more energy than the dispenser in a time instant, we assume the $c_{in} : c_{out} = 2 : 1$ in the simulation.

2. $J_2(k)$ represents the effort to fueling the buffers in the objective which is defined as

$$J_2(k) = (x_{p_H}(k) - x_{pmax})^2 + (x_{p_M}(k) - x_{pmax})^2 + (x_{p_L}(k) - x_{pmax})^2. \tag{7.22}$$

3. $J_3(k)$ only considers the vehicle fueling as the objective that is defined as

$$J_3(k) = (x_{p_V}(k) - x_{pmax})^2. \tag{7.23}$$

The square of the difference of pressure between the vehicle and its maximum value represents the effort to fueling the vehicle in the objective. As a result, $J_3(k)$ is a necessary part of the objective function.

As a result, the objective function of the MINLP at time k with a prediction

Table 7.2: MINLP control methods with three sets of different coefficients of the objective function.

	Coefficients	Objective function
MINLP 1	$c_{eng} = c_b = c_v = 1$	$J(k) = \sum_{k=0}^{t}(J_1 + \sum_{H,M,L,V} J_2)$
MINLP 2	$c_{eng} = c_b = 0$,$c_v = 1$	$J(k) = \sum_{k=0}^{t}(x_p - x_{pmax})^2$
MINLP 3	$c_b = 0$, $c_{eng} = c_v = 1$	$J(k) = \sum_{k=0}^{t}(J_1 + (x_{p_V} - x_{pmax})^2)$

horizon t is summarized as :

$$J(k) = \sum_{i=0}^{t} \left(c_{eng} J_1(k+i) + c_b J_2(k+i) + c_v J_3(k+i)\right), \tag{7.24}$$

where c_{eng}, c_b and c_v are the coefficients of J_1, J_2 and J_3 respectively. By tuning these three parameters, we can adjust the target of the control process. Meanwhile, t represents the prediction horizon of the optimization problem which is also known as the MPC. The performance of the controller will be better if t increased to a proper value, but the computational load will also increase dramatically.

After constructing all the components of the optimization problem, the MINLP is given as:

$$\min \quad \text{Eq. (7.24)} \tag{7.25a}$$

$$\text{s.t.} \quad \text{Eq. (7.1) to Eq. (7.19)} \tag{7.25b}$$

In order to compare the influence of the coefficients in the objective function, we proposed three critical conditions that can represent the trade-off of the MINLP algorithm between energy saving and refueling efficiency. The coefficients and corresponding objective functions of these three conditions are shown in Table 7.2.

- **MINLP 1:** This condition regards J_1, J_2 and J_3 equally important. It is more efficient and aggressive on refueling the vehicle since it has a higher buffer pressure. This strategy tries to fuel the buffers and vehicles as fast as it can to satisfy the objective, which means it will have the most aggressive performance of the waiting time but cost more energy.

- **MINLP 2:** This condition only considers the vehicle refueling target but not energy consumption nor buffer fueling. It means all cost from the compressor are spontaneous which means it will balance the buffer fueling and energy-saving.

- **MINLP 3:** This condition considers the energy and the vehicle, but does not include the buffer fueling, so this condition can save more energy in theory. This strategy is the most energy efficient since it will try to close the compressor as much as it can to reduce the energy consumption.

7.4 Simulation results

In the simulation, we compare the performance of three objective functions. The sampling period of the HRS varies on different conditions and the minimum sampling period is one second during refueling. The MINLP problem is required to be solved within one second. Therefore, all experiments are conducted with the prediction horizon of $t = 1$. We consider four scenarios with vehicle flows following uniform and normal distributions, which are summarized in Table 7.3. The uniform distribution represents the vehicle traffic with equal intervals over a time period, while the normal distribution shows peak and off-peak times. Scenarios S1 and S2 are designed to simulate dense vehicle conditions over a short period, equivalent to 5 vehicles arriving within 17 minutes. Scenarios S3 and S4 illustrate the daily vehicle conditions of 96 vehicles following uniform distribution and normal distribution over 12 hours. The subsequent part compares the control performance of the two systems with different distributions under these varying conditions.

Table 7.3: Four simulation scenarios.

	Distribution	
Number of Vehicles / Time Period	Uniform	Normal
5 / 1000 seconds	S1	S2
96 / 12 hours	S3	S4

Observations from these two tables reveal that under scenarios with a high density of vehicles waiting to refuel in short durations, the results are largely consistent. MINLP 1 always has the shortest waiting time for vehicles and the shortest dispenser operation time for both scenarios S1 and S2; however, it increases the compressor operation time. Conversely, MINLP 3 offers the shortest compressor operation time in both scenarios, indicating it is the most energy-efficient, but it significantly extends vehicle waiting time. Furthermore, comparisons reveal that in scenario S2, other control methods can complete refueling for five vehicles within 2500 seconds, whereas

Table 7.4: Performance of controllers under S1.

Scenario		$t_{total}(s)$		$t_{avg}(s)$		$t_{comp}(s)$		$t_{dis}(s)$	
S1	Logic	1148		230		1420		1836	
	MINLP 1	**959**	**-16.5%**	**191**	**-16.5%**	1995	40.5%	**1729**	**-5.8%**
	MINLP 2	1326	15.5%	255	11.2%	1144	−19.4%	1961	6.8%
	MINLP 3	1740	51.6%	384	67.3%	**363**	**-74.4%**	1786	−2.7%

Table 7.5: Performance of controllers under S2.

Scenario		$t_{total}(s)$		$t_{avg}(s)$		$t_{comp}(s)$		$t_{dis}(s)$	
S2	Logic	1132		226		1397		1806	
	MINLP 1	**951**	**-16.0%**	**190**	**-16.0%**	1995	42.8%	**1661**	**-8.0%**
	MINLP 2	1194	5.5%	239	5.5%	1171	−16.2%	1899	5.2%
	MINLP 3	1314	53.7%	348	53.7%	**363**	**-74.0%**	1786	-1.1%

MINLP 3 cannot finish within this timeframe. MINLP 2 achieves a more balanced outcome, reducing energy consumption without significantly increasing vehicle waiting time. As a result, for scenarios with a high density of vehicles waiting to refuel in short durations, using MINLP 2 can ensure the operational efficiency of the HRS while also achieving energy savings.

In summary, this section presents the simulation results of three optimized control methods, MINLP 1, 2, and 3, across four scenarios (S1-S4), and their comparison with the performance of the logic controller. The various MINLP methods facilitate a balance between minimizing customer waiting time and reducing system energy consumption. In practical control applications, the appropriate controller can be selected based on different vehicle traffic conditions and station requirements. For instance, in scenarios where there is a rapid influx of vehicles queuing at a station, MINLP 1 or MINLP 2 can be used to reduce waiting time in a short period. Conversely, in most cases where vehicle traffic is sparse, MINLP 3 can be utilized, prioritizing energy saving as main objective to control the HRS.

7.5 Conclusion

Based on the HRS refueling, we develop an open-source simulator in Python. The simulation result demonstrates that our simulator is comparable to the HRS simulator in Simulink. Three MINLP (MINLP 1, MINLP 2, MINLP 3) control methods are implemented in the simulator and the simulation results of these control strategies

Table 7.6: Performance of controllers under S3.

Scenario		$t_{total}(s)$		$t_{avg}(s)$		$t_{comp}(s)$		$t_{dis}(s)$	
S3	Logic	36701		382		40686		42876	
	MINLP 1	4799	**-86.9%**	49	**-87.2%**	43352	6.6%	**41810**	**-2.5%**
	MINLP 2	48239	31.4%	502	31.4%	34477	−15.3%	44225	3.2%
	MINLP 3	52250	42.4%	544	42.4%	**33185**	**-18.4%**	44966	4.9%

Table 7.7: Performance of controllers under S4.

Scenario		$t_{total}(s)$		$t_{avg}(s)$		$t_{comp}(s)$		$t_{dis}(s)$	
S4	Logic	43212		450		40560		43140	
	MINLP 1	40021	**-7.4%**	416	**-7.6%**	44068	8.7%	**42184**	**-2.2%**
	MINLP 2	51304	18.7%	534	18.7%	37786	−6.8%	47680	10.5%
	MINLP 3	57309	32.6%	596	32.4%	**37389**	**-7.8%**	50081	16.1%

under four synthetic scenarios.

Based on the characteristics of all methods, these control methods can be selected according to different vehicle traffic patterns and specific station needs. For example, MINLP 1 or MINLP 2 are ideal for scenarios with a sudden surge of vehicles, quickly alleviating waiting time. On the other hand, MINLP 3 is more suitable for conditions with low vehicle density, focusing on energy efficiency as a primary goal for managing the HRS. Based on the evaluation of these control strategies, we provide some suggestions to reduce the energy consumption on four real stations.

Chapter 8

Conclusion and future works

This dissertation presents a comprehensive investigation into stochastic data-driven MPC for constrained systems, with a particular focus on hybrid systems that combine continuous and discrete dynamics. The research makes significant theoretical and practical contributions by addressing the challenges of controlling such systems under uncertainties, proposing novel control methodologies, and demonstrating their applications through case studies.

8.1 Conclusion

The dissertation begins by outlining the fundamental concepts and motivations for studying stochastic data-driven MPC, as detailed in Chapter 1. A broad literature review highlights the increasing relevance of MPC in modern control applications, particularly in areas such as robotics, industrial electronics, and power systems. In Chapter 2, key preliminary concepts such as reachable sets, invariant sets, and stability theories are introduced, laying the theoretical groundwork necessary for the subsequent research.

The central contributions of this research are presented in Chapters 3 to 6. Chapter 3 explores asynchronous stabilization of discrete-time switched linear systems under dwell-time constraints, proposing a novel convex stability criterion. This work improves the ability to control systems that experience mode switching in an asynchronous manner. Chapter 4 extends this investigation by introducing an error reachable set-based stabilization approach for switched linear systems with bounded peak disturbances, providing a robust control strategy that maintains system stability de-

spite external perturbations.

The study then shifts focus to data-driven methods. Chapter 5 presents an innovative integration of DMD into the data-driven MPC framework. This lightweight model-free approach ensures system stability and recursive feasibility, offering a solution for controlling complex systems where obtaining accurate models is challenging. Chapter 6 investigates the application of SCMPC to path planning and obstacle avoidance, providing practical solutions for managing uncertainties in real-time decision-making, particularly in safety-critical applications.

Chapter 7 demonstrates the practical relevance of the proposed methodologies through a case study: energy-saving control for hydrogen refueling stations. This study highlights the potential of data-driven MPC to address real-world energy efficiency challenges.

In conclusion, this dissertation contributes to advancing the field of stochastic data-driven MPC, offering new theoretical insights and practical applications. The work presented here provides a solid foundation for future developments in data-driven control systems, particularly in areas requiring real-time optimization, robustness, and scalability.

8.2 Future works

My future research will focus on the investigation of MPC design for hybrid systems and its applications to the unmanned aerial vehicle (UAV) systems, integrating data-driven methodologies to enhance system stability, robustness, and intelligence. Given the complex and hybrid dynamics of UAVs, traditional model-based control faces challenges in accuracy and adaptability. To address this, I will develop data-driven MPC frameworks that leverage system input-output data for improved performance while ensuring stability and optimality. Additionally, I will investigate intelligent collaborative control for UAV swarms and UAV-unmanned surface vehicle (USV) systems, incorporating AI-driven large models to enhance autonomous decision-making and coordination in complex environments. Furthermore, I will focus on intelligent path planning and trajectory tracking, utilizing computationally efficient online optimization techniques to handle dynamic and uncertain mission scenarios.

My future research aims to achieve both theoretical and practical directions for hybrid system MPC, ensuring optimal UAV operation in critical applications such as disaster response, maritime patrol and precision agriculture.

8.2.1 Data-driven MPC for hybrid systems

Many physical processes exhibit complex hybrid dynamic characteristics, ranging from micro to macro multi-cell systems, UAV systems, and power electronics systems, among others. Accurately describing these systems with precise mathematical formulations remains a significant challenge. Conversely, we often have access to a vast amount of system input-output data. Therefore, optimizing system performance solely based on collected data represents a cutting-edge direction in the field of control. I plan to conduct research on data-driven MPC theory and its applications in hybrid dynamic systems, aiming to establish a new theoretical framework that ensures key performances such as stability, robustness, and optimality. This work seeks to address the contradictions and challenges between the accuracy of data-driven modeling and the optimality of hybrid predictive control.

8.2.2 Advanced control for unmanned aerial vehicle (UAV) systems

In response to the urgent need for precise sensing and intelligent operation in complex and extreme environments, such as earthquake rescue, maritime patrol, and agricultural pest control, I plan to undertake research on the theory and application of collaborative motion control involving multiple UAVs and the integration of UAVs with USVs. This research aims to address the challenges posed by the existing multi-agent frameworks' heavy reliance on model accuracy and insufficient levels of intelligence. By integrating large model theories, such as generative pre-trained transformers, the goal is to achieve coordinated motion control of multiple UAVs and UAV-USV systems endowed with swarm intelligence and autonomous awareness. This approach will be validated through application in significant scenarios, including maritime patrol, demonstrating its efficacy and potential.

8.2.3 Intelligent path planning and trajectory tracking for UAV systems

In future research, the development of intelligent path planning and trajectory tracking for UAV systems remains a critical challenge. Current UAV navigation often faces difficulties such as dynamic environmental changes, obstacle avoidance, uncertainties in wind disturbances, and limited onboard computational resources. Ensur-

ing real-time adaptability while maintaining optimal performance is a key concern. Data-driven and learning methodologies are promising to handle complex and time-varying problems, including complex path planning problems for the UAV systems. Simultaneously, I also intend to exploit a computationally efficient online optimization algorithm to reduce the computational demands of the optimization problem and implement it together with the data-driven path planning scheme.

Appendix A

Publications

- **Journal papers that have been published**

  1. **X. Shang**, S. Zhuang, and Y. Shi, Asynchronous stabilization of discrete-time switched linear systems under dwell-time constraints. *IEEE Transactions on Automatic Control*, DOI: 10.1109/TAC.2024.3428992, 2024.
  (This work is presented in Chapter 3)

  2. **X. Shang**, S. Zhuang, T. Tan, and Y. Shi, Error reachable set based stabilization of switched linear systems with bounded peak disturbances. *Journal of Automation and Intelligence*, 2(2), pp.87-98, 2023.
  (This work is presented in Chapter 4)

  3. S. Zhuang, **X. Shang**, X. Yu, H. Gao, and Y. Shi, A unified framework of convex stability conditions for 2-D switched systems with stable or unstable modes. *Automatica*, 141, p.110264, 2022. (*Regular paper*)

- **Journal papers under review:**

  1. **X. Shang**, S. Zhuang, K. Zhang, and Y. Shi, Dynamic mode decomposition based data-driven model predictive control: Feasibility and stability. Submitted.
  (This work is presented in Chapter 5)

- **Conference papers that have been published or accepted**

  1. **X. Shang**, J. Chen, S. Zhuang, and Y. Shi. Scenario-based model predictive control for path planning and obstacle avoidance. In *the proceeding of 2021 4th IEEE International Conference on Industrial Cyber-Physical Systems*

(ICPS), Victoria, Canada, 10-12 May 2021. IEEE.
(This work is presented in Chapter 6)

2. T. Tan, **X. Shang**, L. Yang, and Y. Shi, Model Predictive Control of asynchronously switched systems with exogenous disturbances, In *the proceedings of 24th IEEE International Conference on Industrial Technology (ICIT 2022)*, Orlando, USA, 04-06 April 2023,

Bibliography

[1] H. Li, A. Dimitrovski, J. B. Song, Z. Han, and L. Qian, "Communication infrastructure design in cyber physical systems with applications in smart grids: A hybrid system framework," *IEEE Communications Surveys & Tutorials*, vol. 16, no. 3, pp. 1689–1708, 2014.

[2] X. D. Koutsoukos, P. J. Antsaklis, J. A. Stiver, and M. D. Lemmon, "Supervisory control of hybrid systems," *Proceedings of the IEEE*, vol. 88, no. 7, pp. 1026–1049, 2000.

[3] J. Lee, S. Bohacek, J. P. Hespanha, and K. Obraczka, "Modeling communication networks with hybrid systems," *IEEE/ACM Transactions on Networking*, vol. 15, no. 3, pp. 630–643, 2007.

[4] M. Gökçek and C. Kale, "Optimal design of a hydrogen refuelling station powered by hybrid power system," *Energy Conversion and Management*, vol. 161, pp. 215–224, 2018.

[5] S.-Y. Park, J. Cho, K. Lee, and E. Yoon, "A PWM buck converter with load-adaptive power transistor scaling scheme using analog-digital hybrid control for high energy efficiency in implantable biomedical systems," *IEEE Transactions on Biomedical Circuits and Systems*, vol. 9, no. 6, pp. 885–895, 2015.

[6] D. Liberzon, *Switching in Systems and Control*. Springer, 2003, vol. 190.

[7] Y. He, M. Wu, G.-P. Liu, and J.-H. She, "Output feedback stabilization for a discrete-time system with a time-varying delay," *IEEE Transactions on Automatic Control*, vol. 53, no. 10, pp. 2372–2377, 2008.

[8] R. M. Palhares and P. L. Peres, "Robust filtering with guaranteed energy-to-peak performance-An LMI approach," *Automatica*, vol. 36, no. 6, pp. 851–858, 2000.

[9] H. Dong, N. Hou, and Z. Wang, "Fault estimation for complex networks with randomly varying topologies and stochastic inner couplings," *Automatica*, vol. 112, p. 108734, 2020.

[10] D. Du, S. Xu, and V. Cocquempot, "Fault detection for nonlinear discrete-time switched systems with persistent dwell time," *IEEE Transactions on Fuzzy Systems*, vol. 26, no. 4, pp. 2466–2474, 2017.

[11] J. Qiu, K. Sun, T. Wang, and H. Gao, "Observer-based fuzzy adaptive event-triggered control for pure-feedback nonlinear systems with prescribed performance," *IEEE Transactions on Fuzzy Systems*, vol. 27, no. 11, pp. 2152–2162, 2019.

[12] P. Shi, H. Wang, and C.-C. Lim, "Network-based event-triggered control for singular systems with quantizations," *IEEE Transactions on Industrial Electronics*, vol. 63, no. 2, pp. 1230–1238, 2015.

[13] M. V. Basin and P. C. Rodriguez-Ramirez, "Sliding-mode filter design for linear systems with unmeasured states," *IEEE Transactions on Industrial Electronics*, vol. 58, no. 8, pp. 3616–3622, 2010.

[14] M. Basin and P. Rodriguez-Ramirez, "Sliding mode filtering for stochastic systems with polynomial state and observation equations," *Journal of the Franklin Institute*, vol. 351, no. 4, pp. 2203–2217, 2014.

[15] L. I. Allerhand and U. Shaked, "Robust stability and stabilization of linear switched systems with dwell time," *IEEE Transactions on Automatic Control*, vol. 56, no. 2, pp. 381–386, 2011.

[16] H. Lin and P. J. Antsaklis, "Stability and stabilizability of switched linear systems: A survey of recent results," *IEEE Transactions on Automatic control*, vol. 54, no. 2, pp. 308–322, 2009.

[17] H. R. Karimi, "Robust delay-dependent H_∞ control of uncertain time-delay systems with mixed neutral, discrete, and distributed time-delays and Markovian switching parameters," *IEEE Transactions on Automatic Control*, vol. 58, no. 8, pp. 1910–1923, 2011.

[18] J. Lam, Z. Shu, S. Xu, and E.-K. Boukas, "Robust control of descriptor discrete-time Markovian jump systems," *International Journal of Control*, vol. 80, no. 3, pp. 374–385, 2007.

[19] S. Xu, T. Chen, and J. Lam, "Robust H_∞ filtering for uncertain Markovian jump systems with mode-dependent time delays," *IEEE Transactions on Automatic Control*, vol. 48, no. 5, pp. 900–907, 2003.

[20] S. Xu, J. Lam, and X. Mao, "Delay-dependent H_∞ control and filtering for uncertain Markovian jump systems with time-varying delays," *IEEE Transactions on Circuits and Systems I: Regular Papers*, vol. 54, no. 9, pp. 2070–2077, 2007.

[21] J. P. Hespanha and A. S. Morse, "Stability of switched systems with average dwell-time," in *Proceedings of the 38th IEEE Conference on Decision and Control (CDC)*, vol. 3. IEEE, 1999, pp. 2655–2660.

[22] T.-T. Han, S. S. Ge, and T. H. Lee, "Persistent dwell-time switched nonlinear systems: Variation paradigm and gauge design," *IEEE Transactions on Automatic Control*, vol. 55, no. 2, pp. 321–337, 2009.

[23] C. E. García, D. M. Prett, and M. Morari, "Model predictive control: Theory and practice—A survey," *Automatica*, vol. 25, no. 3, pp. 335–348, 1989.

[24] D. W. Clarke, C. Mohtadi, and P. Tuffs, "Generalized predictive control—Part I. The basic algorithm," *Automatica*, vol. 23, no. 2, pp. 137–148, 1987.

[25] D. Q. Mayne, "Model predictive control: Recent developments and future promise," *Automatica*, vol. 50, no. 12, pp. 2967–2986, 2014.

[26] J. B. Rawlings and D. Q. Mayne, *Model Predictive Control Theory and Design*. Nob Hill Publishing, Madison, WI, 2009.

[27] D. H. Shim, H. J. Kim, and S. Sastry, "Decentralized nonlinear model predictive control of multiple flying robots," in *Proceedings of the 42nd IEEE International Conference on Decision and Control (CDC)*, vol. 4. IEEE, Oct. 2003, pp. 3621–3626.

[28] N. Slegers and M. Costello, "Model predictive control of a parafoil and payload system," *Journal of Guidance, Control, and Dynamics*, vol. 28, no. 4, pp. 816–821, 2005.

[29] H. Xiao, Z. Li, C. Yang, L. Zhang, P. Yuan, L. Ding, and T. Wang, "Robust stabilization of a wheeled mobile robot using model predictive control based on neurodynamics optimization," *IEEE Transactions on Industrial Electronics*, vol. 64, no. 1, pp. 505–516, 2016.

[30] S. Mariéthoz and M. Morari, "Explicit model predictive control of a PWM inverter with an LCL filter," *IEEE Transactions on Industrial Electronics*, vol. 56, no. 2, pp. 389–399, 2008.

[31] P. Cortes, J. Rodríguez, P. Antoniewicz, and M. Kazmierkowski, "Direct power control of an AFE using predictive control," *IEEE Transactions on Power Electronics*, vol. 23, no. 5, pp. 2516–2523, 2008.

[32] S. Kouro, P. Cortés, R. Vargas, U. Ammann, and J. Rodríguez, "Model predictive control—A simple and powerful method to control power converters," *IEEE Transactions on Industrial Electronics*, vol. 56, no. 6, pp. 1826–1838, 2008.

[33] J. Rodriguez, M. P. Kazmierkowski, J. R. Espinoza, P. Zanchetta, H. Abu-Rub, H. A. Young, and C. A. Rojas, "State of the art of finite control set model predictive control in power electronics," *IEEE Transactions on Industrial Informatics*, vol. 9, no. 2, pp. 1003–1016, 2012.

[34] A. Narasingam and J. S.-I. Kwon, "Koopman Lyapunov-based model predictive control of nonlinear chemical process systems," *AIChE Journal*, vol. 65, no. 11, p. e16743, 2019.

[35] T. Wang, H. Gao, and J. Qiu, "A combined adaptive neural network and nonlinear model predictive control for multirate networked industrial process control," *IEEE Transactions on Neural Networks and Learning Systems*, vol. 27, no. 2, pp. 416–425, 2015.

[36] P. Sindareh-Esfahani, S. S. Tabatabaei, and J. K. Pieper, "Model predictive control of a heat recovery steam generator during cold start-up operation using piecewise linear models," *Applied Thermal Engineering*, vol. 119, pp. 516–529, 2017.

[37] J. B. Rawlings and R. Amrit, "Optimizing process economic performance using model predictive control," in *Nonlinear Model Predictive Control*. Springer, 2009, pp. 119–138.

[38] X. Wu, J. Shen, Y. Li, and K. Y. Lee, "Fuzzy modeling and predictive control of superheater steam temperature for power plant," *ISA Transactions*, vol. 56, pp. 241–251, 2015.

[39] Y. Huang, H. Wang, A. Khajepour, H. He, and J. Ji, "Model predictive control power management strategies for HEVs: A review," *Journal of Power Sources*, vol. 341, pp. 91–106, 2017.

[40] J. Hu, Y. Shan, J. M. Guerrero, A. Ioinovici, K. W. Chan, and J. Rodriguez, "Model predictive control of microgrids—An overview," *Renewable and Sustainable Energy Reviews*, vol. 136, p. 110422, 2021.

[41] J. Tarragona, A. L. Pisello, C. Fernández, A. de Gracia, and L. F. Cabeza, "Systematic review on model predictive control strategies applied to active thermal energy storage systems," *Renewable and Sustainable Energy Reviews*, vol. 149, p. 111385, 2021.

[42] G. Ferrari-Trecate, L. Galbusera, M. P. E. Marciandi, and R. Scattolini, "Model predictive control schemes for consensus in multi-agent systems with single-and double-integrator dynamics," *IEEE Transactions on Automatic Control*, vol. 54, no. 11, pp. 2560–2572, 2009.

[43] R. R. Negenborn, B. De Schutter, and J. Hellendoorn, "Multi-agent model predictive control for transportation networks: Serial versus parallel schemes," *Engineering Applications of Artificial Intelligence*, vol. 21, no. 3, pp. 353–366, 2008.

[44] Q. Sun, K. Zhang, and Y. Shi, "Resilient model predictive control of cyber–physical systems under DoS attacks," *IEEE Transactions on Industrial Informatics*, vol. 16, no. 7, pp. 4920–4927, 2019.

[45] L. Zhang, B. Wang, Y. Li, and Y. Tang, "Distributed stochastic model predictive control for cyber–physical systems with multiple state delays and probabilistic saturation constraints," *Automatica*, vol. 129, p. 109574, 2021.

[46] P. O. Scokaert and D. Q. Mayne, "Min-max feedback model predictive control for constrained linear systems," *IEEE Transactions on Automatic control*, vol. 43, no. 8, pp. 1136–1142, 1998.

[47] D. M. Raimondo, D. Limon, M. Lazar, L. Magni, and E. F. Camacho, "Min-max model predictive control of nonlinear systems: A unifying overview on stability," *European Journal of Control*, vol. 15, no. 1, pp. 5–21, 2009.

[48] M. Lazar, D. M. De La Pena, W. M. H. Heemels, and T. Alamo, "On input-to-state stability of min–max nonlinear model predictive control," *Systems & Control Letters*, vol. 57, no. 1, pp. 39–48, 2008.

[49] C. Liu, H. Li, J. Gao, and D. Xu, "Robust self-triggered min–max model predictive control for discrete-time nonlinear systems," *Automatica*, vol. 89, pp. 333–339, 2018.

[50] C. Løvaas, M. M. Seron, and G. C. Goodwin, "Robust output-feedback model predictive control for systems with unstructured uncertainty," *Automatica*, vol. 44, no. 8, pp. 1933–1943, 2008.

[51] D. Q. Mayne, M. M. Seron, and S. Raković, "Robust model predictive control of constrained linear systems with bounded disturbances," *Automatica*, vol. 41, no. 2, pp. 219–224, 2005.

[52] J. Fleming, B. Kouvaritakis, and M. Cannon, "Regions of attraction and recursive feasibility in robust MPC," in *Proceedings of the 21st Mediterranean Conference on Control and Automation (MED)*. IEEE, Jun. 2013, pp. 801–806.

[53] D. Q. Mayne, E. C. Kerrigan, E. Van Wyk, and P. Falugi, "Tube-based robust nonlinear model predictive control," *International Journal of Robust and Nonlinear Control*, vol. 21, no. 11, pp. 1341–1353, 2011.

[54] S. V. Raković, B. Kouvaritakis, R. Findeisen, and M. Cannon, "Homothetic tube model predictive control," *Automatica*, vol. 48, no. 8, pp. 1631–1638, 2012.

[55] J. Fleming, B. Kouvaritakis, and M. Cannon, "Robust tube MPC for linear systems with multiplicative uncertainty," *IEEE Transactions on Automatic Control*, vol. 60, no. 4, pp. 1087–1092, 2014.

[56] P. Falugi and D. Q. Mayne, "Getting robustness against unstructured uncertainty: A tube-based MPC approach," *IEEE Transactions on Automatic Control*, vol. 59, no. 5, pp. 1290–1295, 2013.

[57] B. Kouvaritakis, M. Cannon, S. V. Raković, and Q. Cheng, "Explicit use of probabilistic distributions in linear predictive control," *Automatica*, vol. 46, no. 10, pp. 1719–1724, 2010.

[58] M. Farina, L. Giulioni, L. Magni, and R. Scattolini, "An approach to output-feedback MPC of stochastic linear discrete-time systems," *Automatica*, vol. 55, pp. 140–149, 2015.

[59] M. Korda, R. Gondhalekar, F. Oldewurtel, and C. N. Jones, "Stochastic MPC framework for controlling the average constraint violation," *IEEE Transactions on Automatic Control*, vol. 59, no. 7, pp. 1706–1721, 2014.

[60] M. Cannon, Q. Cheng, B. Kouvaritakis, and S. V. Raković, "Stochastic tube MPC with state estimation," *Automatica*, vol. 48, no. 3, pp. 536–541, Mar. 2012.

[61] C. Liu, A. Gray, C. Lee, J. K. Hedrick, and J. Pan, "Nonlinear stochastic predictive control with unscented transformation for semi-autonomous vehicles," in *Proceedings of 2014 American Control Conference (ACC)*. IEEE, Jun. 2014, pp. 5574–5579.

[62] A. Mesbah, S. Streif, R. Findeisen, and R. D. Braatz, "Stochastic nonlinear model predictive control with probabilistic constraints," in *Proceedings of 2014 American Control Conference (ACC)*. IEEE, Jun. 2014, pp. 2413–2419.

[63] D. Munoz-Carpintero and M. Cannon, "Convergence of stochastic nonlinear systems and implications for stochastic model predictive control," *IEEE Transactions on Automatic Control*, vol. 66, no. 6, pp. 2832–2839, 2020.

[64] J. A. Primbs and C. H. Sung, "Stochastic receding horizon control of constrained linear systems with state and control multiplicative noise," *IEEE Transactions on Automatic Control*, vol. 54, no. 2, pp. 221–230, 2009.

[65] M. Cannon, B. Kouvaritakis, and X. Wu, "Probabilistic constrained MPC for multiplicative and additive stochastic uncertainty," *IEEE Transactions on Automatic Control*, vol. 54, no. 7, pp. 1626–1632, 2009.

[66] L. Fagiano and M. Khammash, "Nonlinear stochastic model predictive control via regularized polynomial chaos expansions," in *Proceedings of the 51st IEEE Conference on Decision and Control (CDC)*. IEEE, Dec. 2012, pp. 142–147.

[67] L. Blackmore, M. Ono, A. Bektassov, and B. C. Williams, "A probabilistic particle-control approximation of chance-constrained stochastic predictive control," *IEEE Transactions on Robotics*, vol. 26, no. 3, pp. 502–517, 2010.

[68] L. Hewing and M. N. Zeilinger, "Scenario-based probabilistic reachable sets for recursively feasible stochastic model predictive control," *IEEE Control Systems Letters*, vol. 4, no. 2, pp. 450–455, 2019.

[69] G. Schildbach, L. Fagiano, C. Frei, and M. Morari, "The scenario approach for stochastic model predictive control with bounds on closed-loop constraint violations," *Automatica*, vol. 50, no. 12, pp. 3009–3018, 2014.

[70] J. Fleming and M. Cannon, "Stochastic MPC for additive and multiplicative uncertainty using sample approximations," *IEEE Transactions on Automatic Control*, vol. 64, no. 9, pp. 3883–3888, 2018.

[71] M. Lorenzen, F. Allgöwer, F. Dabbene, and R. Tempo, "Scenario-based stochastic MPC with guaranteed recursive feasibility," in *Proceedings of the 54th IEEE Conference on Decision and Control (CDC)*. IEEE, Dec. 2015, pp. 4958–4963.

[72] S. Grammatico, X. Zhang, K. Margellos, P. Goulart, and J. Lygeros, "A scenario approach for non-convex control design," *IEEE Transactions on Automatic Control*, vol. 61, no. 2, pp. 334–345, 2015.

[73] B. Kouvaritakis and M. Cannon, *Model Predictive Control–Classical, Robust and Stochastic*. Springer, 2016.

[74] T. Yang, X. Yi, J. Wu, Y. Yuan, D. Wu, Z. Meng, Y. Hong, H. Wang, Z. Lin, and K. H. Johansson, "A survey of distributed optimization," *Annual Reviews in Control*, vol. 47, pp. 278–305, 2019.

[75] M. Farina, L. Giulioni, and R. Scattolini, "Stochastic linear model predictive control with chance constraints—A review," *Journal of Process Control*, vol. 44, pp. 53–67, 2016.

[76] A. Mesbah, "Stochastic model predictive control: An overview and perspectives for future research," *IEEE Control Systems Magazine*, vol. 36, no. 6, pp. 30–44, 2016.

[77] M. Ono and B. C. Williams, "Iterative risk allocation: A new approach to robust model predictive control with a joint chance constraint," in *Proceedings of the 47th IEEE Conference on Decision and Control (CDC)*. IEEE, Dec. 2008, pp. 3427–3432.

[78] Z. Zhou and R. Cogill, "Reliable approximations of probability-constrained stochastic linear-quadratic control," *Automatica*, vol. 49, no. 8, pp. 2435–2439, 2013.

[79] P. Li, M. Wendt, and G. Wozny, "A probabilistically constrained model predictive controller," *Automatica*, vol. 38, no. 7, pp. 1171–1176, 2002.

[80] E. Cinquemani, M. Agarwal, D. Chatterjee, and J. Lygeros, "Convexity and convex approximations of discrete-time stochastic control problems with constraints," *Automatica*, vol. 47, no. 9, pp. 2082–2087, Sep. 2011.

[81] G. C. Calafiore and L. Fagiano, "Robust model predictive control via scenario optimization," *IEEE Transactions on Automatic Control*, vol. 58, no. 1, pp. 219–224, 2013.

[82] M. Evans, M. Cannon, and B. Kouvaritakis, "Linear stochastic MPC under finitely supported multiplicative uncertainty," in *Proceedings of 2012 American Control Conference (ACC)*. IEEE, Jun. 2012, pp. 442–447.

[83] F. Oldewurtel, A. Parisio, C. N. Jones, M. Morari, D. Gyalistras, M. Gwerder, V. Stauch, B. Lehmann, and K. Wirth, "Energy efficient building climate control using stochastic model predictive control and weather predictions," in *Proceedings of 2010 American Control Conference (ACC)*. IEEE, Jun. 2010, pp. 5100–5105.

[84] J. Yan and R. R. Bitmead, "Incorporating state estimation into model predictive control and its application to network traffic control," *Automatica*, vol. 41, no. 4, pp. 595–604, 2005.

[85] L. Dai, Y. Xia, Y. Gao, B. Kouvaritakis, and M. Cannon, "Cooperative distributed stochastic MPC for systems with state estimation and coupled probabilistic constraints," *Automatica*, vol. 61, pp. 89–96, 2015.

[86] L. Dai, Y. Xia, and Y. Gao, "Distributed model predictive control of linear systems with stochastic parametric uncertainties and coupled probabilistic constraints," *SIAM Journal on Control and Optimization*, vol. 53, no. 6, pp. 3411–3431, 2015.

[87] L. Dai, Y. Xia, Y. Gao, and M. Cannon, "Distributed stochastic MPC of linear systems with additive uncertainty and coupled probabilistic constraints," *IEEE Transactions on Automatic Control*, vol. 62, no. 7, pp. 3474–3481, 2016.

[88] G. C. Calafiore and M. C. Campi, "The scenario approach to robust control design," *IEEE Transactions on Automatic Control*, vol. 51, no. 5, pp. 742–753, 2006.

[89] D. Bernardini and A. Bemporad, "Scenario-based model predictive control of stochastic constrained linear systems," in *Proceedings of the 48h IEEE Conference on Decision and Control (CDC) held jointly with 2009 28th Chinese Control Conference (CCC)*. IEEE, Dec. 2009, pp. 6333–6338.

[90] S. Singh, Y. Chow, A. Majumdar, and M. Pavone, "A framework for time-consistent, risk-sensitive model predictive control: Theory and algorithms," *IEEE Transactions on Automatic Control*, vol. 64, no. 7, pp. 2905–2912, 2018.

[91] P. Sopasakis, D. Herceg, A. Bemporad, and P. Patrinos, "Risk-averse model predictive control," *Automatica*, vol. 100, pp. 281–288, 2019.

[92] V. Belenko, V. Chernenko, V. Krundyshev, and M. Kalinin, "Data-driven failure analysis for the cyber physical infrastructures," in *Proceedings of 2019 IEEE International Conference on Industrial Cyber Physical Systems (ICPS)*. IEEE, May 2019, pp. 1–5.

[93] L. Hewing, K. P. Wabersich, M. Menner, and M. N. Zeilinger, "Learning-based model predictive control: Toward safe learning in control," *Annual Review of Control, Robotics, and Autonomous Systems*, vol. 3, pp. 269–296, 2020.

[94] V. Krishnan and F. Pasqualetti, "On direct vs indirect data-driven predictive control," *arXiv preprint arXiv:2103.14936*, 2021.

[95] T. Zhang, G. Kahn, S. Levine, and P. Abbeel, "Learning deep control policies for autonomous aerial vehicles with MPC-guided policy search," in *Proceedings*

of 2016 IEEE International Conference on Robotics and Automation (ICRA). IEEE, May 2016, pp. 528–535.

[96] S. Kamthe and M. Deisenroth, "Data-efficient reinforcement learning with probabilistic model predictive control," in *Proceedings of International Conference on Artificial Intelligence and Statistics (AISTAS)*. PMLR, Apr. 2018, pp. 1701–1710.

[97] I. Mitsioni, Y. Karayiannidis, J. A. Stork, and D. Kragic, "Data-driven model predictive control for the contact-rich task of food cutting," in *Proceedings of the 19th IEEE-RAS International Conference on Humanoid Robots (Humanoids)*. IEEE, Oct. 2019, pp. 244–250.

[98] S. Peitz and S. Klus, "Koopman operator-based model reduction for switched-system control of PDEs," *Automatica*, vol. 106, pp. 184–191, 2019.

[99] J. Berberich, J. Köhler, M. A. Müller, and F. Allgöwer, "Data-driven model predictive control with stability and robustness guarantees," *IEEE Transactions on Automatic Control*, vol. 66, no. 4, pp. 1702–1717, 2020.

[100] G. Baggio, D. S. Bassett, and F. Pasqualetti, "Data-driven control of complex networks," *Nature Communications*, vol. 12, no. 1, pp. 1–13, 2021.

[101] K. Bieker, S. Peitz, S. L. Brunton, J. N. Kutz, and M. Dellnitz, "Deep model predictive flow control with limited sensor data and online learning," *Theoretical and Computational Fluid Dynamics*, vol. 34, no. 4, pp. 577–591, 2020.

[102] A. Bemporad and M. Morari, "Control of systems integrating logic, dynamics, and constraints," *Automatica*, vol. 35, no. 3, pp. 407–427, 1999.

[103] P. Mhaskar, N. H. EI-Farra, and P. D. Christofides, "Predictive control of switched nonlinear systems with scheduled mode transitions," *IEEE Transactions on Automatic Control*, vol. 50, no. 11, pp. 1670–1680, 2007.

[104] D. Görges, M. Izák, and S. Liu, "Optimal control and scheduling of switched systems," *IEEE Transactions on Automatic Control*, vol. 56, no. 1, pp. 135–140, 2010.

[105] C.-J. Ong, Z. Wang, and M. Dehghan, "Model predictive control for switching systems with dwell-time restriction," *IEEE Transactions on Automatic Control*, vol. 61, no. 12, pp. 4189–4195, 2016.

[106] M. A. Müller, P. Martius, and F. Allgöwer, "Model predictive control of switched nonlinear systems under average dwell-time," *Journal of Process Control*, vol. 22, no. 9, pp. 1702–1710, 2012.

[107] S. Zhuang, H. Gao, and Y. Shi, "Model predictive control of switched linear systems with persistent dwell-time constraints: Recursive feasibility and stability," *IEEE Transactions on Automatic Control*, vol. 68, no. 12, pp. 7887–7894, 2023.

[108] F. Blanchini and S. Miani, *Set-Theoretic Methods in Control*. Springer, 2008, vol. 78.

[109] F. Blanchini, "Ultimate boundedness control for uncertain discrete-time systems via set-induced Lyapunov functions," *IEEE Transactions on automatic control*, vol. 39, no. 2, pp. 428–433, 1994.

[110] D. Liberzon, *Switching in Systems and Control*. Berlin, Germany: Birkhäuser, 2003.

[111] F. Zhu and P. J. Antsaklis, "Optimal control of hybrid switched systems: A brief survey," *Discrete Event Dynamic Systems*, vol. 25, pp. 345–364, 2015.

[112] A. S. Morse, "Supervisory control of families of linear set-point controllers-Part 1: Exact matching," *IEEE Transactions on Automatic Control*, vol. 41, no. 10, pp. 1413–1431, 1996.

[113] J. P. Hespanha, "Uniform stability of switched linear systems: Extensions of LaSalle's invariance principle," *IEEE Transactions on Automatic Control*, vol. 49, no. 4, pp. 470–482, 2004.

[114] H. Michalska and D. Q. Mayne, "Robust receding horizon control of constrained nonlinear systems," *IEEE Transactions on Automatic Control*, vol. 38, no. 11, pp. 1623–1633, 1993.

[115] J. Hopcroft and R. Kannan, *Computer Science Theory for the Information Age*. Carnegie Mellon University, 2011.

[116] L. Hogben, *Handbook of Linear Algebra*. CRC press, 2006.

[117] S. L. Brunton, M. Budišić, E. Kaiser, and J. N. Kutz, "Modern Koopman theory for dynamical systems," *arXiv preprint arXiv:2102.12086*, 2021.

[118] P. J. Schmid, "Dynamic mode decomposition of numerical and experimental data," *Journal of Fluid Mechanics*, vol. 656, pp. 5–28, 2010.

[119] P. J. Schmid, L. Li, M. P. Juniper, and O. Pust, "Applications of the dynamic mode decomposition," *Theoretical and Computational Fluid Dynamics*, vol. 25, no. 1, pp. 249–259, 2011.

[120] J. L. Proctor, S. L. Brunton, and J. N. Kutz, "Dynamic mode decomposition with control," *SIAM Journal on Applied Dynamical Systems*, vol. 15, no. 1, pp. 142–161, 2016.

[121] A. Narasingam and J. S.-I. Kwon, "Development of local dynamic mode decomposition with control: Application to model predictive control of hydraulic fracturing," *Computers & Chemical Engineering*, vol. 106, pp. 501–511, 2017.

[122] Q. Lu and V. M. Zavala, "Image-based model predictive control via dynamic mode decomposition," *Journal of Process Control*, vol. 104, pp. 146–157, 2021.

[123] C. Patyn and G. Deconinck, "Dynamic mode decomposition for nonintrusive and robust model predictive control of residential heating systems," *Energy and Buildings*, vol. 254, p. 111450, 2022.

[124] M. O. Williams, I. G. Kevrekidis, and C. W. Rowley, "A data–driven approximation of the Koopman operator: Extending dynamic mode decomposition," *Journal of Nonlinear Science*, vol. 25, no. 6, pp. 1307–1346, 2015.

[125] M. Korda and I. Mezić, "Linear predictors for nonlinear dynamical systems: Koopman operator meets model predictive control," *Automatica*, vol. 93, pp. 149–160, 2018.

[126] N. V. Sahinidis, "Mixed-integer nonlinear programming 2018," *Optimization and Engineering*, vol. 20, pp. 301–306, 2019.

[127] L. Ni and D. Wang, "A gain-switching control scheme for position-error-based bilateral teleoperation: Contact stability analysis and controller design," *International Journal of Robotics Research*, vol. 23, no. 3, pp. 255–274, 2004.

[128] L. Hetel, J. Daafouz, and C. Iung, "Stability analysis for discrete time switched systems with temporary uncertain switching signal," in *Proceedings of the 46th IEEE Conference on Decision and Control (CDC)*. IEEE, 2007, pp. 5623–5628.

[129] P. Mhaskar, N. H. El-Farra, and P. D. Christofides, "Robust predictive control of switched systems: Satisfying uncertain schedules subject to state and control constraints," *International Journal of Adaptive Control and Signal Processing*, vol. 22, no. 2, pp. 161–179, 2008.

[130] G. Zhang and A. Tanwani, "ISS Lyapunov functions for cascade switched systems and sampled-data control," *Automatica*, vol. 105, pp. 216–227, 2019.

[131] S. Liu, A. Tanwani, and D. Liberzon, "ISS and integral-ISS of switched systems with nonlinear supply functions," *Mathematics of Control, Signals, and Systems*, vol. 34, pp. 297–327, 2021.

[132] J.-W. Lee and G. E. Dullerud, "Uniform stabilization of discrete-time switched and Markovian jump linear systems," *Automatica*, vol. 42, pp. 205–218, 2006.

[133] Y. Chitour, N. Guglielmi, V. Y. Protasov, and M. Sigalotti, "Switching systems with dwell time: Computing the maximal Lyapunov exponent," *Nonlinear Analysis: Hybrid Systems*, vol. 40, no. 101021, 2021.

[134] M. Della Rossa, M. Pasquini, and D. Angeli, "Continuous-time switched systems with swithcing frequency constraints: Path-complete stability criteria," *Automatica*, vol. 137, p. 110099, 2022.

[135] J. C. Geromel and P. Colaneri, "Stability and stabilization of discrete time switched systems," *International Journal of Control*, vol. 79, no. 7, pp. 719–728, 2006.

[136] F. Blanchini, S. Miani, and C. Savorgnan, "Stability results for linear parameter varying and switching systems," *Automatica*, vol. 43, pp. 1817–1823, 2007.

[137] L. Zhang and P. Shi, "Stability, l_2-gain and asynchronous H_∞ control of discrete-time switched systems with average dwell time," *IEEE Transactions on Automatic Control*, vol. 54, no. 9, pp. 2193–2200, 2009.

[138] J. Hespanha, "l_2-induced gains of switched linear systems," *Unsolved Problems in Mathematical Systems and Control Theory*, vol. in: V. D. Blondel, A. Megretski (Eds.), Princeton, NJ, USA: Princeton Univ. Press, pp. 131–133, 2003.

[139] J. Xiao and M. Xiang, "New results on asynchronous H_∞ control for switched discrete-time linear systems under dwell time constraint," *Applied Mathematics and Computation*, vol. 242, pp. 601–611, 2014.

[140] L. Zhang, S. Zhuang, and P. Shi, "Non-weighted quasi-time-dependent H_∞ filtering for switched linear systems with persistent dwell-time," *Automatica*, vol. 54, pp. 201–209, 2015.

[141] S. Yuan, L. Zhang, B. De Schutter, and S. Baldi, "A novel Lyapunov function for a non-weighted l_2 gain of asynchronously switched linear systems," *Automatica*, vol. 87, pp. 310–317, 2018.

[142] T. Tan, S. Zhuang, and Y. Shi, "Model predictive control for asynchronously switched linear systems with mode-dependent dwell time," *Automatica*, vol. 162, p. 111524, 2024.

[143] S. Zhuang, X. Yu, J. Qiu, Y. Shi, and H. Gao, "Meta-sequence-dependent H_∞ filteirng for switched linear systems under persistent dwell-time constraint," *Automatica*, vol. 123, p. 109348, 2021.

[144] W. Xiang, H.-D. Tran, and T. Johnson, "Nonconservative lifted convex conditions for stability of discrete-time switched systems under minimum dwell-time constraint," *IEEE Transactions on Automatic Control*, vol. 64, no. 8, pp. 3407–3414, 2019.

[145] M. Philippe, R. Essick, G. E. Dullerud, and R. M. Jungers, "Stability of discrete-time switching systems with constrained switching sequences," *Automatica*, vol. 72, pp. 242–250, 2016.

[146] C. Briat, "Convex lifted conditions for robust l_2-stability analysis and l_2-stabilization of linear discrete-time switched systems with minimum dwell-time constriant," *Automatica*, vol. 50, pp. 976–983, 2014.

[147] M. Della Rossa, T. Alves Lima, M. Jungers, and R. M. Jungers, "Graph-based conditions for feedback stabilization of switched and LPV systems," *Automatica*, vol. 160, p. 111427, 2024.

[148] R. Yang and W. Zheng, "H_∞ filtering for discrete-time 2-D switched systems: an extended average dwell time approach," *Automatica*, vol. 98, pp. 302–313, 2018.

[149] C. Briat, "Stability analysis and stabilization of stochastic linear impulsive, switched and sampled-data systems under dwell-time constraints," *Automatica*, vol. 74, pp. 279–287, 2016.

[150] W. Xiang, H.-D. Tran, and T. T. Johnson, "Robust exponential stability and disturbance attenuation for discrete-time switched systems under arbitrary switching," *IEEE Transactions on Automatic Control*, vol. 63, no. 5, pp. 1450–1456, 2017.

[151] Z. Fei, S. Shi, Z. Wang, and L. Wu, "Quasi-time-dependent output control for discrete-time switched system with mode-dependent average dwell time," *IEEE Transactions on Automatic Control*, vol. 63, no. 8, pp. 2647–2653, 2018.

[152] H. Shen, Z. Huang, X. Yang, and Z. Wang, "Quantized energy-to-peak state estimation for persistent dwell-time switched neural networks with packet dropouts," *Nonlinear Dynamics*, vol. 93, pp. 2249–2262, 2018.

[153] S. Shi, Z. Fei, T. Wang, and Y. Xu, "Filtering for switched T–S fuzzy systems with persistent dwell time," *IEEE Transactions on Cybernetics*, vol. 49, no. 5, pp. 1923–1931, 2018.

[154] H. Gao, T. Chen, and J. Lam, "A new delay system approach to network-based control," *Automatica*, vol. 44, no. 1, pp. 39–52, 2008.

[155] H. Gao, X. Meng, and T. Chen, "Stabilization of networked control systems with a new delay characterization," *IEEE Transactions on Automatic Control*, vol. 53, no. 9, pp. 2142–2148, 2008.

[156] H. R. Karimi, "A sliding mode approach to H_∞ synchronization of master–slave time-delay systems with Markovian jumping parameters and nonlinear uncertainties," *Journal of the Franklin Institute*, vol. 349, no. 4, pp. 1480–1496, 2012.

[157] R. Palhares, C. Campos, P. Y. Ekel, M. Leles, and M. D'Angelo, "Delay-dependent robust H_∞ control of uncertain linear systems with lumped delays,"

IEE Proceedings-Control Theory and Applications, vol. 152, no. 1, pp. 27–33, 2005.

[158] X.-M. Sun, J. Zhao, and D. J. Hill, "Stability and l_2-gain analysis for switched delay systems: A delay-dependent method," *Automatica*, vol. 42, no. 10, pp. 1769–1774, 2006.

[159] G. Zhai, B. Hu, K. Yasuda, and A. N. Michel, "Disturbance attenuation properties of time-controlled switched systems," *Journal of the Franklin Institute*, vol. 338, no. 7, pp. 765–779, 2001.

[160] J. Zhao and D. J. Hill, "On stability, l_2-gain and H_∞ control for switched systems," *Automatica*, vol. 44, no. 5, pp. 1220–1232, 2008.

[161] M. Dehghan and C.-J. Ong, "Characterization and computation of disturbance invariant sets for constrained switched linear systems with dwell time restriction," *Automatica*, vol. 48, no. 9, pp. 2175–2181, 2012.

[162] L. Zhang, S. Zhuang, P. Shi, and Y. Zhu, "Uniform tube based stabilization of switched linear systems with mode-dependent persistent dwell-time," *IEEE Transactions on Automatic Control*, vol. 60, no. 11, pp. 2994–2999, 2015.

[163] Z. Feng and J. Lam, "On reachable set estimation of singular systems," *Automatica*, vol. 52, pp. 146–153, 2015.

[164] Z. Feng and W. X. Zheng, "On reachable set estimation of delay Markovian jump systems with partially known transition probabilities," *Journal of the Franklin Institute*, vol. 353, no. 15, pp. 3835–3856, 2016.

[165] J. Lam, B. Zhang, Y. Chen, and S. Xu, "Reachable set estimation for discrete-time linear systems with time delays," *International Journal of Robust and Nonlinear Control*, vol. 25, no. 2, pp. 269–281, 2015.

[166] W. Xiang, H.-D. Tran, and T. T. Johnson, "Output reachable set estimation for switched linear systems and its application in safety verification," *IEEE Transactions on Automatic Control*, vol. 62, no. 10, pp. 5380–5387, 2017.

[167] Y. Chen and J. Lam, "Estimation and synthesis of reachable set for discrete-time periodic systems," *Optimal Control Applications and Methods*, vol. 37, no. 5, pp. 885–901, 2016.

[168] Y. Chen, J. Lam, and B. Zhang, "Estimation and synthesis of reachable set for switched linear systems," *Automatica*, vol. 63, pp. 122–132, 2016.

[169] L. Zhang, S. Zhuang, and P. Shi, "Non-weighted quasi-time-dependent H_∞ filtering for switched linear systems with persistent dwell-time," *Automatica*, vol. 54, pp. 201–209, 2015.

[170] E. Bradford, L. Imsland, D. Zhang, and E. A. del Rio Chanona, "Stochastic data-driven model predictive control using gaussian processes," *Computers & Chemical Engineering*, vol. 139, p. 106844, 2020.

[171] A. Carron, E. Arcari, M. Wermelinger, L. Hewing, M. Hutter, and M. N. Zeilinger, "Data-driven model predictive control for trajectory tracking with a robotic arm," *IEEE Robotics and Automation Letters*, vol. 4, no. 4, pp. 3758–3765, 2019.

[172] J. N. Kutz, S. L. Brunton, B. W. Brunton, and J. L. Proctor, *Dynamic Mode Decomposition: Data-driven Modeling of Complex Systems*. SIAM, 2016.

[173] V. Gunes, S. Peter, T. Givargis, and F. Vahid, "A survey on concepts, applications, and challenges in cyber-physical systems." *KSII Transactions on Internet & Information Systems*, vol. 8, no. 12, 2014.

[174] G. Xiong, F. Zhu, X. Liu, X. Dong, W. Huang, S. Chen, and K. Zhao, "Cyber-physical-social system in intelligent transportation," *IEEE/CAA Journal of Automatica Sinica*, vol. 2, no. 3, pp. 320–333, 2015.

[175] J. M. Bradley and E. M. Atkins, "Optimization and control of cyber-physical vehicle systems," *Sensors*, vol. 15, no. 9, pp. 23 020–23 049, 2015.

[176] J. Wan, H. Yan, D. Li, K. Zhou, and L. Zeng, "Cyber-physical systems for optimal energy management scheme of autonomous electric vehicle," *The Computer Journal*, vol. 56, no. 8, pp. 947–956, 2013.

[177] C. Lv, X. Hu, A. Sangiovanni-Vincentelli, Y. Li, C. M. Martinez, and D. Cao, "Driving-style-based codesign optimization of an automated electric vehicle: A cyber-physical system approach," *IEEE Transactions on Industrial Electronics*, vol. 66, no. 4, pp. 2965–2975, 2018.

[178] M. Sniedovich, "Dijkstra's algorithm revisited: The dynamic programming connexion," *Control and Cybernetics*, vol. 35, no. 3, pp. 599–620, 2006.

[179] A. R. Soltani, H. Tawfik, J. Y. Goulermas, and T. Fernando, "Path planning in construction sites: Performance evaluation of the Dijkstra, A*, and GA search algorithms," *Advanced Engineering Informatics*, vol. 16, no. 4, pp. 291–303, 2002.

[180] P. Vadakkepat, K. C. Tan, and W. Ming-Liang, "Evolutionary artificial potential fields and their application in real time robot path planning," in *Proceedings of Congress on Evolutionary Computation*, vol. 1. IEEE, 2000, pp. 256–263.

[181] M. B. Montaner and A. Ramirez-Serrano, "Fuzzy knowledge-based controller design for autonomous robot navigation," *Expert Systems with Applications*, vol. 14, no. 1-2, pp. 179–186, 1998.

[182] V. Roberge, M. Tarbouchi, and G. Labonté, "Comparison of parallel genetic algorithm and particle swarm optimization for real-time UAV path planning," *IEEE Transactions on Industrial Informatics*, vol. 9, no. 1, pp. 132–141, 2012.

[183] J. J. Kuffner and S. M. LaValle, "RRT-connect: An efficient approach to single-query path planning," in *Proceedings of 2000 IEEE International Conference on Robotics and Automation (ICRA)*, vol. 2. IEEE, 2000, pp. 995–1001.

[184] L. E. Kavraki, P. Svestka, J.-C. Latombe, and M. H. Overmars, "Probabilistic roadmaps for path planning in high-dimensional configuration spaces," *IEEE transactions on Robotics and Automation*, vol. 12, no. 4, pp. 566–580, 1996.

[185] Y. Koren and J. Borenstein, "Potential field methods and their inherent limitations for mobile robot navigation." in *Proceedings of 1991 IEEE International Conference on Robotics and Automation (ICRA)*, vol. 2, no. 1991, 1991, pp. 1398–1404.

[186] J. Ji, A. Khajepour, W. W. Melek, and Y. Huang, "Path planning and tracking for vehicle collision avoidance based on model predictive control with multi-constraints," *IEEE Transactions on Vehicular Technology*, vol. 66, no. 2, pp. 952–964, 2016.

[187] H. Guo, C. Shen, H. Zhang, H. Chen, and R. Jia, "Simultaneous trajectory planning and tracking using an MPC method for cyber-physical systems: A case study of obstacle avoidance for an intelligent vehicle," *IEEE Transactions on Industrial Informatics*, vol. 14, no. 9, pp. 4273–4283, 2018.

[188] U. Rosolia, S. De Bruyne, and A. G. Alleyne, "Autonomous vehicle control: A nonconvex approach for obstacle avoidance," *IEEE Transactions on Control Systems Technology*, vol. 25, no. 2, pp. 469–484, 2016.

[189] C. Shen, Y. Shi, and B. Buckham, "Trajectory tracking control of an autonomous underwater vehicle using Lyapunov-based model predictive control," *IEEE Transactions on Industrial Electronics*, vol. 65, no. 7, pp. 5796–5805, 2017.

[190] T. Schouwenaars, B. De Moor, E. Feron, and J. How, "Mixed integer programming for multi-vehicle path planning," in *Proceedings of 2001 European Control Conference (ECC)*. IEEE, Jun. 2001, pp. 2603–2608.

[191] S. V. Raković and D. Q. Mayne, "Robust model predictive control for obstacle avoidance: Discrete time case," in *Assessment and Future Directions of Nonlinear Model Predictive Control*. Springer, 2007, pp. 617–627.

[192] L. Dai, Q. Cao, Y. Xia, and Y. Gao, "Distributed MPC for formation of multi-agent systems with collision avoidance and obstacle avoidance," *Journal of the Franklin Institute*, vol. 354, no. 4, pp. 2068–2085, 2017.

[193] Y. Long, S. Liu, L. Xie, and K. H. Johansson, "A scenario-based distributed stochastic MPC for building temperature regulation," in *2014 IEEE International Conference on Automation Science and Engineering (CASE)*. IEEE, 2014, pp. 1091–1096.

[194] M. Bornapour, R.-A. Hooshmand, and M. Parastegari, "An efficient scenario-based stochastic programming method for optimal scheduling of CHP-PEMFC, WT, PV and hydrogen storage units in micro grids," *Renewable Energy*, vol. 130, pp. 1049–1066, 2019.

[195] A. Gray, Y. Gao, T. Lin, J. K. Hedrick, and F. Borrelli, "Stochastic predictive control for semi-autonomous vehicles with an uncertain driver model," in

Proceedings of the 16th International IEEE Conference on Intelligent Transportation Systems (ITSC 2013). IEEE, 2013, pp. 2329–2334.

[196] M. Genovese, V. Cigolotti, E. Jannelli, and P. Fragiacomo, "Hydrogen refueling process: Theory, modeling, and in-force applications," *Energies*, vol. 16, no. 6, p. 2890, 2023.

[197] Y. Wang and C. Decès-Petit, "Predicting fueling process on hydrogen refueling stations using multi-task machine learning," *International Journal of Hydrogen Energy*, vol. 45, no. 56, pp. 32 743–32 752, 2020.